Dissertation
submitted to the
Combined Faculties for the Natural Sciences and for Mathematics
of the Ruperto-Carola University of Heidelberg, Germany
for the degree of
Doctor of Natural Sciences

presented by
Dipl.-Phys. Babak Hadji Hosseini
born in Tehran, Iran

Oral examination: November 14th, 2008

Cellular Separation Forces Studied by Force Spectroscopy and Microplate Manipulation

Refeeres:	Prof. Dr. Joachim P. Spatz
	Prof. Dr. Heinz Horner

Zusammenfassung

In unserem Immunsystem tasten T-Zellen beständig antigenpräsentierende Zellen (AP-Zellen) nach antigen-beladenen MHC Molekülen ab, um mit ihren spezifischen T-Zell-Rezeptoren (TZR) fremdartige Mikroorganismen zu erkennen, welche in den Körper eingedrungen sind. In den letzten Jahren wurde deutlich, dass die Adhäsion zwischen T-Zellen und AP-Zellen durch eine spezielle Anordnung der Oberflächenmoleküle gekennzeichnet ist. Die hierbei auftretenden biophysikalischen Effekte sind noch weitgehend unerforscht.

In der vorliegenden Dissertation vergleichen wir die zeitabhängigen Adhäsionskräfte zwischen T-Zell/AP-Zell Paaren bei An- bzw. Abwesenheit von Antigenen an deren Oberfläche. Die Interaktion der Zellpaare wurde hierbei mit einer Zellziehaparatur visualisiert und mit den am Rasterkraftmikroskop gemessenen Kraftspektren korreliert.

Wir konnten zeigen, dass die Adhäsionskräfte bei Vorhandensein von Antigenen mit ca. 14 nN bis zu zehnmal höher sind als im Falle ihrer Abwesenheit. Hierbei liegen die gemessenen Kräfte zwischen den unterschiedlichen Zellpaaren in den ersten 2 Minuten bei ca. 2nN. Nach einer Adhäsionszeit von 15 min steigen die Kräfte bei Paaren mit Antigen an, um nach 30 min ein Maximum zu erreichen. Die Adhäsionskräfte bleiben bei Paaren ohne Antigen im gleichen Zeitraum niedrig. Neben der Gesamtadhäsionskraft zwischen den Zellen wurden desweiteren Einzelmolekülabrisse ausgewertet und mit Hilfe theoretischer Modelle Einblicke in das Interaktionspotenzial der Proteine gewonnen.

Die vorliegende Arbeit zeigt, dass fremdartige Antigene an der Zelloberfläche von AP-Zellen starke Zelladhäsion mit T-Zellen auslösen und trägt demzufolge entscheidend zum besseren Verständis der Rolle von Kraft in Zell-Zellinteraktion bei.

Abstract

During adaptive immune response, peptides from foreign microorganisms are processed and displayed on the surface of Antigen Presenting Cells (APCs) within the cleft of major histocompatibility complexes (pMHC), which are recognized by T cells that patrol the body. In recent years, a large spatially organized molecular cluster called immune synapse (IS) has been identified, which forms at the T cell/APC interface. Little is known about the biophysics of these cell conjugates and it is generally believed that cell adhesion molecules are activated on the T cell surface after recognition which should subsequently lead to higher adhesion forces between the two cells. Thus, the goal of this thesis was to measure the change of total adhesion forces between T cells and APCs when peptide was present compared to the case when peptide was absent.

In this work, we report the first measurement of separation forces between T cells and APCs employing a cell stretcher device and Atomic Force Microscopy (AFM). We analyze the kinetics of T cells that interact with APCs presenting a foreign peptide by their MHC (pulsed), and APCs carrying no peptide (unpulsed) for contact times of 0 to 60 minutes. Unlike pulsed cells, unpulsed APCs did not show the formation of immune synapses. Forces are comparable for short time points but start to deviate after 15 min to reach a maximum after 30 min in the pulsed case.

We could correlate single rupture events found in AFM spectra to protein unbinding theories gaining a deeper insight into the molecular basis for the increase in adhesion forces. Thus, this work provides an important contribution to the physical understanding of cell-cell adhesion.

Contents

Abstract iii

I Introduction 1

1 Cellular Adhesion 3
- 1.1 Cellular structure . . . 3
- 1.2 Development of adhesion . . . 4
- 1.3 Principles of adhesion . . . 5
- 1.4 Proteins in adhesion . . . 7
- 1.5 Physics of adhesion bonds . . . 9

2 The Immunological Synapse 15
- 2.1 Adaptive immune system . . . 15
- 2.2 Immune synapse formation . . . 16
- 2.3 Significance . . . 19

3 Techniques Measuring Forces in Living Cells 21
- 3.1 Micropipette aspiration . . . 22
- 3.2 Optical tweezers . . . 26
- 3.3 Magnetic tweezers . . . 28
- 3.4 The Optical Stretcher . . . 29
- 3.5 Substrate Stretcher . . . 31

II Experimental Measurement Techniques 33

4 The Cell Stretcher and its Applications 35
- 4.1 Introduction . . . 35
- 4.2 Experimental setup . . . 37
- 4.3 Enhanced experimental setup . . . 38
- 4.4 Adhesion contrast . . . 40

5 The Atomic Force Microscope 45

5.1 Introduction . . . 45
5.2 Applications . . . 46
5.3 Setup . . . 48

6 Fluorescent-activated Cell Sorting 53

III Separation Experiments 57

7 Motivation 59

8 Qualitative Observations - Cell Stretcher 63
8.1 Modified cell stretcher . . . 63
8.2 Experiment preparation . . . 65
8.3 Experiments . . . 67
8.4 Conclusion . . . 70

9 AFM Separation Experiments 71
9.1 Characterization of 3B11/LK35.2 conjugates . . . 71
9.2 Experiment preparation . . . 74
9.3 Experimental procedure . . . 76
9.4 Total separation force dynamics for 3B11/LK35.2 pairs . . . 76
9.5 Single rupture events . . . 81
9.6 1934.4/L cells experiments . . . 89
9.7 Discussion . . . 90

IV Conclusion and Outlook 93

10 Conclusion 95

11 Outlook 97

List of Figures 100

References 114

A Appendix 117
A.1 Abbreviations . . . 117
A.2 IL2 Sandwich ELISA . . . 118
A.3 Analysis of the Immune Synapse Using ImageStream . . . 118

Part I

Introduction

Chapter

1

Cell Adhesion

Cells form the basic structural subunit of our human body. A high level of communication, cooperativity and synergism is required to ensure the development and function of this highly complex living entity, which consists of about 10^{14} single cells[1]. The ability of cells to initiate, control and maintain adhesion to each other and their capacity to communicate with their surrounding is essential for a multicellular existence. Carefully regulated cell-cell and cell-environment interactions orchestrate the formation of tissues and organs during embryogenesis. Our skin is made of interconnected cells that tightly adhere to each other and the underlying connective tissue. Muscle cells form tight bonds to transfer stress and to produce forces. Transient cell encounters in the lymph nodes trigger specific immune responses to initiate the extinction of foreign pathogens that have entered our body.

In this chapter we will take a closer look at the different forms of cell adhesion and the mechanisms involved therein. Before, we will briefly introduce the basic structure of cells.

1.1 Cellular structure

Structural components, which make up a cell are displayed in Fig. 1.1. A lipid bilayer *membrane* separates the cytosol, the internal fluid of the cell where most chemical reactions take place, from the outside. Inside the intracellular domain, the *nucleus* carries genetic code in form of Deoxyribonucleic Acid (DNA). The *cytoskeleton* is a highly versatile set of networks composed of proteins differing in size and lengths. It enables cells to adapt to their environment, maintain their structural integrity and; furthermore, it is indispensable for directed cell movement, cell division and intracellular transport. The cytoskeleton is constituted of three distinct protein filament structures [1]:

Actin Filaments
are linear assemblages of globular actin, which is the most abundant protein in animal cells. It has a diameter of 7 nm and is mostly allocated beneath the cell membrane, see Fig. 1.1. Actin is vital to many cellular processes like cell locomotion and stress propagation through cells [2]. In muscle cells, actin filaments together with a motor protein, termed myosin II, are employed to contract muscles.

Intermediate Filaments
are composed of a class of proteins with limited sequence identity [3]. They have a

---

[1] In comparison, the milky way has approximately 10^{11} stars.

diameter of 8-12 nm and help cells, among other things, to maintain their shape [4].

Microtubules
are hollow cylinders, about 25 nm in diameter, made of proteins called tubulin. These biopolymers are very rigid with a bending rigidity ≈100 times that of actin filaments. Hence, they are thought to resist compressive forces, which are exerted by the other contractile cytoskeletal protein filaments [5].

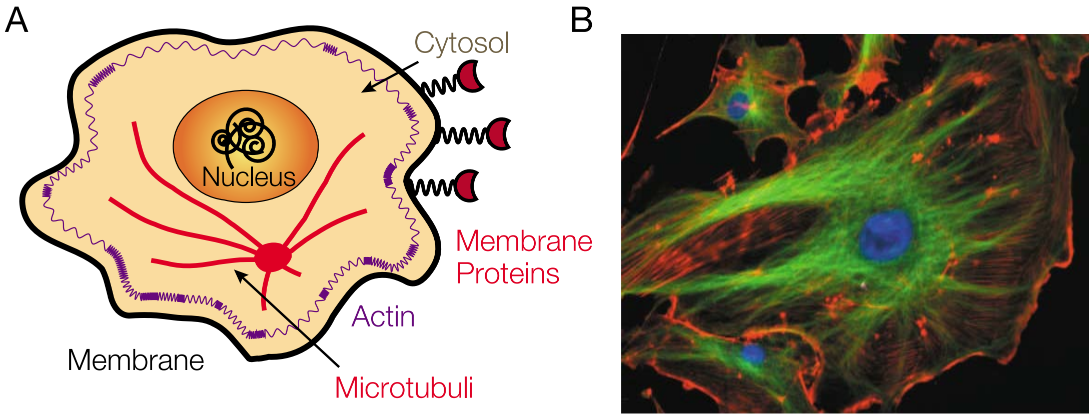

Figure 1.1: Structural components of a cell: (A) Schematic view of a cell: a lipid membrane separates the intracellular from the extracellular domain. The cytosol is the internal fluid of the cell, where most chemical reactions take place. Microtubuli and actin, which are shape-maintaining cytoskeleton components are shown. (B) Fluorescent image of an endothelial cell. Adapted from http://rsb.info.nih.gov.

Each of these three key filament systems of the cytoskeleton exhibits distinct mechanical properties. The filament networks are associated by linker proteins like plectin [6] and, in adhered cells, these filaments are connected through a myriad of other molecules to membrane proteins and the nucleus [7, 8]. Hence, a network spanning the entire cell is created which provides a mechanical continuum from the membrane to the DNA inside the nucleus [9]. The cytoskeleton responds to both, stimulation by mechanical forces and biochemical signaling. Cellular signaling may be induced, for instance, by surface recognition via Cell Adhesion Molecules (CAMs) (discussed in the next section), causing cascades of biochemical reactions, which lead to the precise regulation of cytoskeletal structure and cell adhesion forces.

1.2 Development of adhesion

Life emerged around 4 billion years ago on this planet in the form of primitive single-cell organisms. It is assumed that these ancestral precursor cells had about 1000 protein encoding genes, which diversified later to provide a selective advantage over other cell types [10]. Cells needed to scan their microenvironment, detect prey and foreign pathogens, therefore key principles of mechanosensitivity - the ability to specifically respond to external mechanical stimuli - and underlying mechanisms by which cells convert mechanical stimulus into chemical activity, called mechanotransduction, were developed at this early stage [11]. These genes laid then the basis for the subsequent development of multicellular organisms about 1 billion years ago, which is considered to be one of the *major transitions* in the evolution of life [12]. During this transition, adhesion and signaling between cells played a vital role: For the simplest of all reasons, cells needed to cohere to each other to establish stable aggregates. Moreover, in order to advance from simple cell colonies into a multicellular organisms basic communication for the overall coordination within such an organism is a necessary prerequisite.

1.3 Principles of adhesion

In our bodies, the regulation of adhesion and the communication of cells has reached an utterly high complexity. The correct migration, positioning, adhesion and communication of cells form the basis for the successful cooperation and synchronization of this many individual cells. Surprisingly, cells use a relatively small set of molecular adhesion mechanisms to interact with their environment. Principle proteins that mediate cell attachment or defense against infectious agents have probably evolved from mechanisms already present in uni-cellular organisms and many animal cell signaling and adhesion genes were in place at a very early stage in evolution [13]. We will now discuss which principle mechanisms cells use to control their propensity of adhesion.

1.3.1 One-to-one ligand-receptor pairing

Cells control their ability to adhere by a repertoire of transmembrane proteins on their surface. These surface receptors are composed of three domains: a large extracellular part, a transmembrane part, and a short intracellular domain [1]. The major classes of CAMs and their basic structures are displayed schematically in Fig. 1.2. We will review some of the protein families involved in adhesion and elucidate their specific importance and respective roles in Sec. 1.4.

These surface receptors usually recognize and bind to one specific *counterreceptor* termed ligand and thus mediate adhesion. Although many exceptions from this one-to-one binding rule exists, this basic principle is the corner stone of cellular adhesion. Specific binding of receptors to ligands and their precise recognition is the key element in controlling adhesive interactions between cells and their surroundings. Deviations from this elaborate molecular recognition and signaling machinery can lead to cellular dysfunction resulting in many pathologies like cancer [14, 15]. Basically, receptor-ligand interactions can be grouped into two types:

homophilic:
two receptors of the same kind bind together, i.e. ligand and receptor are identical

heterophilic:
two unlike molecules associate to form a stable bond

The type of CAMs and their level of expression depends on cell type and context and is usually determined by the genetic program that led to the differentiation of the cell. Consequently, bonds formed between two cells or between cells and their environment can be vastly different in their nature [16].

1.3.2 Avidity regulation

In interactions, which include multiple proteins, *avidity* is a relative measure to describe the overall strength of the combined bond interactions. It should not be confused with *affinity*, which describes the strength of a single bond. Cells have developed several ways to regulate avidity in adhesion:

Affinity regulation Cell adhesion receptors can change their individual conformational state and, thus, their ability to bind to ligands. Basically, three conformations are distinguished: inactivated, activated (also called primed) and bound state. Complicating the situation, there exist multiple intermediate states between activated and inactivated states. Thus, overall affinity has to be defined as equilibrium shifts between these states. Structural changes in integrins, one of the major families of CAMs, are rapid and reversible [17]. They dramatically regulate adhesion propensity of receptor-ligand interactions. The extracellular conformational conversion is controlled by the short cytoplasmic tail domain. Cells can thus, convert their adhesive surface proteins pretty accurately from the inside. This process is thus termed “inside-out-signaling”. In integrins, affinity changes were well studied in recent years and it has become evident that they undergo striking structural changes [18, 19].

Valency regulation Another mechanism to control the overall adhesion strength is achieved by regulating the number of molecules involved in adhesion. This is accomplished by either increasing the interaction interface or by facilitating diffusion of CAMs into the membrane area where interaction takes place. The latter mechanism is probably the reason why CAMs all have short cytoplasmic domains that can rapidly bind and unbind to the cytoskeleton and thus facilitate anchoring or high diffusivity of these membrane proteins, respectively. Finally, cells can up-regulate the number of CAMs in the interaction area storing them internally in vesicles before adhesion occurs. Upon adhesion, these proteins can be transported to the membrane and inserted there [20]. Recently, evidence is accumulating that a similar mechanism is used in directed cell movement [21–23]. To this end, cells detach their back part, collect adhesion proteins which are present there and recirculate them internally to their front part to facilitate forward movement.

1.3.3 Regulatory events

Another feature of cell adhesion are regulatory events which happen in the course of adhesion events.

Outside-in signaling Some CAMs do not only mediate adhesion but also serve as signaling proteins [24, 25]. Even though the term *integrin activation* is used to describe affinity state conversions it is also used to describe signals received from the cell by their CAMs surface receptors. These signals are important for cell viability and many cells die if they do not receive appropriate adhesion signals[2] [26].

---

[2] Cell death as response to the absence of cell adhesion is called *anoikis*.

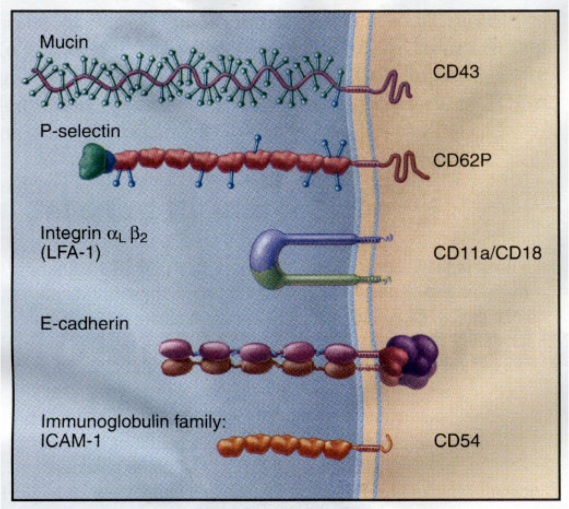

Figure 1.2: Transmembrane adhesion molecules: The major classes of Cell Adhesion Molecules (CAMs) are shown. Mucin and P-selectin represent various carbohydrates and (carbohydrate-binding) lectins for cell interactions, respectively. Lymphocyte Function-associated Antigen-1 (LFA-1) illustrates the integrin family. Integrins are heterodimeric CAMs composed of two non-covalently bound polypeptides called α (blue) and β (green) chain. They facilitate heterophilic cell adhesion to the Extracellular Matrix (ECM) and sometimes to other cells. E-cadherin represents the cell-cell binding protein family called cadherins. They have a central role in tight bonds present in cell assemblies, where structural integrity and mechanical stress resistance is essential, like in muscle or epithelial tissue. Intercellular Adhesion Molecule-1 (ICAM-1) belongs to the large Immunoglobulin Superfamily (IgSF). Adapted from [10].

Inside-out signaling Since in low-affinity states CAMs cannot interact with there environment, cells need a mechanism to activate them by other means. Usually, other receptors on the cell surface will receive signals and transduce them to the inside. There, other proteins will circulate these signals and finally changes in the cytoplasmic domain will lead to an activation of CAMs. This activation or *priming* process is thus called inside-out signaling.

Adhesion strengthening Adhesion strengthening occurs after initial adhesion and reinforces overall adhesion strength by either increasing avidity or coupling of cytoskeletal networks to the membrane bound receptors [27].

1.4 Proteins in adhesion

1.4.1 Cadherins

Evidently, cells are organized hierarchically in animal bodies. On a first level, cells cluster into cooperative assemblies, called tissues, which perform specific functions. In turn, on the next level tissues group to build larger functional units called organs, like the heart, lung and skin. To this end, tight cell-cell junctions form highly stable bonds that are necessary to preserve tissue integrity and architecture. In animals, there are five basic tissue types, which perform specific functions: epithelium, connective tissue, blood, muscle, and nervous tissue. Except for blood, which is a *fluid connective tissue* like lymph, tissues need to maintain a high grade of structural integrity. In this context, cell-cell adhesion is mostly mediated by the surface protein family termed **cadherins**[3]. Cadherin induced adhesion is strongly homophilic, and even within this family binding between same cadherins is highly favored. For example, E-cadherin (epithelial cadherin) on one cell will bind only to E-cadherin on another cell. Due to this homophilic specificity cells having the same cadherin molecule on their surface tend to associate during development [28]. Perturbations in the function and expression of E-cadherin and its associated proteins during cancer can result in loss of adhesion and tumor spreading through metastasis [29].

Separation force measurements revealed that E-cadherin is the key adhesion molecule involved in cell-cell adhesion bearing the major part of adhesion strength [30]. An example of E-cadherin mediated adhesion is displayed in Fig. 1.3. Neighboring cells form firm adherens junctions and interlink not only their membranes but also their cytoskeleton [31]. Thus, adherens junctions form cell-cell bonds that provide strong mechanical attachments between adjacent cells in tissues. Especially cells in mechanically active environments rely strongly on cadherin-based intercellular junctions to withstand forces: e.g. muscle cells in the heart are tightly held together and tension is transmitted throughout the tissue by this type of connection [32].

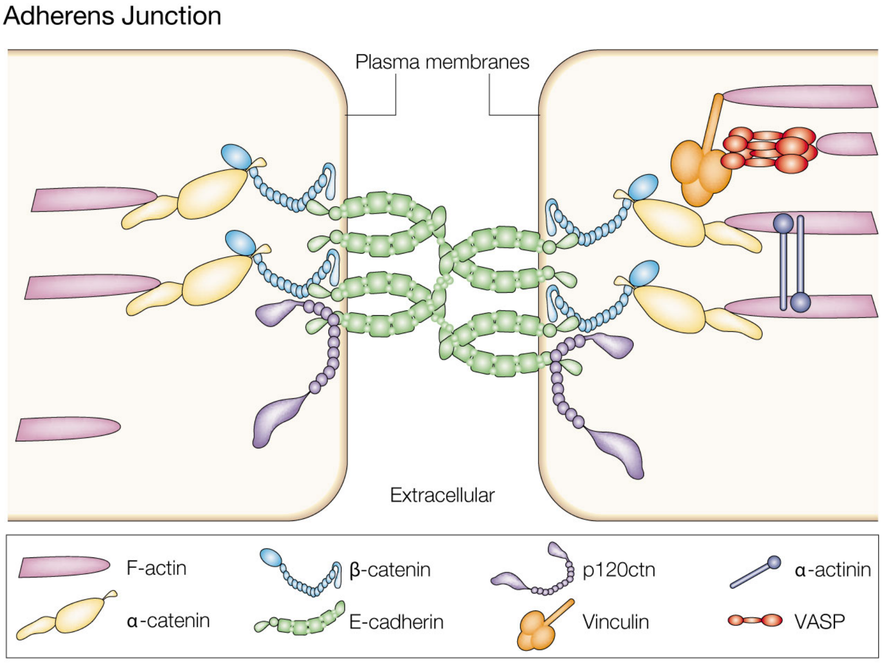

Figure 1.3: Schematic of an adherens junction: Cells connect through homophilic E-cadherin mediated cell-cell adhesion. These CAMs on the cell surface are chained to the actin cytoskeleton through a number of associated proteins called catenins on the intracellular side. This results in strong attachment of the cells and subsequently forces are transmitted . Adapted from [33].

---

[3] Derived from *Calcium Dependent Adhesion* protein.

1.4.2 Integrins

Integrins form one of the major family of homophilic cell adhesion receptors [24, 34, 35]. All integrins are non-covalently linked heterodimeric molecules containing an α and β polypeptide subunit (see Fig. 1.2). Integrins facilitate interactions with a few ligands on other cells but are mainly responsible for the adhesion of cells to the ECM. The ECM is a major part of connective tissue which is composed of many different protein structures, e.g. laminin, fibronectin, collagen etc. and provides a physical microenvironment for cells. In turn, it is cells that assemble the ECM. Thus, cells interact with the ECM and their function is often determined by the properties of their extracellular microenvironment [36]. Integrin mediated adhesion is present in almost every animal and regulate many biological functions like cell migration and morphogenesis, cell proliferation, cell differentiation, cell death, embryonic development, wound repair, tissue formation and cell migration [37–39]. Adhesion to the ECM trigger certain signaling pathways in cells and controls how they spread and remodel their cytoskeleton [40, 41].

In recent years, evidence has been accumulating that cells can "sense" and scan their mechanical environment using protein complexes built around integrin-mediated adhesion sites called focal adhesions [42–48]. The elasticity of substrates is clearly recognized by cells and can affect, for example, differentiation of certain stem cells [49].

1.4.3 Immunoglobulin family

The Immunoglobulin Superfamily (IgSF) is made up of a large number of CAMs which all possess a part termed immunoglobulin domain. This family of molecules plays an important role in our immune system [50] and their structure and properties are pretty well studied today [51]. Important members for this work are the T Cell Receptor (TCR) and ICAM-1, both present on T cells. The TCR helps T cells to recognize foreign peptide sequences, which are presented by other immune cells on their surface through Major Histocompatibility Complex (MHC) proteins. We will discuss the interaction of TCR and ICAM-1 in detail in Chapter 2.

1.5 Physics of adhesion bonds

We have learned that specific biological interactions are induced by numerous receptor-ligand pairs. Since cells have to be able to adapt to their environment rather quickly, these molecular bonds are reversible, have short life-times and dissociate spontaneously after a certain time even without application of external forces. This is one of the reasons why receptor-ligand interactions are non-covalent: the stability of these protein-protein couplings is mainly mediated through small free energy changes in electrostatic, van der Waals bond and weak hydrogen bond interactions at the receptor-ligand interface.

1.5.1 Single adhesion bonds

Suppose a molecule-molecule interaction which is conceptually governed by an attractive potential like in Fig. 1.4. If an external force F is applied on the bond, its energy landscape is tilted and deformed. A higher external force will result in a lower potential barrier which in turn will increase the likelihood of the bound state to dissociate.

George Irving Bell[4] was the first to introduce a model where force rate dependent effects in receptor-ligand interaction at cell surfaces were correctly accounted for [52]. His fairly simple and powerful theoretical model has been expanded and enhanced ever since [53–57], but is still regarded as cornerstone in cell surface molecule interactions. Bell was the first to realize, that kinetics and reaction rates of molecules bound in a cell membrane (2-D system) vary significantly from those in solution (3-D system). Furthermore, following the kinetic theory of the strength of solids, Bell proposed that the life-time of a reversible receptor-ligand bond is given by

$$\tau = \tau_0 \exp\left(\frac{E_0 - \rho f}{k_B T}\right) \tag{1.1}$$

where E_0 is the free energy change upon binding of the proteins, k_B is the Boltzmann constant, f the force acting on the bond and ρ is of the order of the distance between the potential's minimum and its barrier. A direct consequence is that the instantaneous, force-dependent dissociation rate, or off-rate, for the receptor-ligand molecule increases exponentially as a function of the external force f according to a formula which is termed "Bell's equation":

$$k_{\text{off}}(f) = k_{\text{off}}^0 \exp\left(\frac{r_0 f}{k_B T}\right) = k_{\text{off}}^0 \exp\left(\frac{f}{f_0}\right). \tag{1.2}$$

Bell's work was based on pioneering efforts by Eyring and Kramers[5] [58–60]. An interpretation of the formula above is to say: the rate of bond dissociation is the product of the probability of success k_{off} and the "trial frequency" e^{f/f_0}. Increasing the force f will thus lower the dissociation barrier and improve chances for unbinding by the Boltzmann factor e^{f/f_0}. In recent years single molecule force spectroscopy has made it possible to experimentally measure bond strengths by Atomic Force Microscope, Optical Tweezers (OT) and the Bio-membrane Force Probe (BFP). We will review these techniques in Chapter 3. Using Eq. 1.2, we can estimate the typical force scale of single rupture events using $\rho \approx 0.5 - 1$ nm, $T = 300$ K as $f_0 = 4 - 8$ pN. To get an estimate for the rupture force we follow Bell's paper [52]: Since $f_0 = E_0/\rho$ we can estimate $f_0 \approx 120$ pN using $E_0 = 0.37$ eV for a typical antigen-antibody bond, which is closer to experiments.

In laboratory situations, bond rupture forces are to be considered as stochastically distributed around a *most probable rupture force* f^*. Additionally, the forces applied in experiments are not constant and are coupled to the velocity of the retracted force probe. Evans and Ritchie were the first to realize that f^* should thus depend on the **loading rate** r_f, i.e. the increase of force per time, by the relationship

$$f^* = f_0 \ln\left(\frac{r_f}{k_{\text{off}}^0 f_0}\right), \tag{1.3}$$

which has been verified in the past ten years by a number of experiments [61–64]. For a linear relationship, r_f is written as

$$r_f = v \cdot \kappa,$$

---

[4] Theoretical Physicist at Los Alamos Scientific Laboratory, ⋆1926 - †2000.

[5] Kramers developed his equations parallel to the development of rate theory in the chemistry community by Eyring and Wigner.

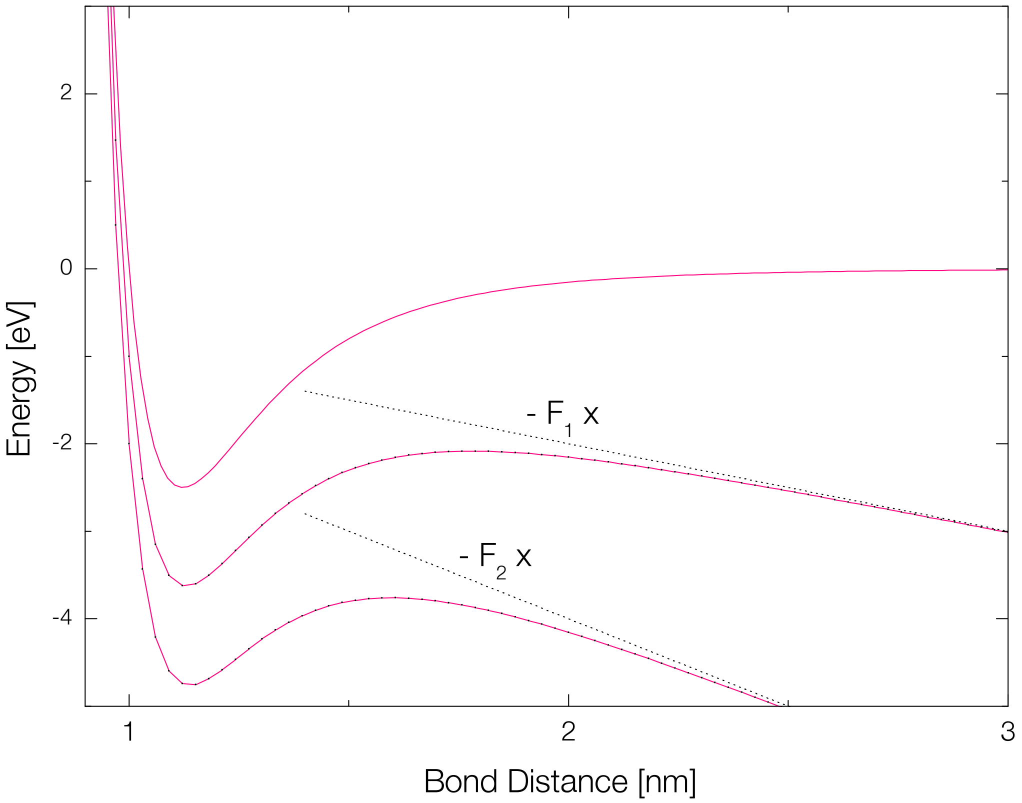

Figure 1.4: Constant force applied to a bond: Schematic diagram of a reaction pathway in unbonding. A simple Lennard-Jones potential is plotted. If an external force is applied the energy landscape is tilted and deformed. The potential's barrier is lowered if higher forces are applied. Thus, the probability of dissociation grows with increasing external force.

where v is the retraction velocity of the force probe (cantilever in case of an atomic force microscope) and κ is the probe's force constant. In 1999, Merkel et al. measured the rupture force of streptavidin-biotin complex which is amongst the strongest bonds in biology using the BFP. They showed that rupture force experiments performed by earlier AFM measurements [65] yielded high values due to Eq. 1.3 (see Fig. 1.5) since AFM cantilevers are pretty stiff.

1.5.2 Adhesion clusters

Adhesion between cells includes more than just a single receptor-ligand linkage. A multivalent approach has to be considered, which accounts for the thermodynamical aspects of the interaction. Many aspects of multiple cell-environment bridges alter adhesion dynamics: molecules might be cross-linked intercellularly or through co-proteins on the cell surface and thus establish adhesion clusters. We will study specialized molecule clusters, which occur in our immune system in Chapter 2. Additionally, adhesive proteins on a surface associate with the intra-cellular cytoskeleton to strengthen cohesion [66], which in

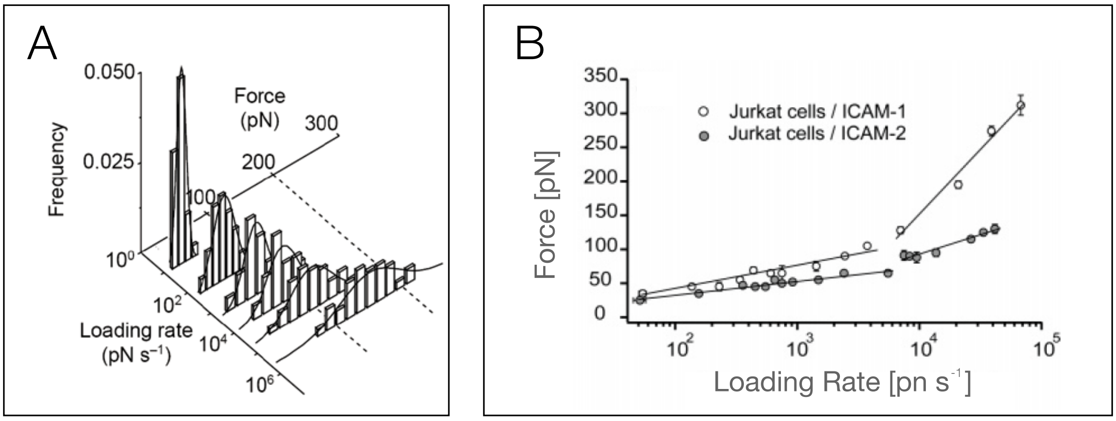

Figure 1.5: Loading rate dependence of adhesion bonds: (A) Rupture force distributions of single biotin-streptavidin bonds show a shifting peak location and enlarging width with increasing loading rate. Bond rupture was measured with the BFP, see 3.1 for details. Graph taken from [61]. (B) Force spectra of the LFA-1/ICAM-1 and LFA-1/ICAM-2 interactions measured by Atomic Force Microscope (AFM) exhibit a fast loading regime and a slow loading regime. Each regime belongs to a separate potential well in the reaction pathway. Taken from [62].

turn regulates diffusivity within the 2-D membrane. Adding to this, rebinding lifetimes, i.e. rebinding coefficients k_{on}, are reported to be strongly altered through heterogeneous protein pattern patches and clusters (known as lipid rafts) on the cell surface [67]. These complicating issues explain why single molecule studies have been at the center of focus in the past years. In contrast to single bond physics, the connection between theory and experiments has not been established precisely, so far. Nevertheless, some attempts have been made to account for the complex interactions in multi-bond adhesion [68–71].

Let us consider receptor-ligand mediated adhesion between two surfaces like displayed in Fig. 1.6 . Suppose an associated bond behaves like an idealized spring with a constant of κ and that the bonds bind and unbind with the rates of k_{on} and k_{off}, respectively. A force F, mediated by a spring-like force transducers detangles the proteins at a speed of v. The bonds might break through different mechanisms: On the one extreme, bonds might break one after another, like in a zipper, or, they all break at the same time. In the first case the load is concentrated on one bond at a time and after bond failure the next bond is loaded. This yields a total rupture time which is proportional to the total number of bonds N_b. In the second case, the force is distributed evenly among all bonds and we can infer by Newton's third law that:

$$\begin{aligned}\kappa_b r_0 &= \frac{1}{N_b(t)}\kappa_t x_t \\ &= \frac{\kappa_n \kappa_t}{N_b(t)\kappa_b + \kappa_t}\, vt \qquad (1.4)\end{aligned}$$

where κ_b and κ_t are the force constants of the bonds and the transducer, respectively. Using this equation, U. Seifert was able to approximate maximal forces in rupture experiments

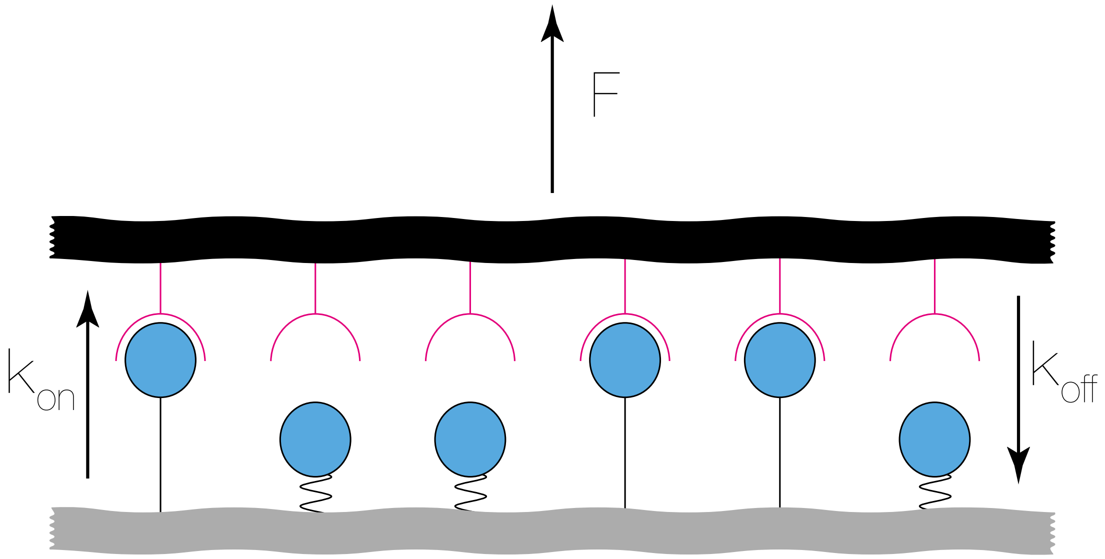

Figure 1.6: Separation of two surfaces connected by receptor/ligand pairs: Two opposing surfaces carrying adhesion receptor-ligand molecules. The upper surface is retracted by a force F. Pairs bind and unbind at rate coefficients $k_{\rm on}$ and $k_{\rm off}$.

with a *stiff transducer*, i.e. $\kappa_t \lesssim \kappa_b$ as

$$F^* \sim N_b(0)\,\bar{\mu} \quad \text{for } \bar{\mu} \lesssim 1 \tag{1.5}$$

$$\sim N_b(0)\,\ln(\bar{\mu}) \quad \text{for } \bar{\mu} \gtrsim 1 \tag{1.6}$$

with a loading parameter of $\bar{\mu} = \kappa_b r_0 v / k_B T k^0_{\rm off}$.

1.5.3 Leukocyte rolling adhesion

An example of the complex interplay between several adhesion receptors is found in leukocyte resting. Blood leukocytes flow through blood vessels at high velocities but during inflammation and immune surveillance they slow down on vascular surfaces. This is a multi-step process where different ligands with different bond properties are important, see Fig. 1.7. First the cell slows down by a factor of 100 through adhesion molecule pairs belonging to the selectin family. The receptors are present on long membrane tethers [72] on the leukocyte and responsible for the initial slow-down and subsequent rolling. The complete stop, which is necessary for the exit of the cell is then mediated by integrin receptors which became activated during rolling. The selectin bonds have a high dissociation constant $k_{\rm off}$ [73] but can resist forces up 165 pN [74]. In contrast, integrins resist lower forces but are required for the stable adhesion step. It was shown that selectins can slow down the cell but they are unable to stop them entirely. In contrast, integrins alone mediate firm adhesion only, if the cells are slowed down before by selectins [75]. This shows that the strength of binding combined with force-dependent rate constants and the cooperation between different adhesion molecule families is tailored to solve one of the most complicated adhesion events.

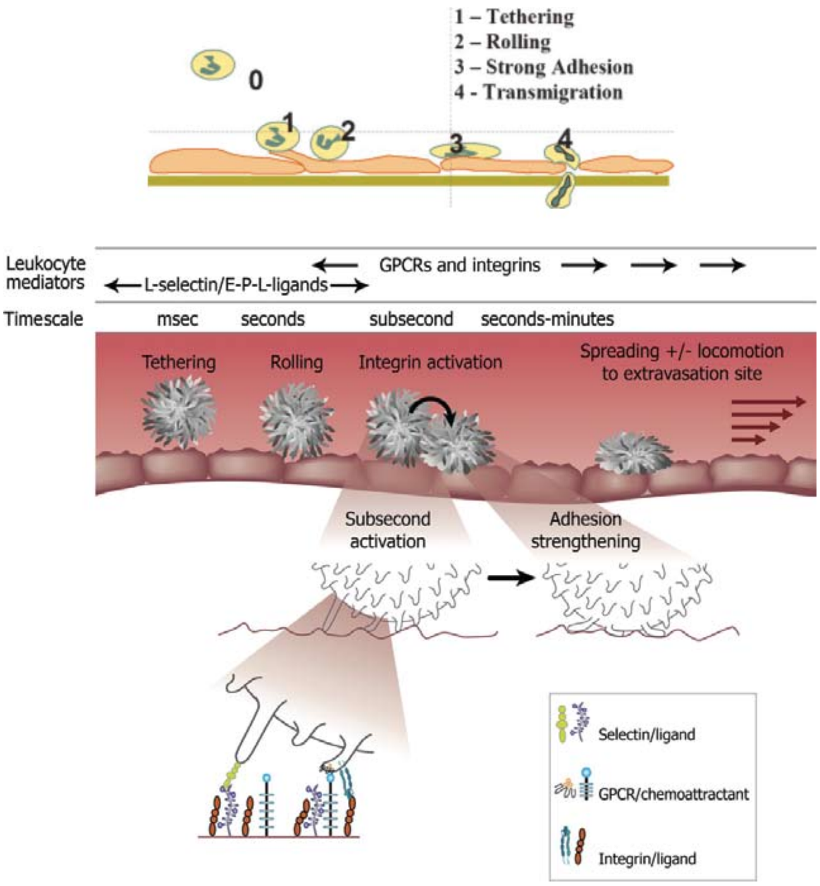
1 – Tethering
2 – Rolling
3 – Strong Adhesion
4 - Transmigration
0
1
2
3
4
Leukocyte mediators
GPCRs and integrins
L-selectin/E-P-L-ligands
Timescale
msec
seconds
subsecond
seconds-minutes
Tethering
Rolling
Integrin activation
Spreading +/- locomotion to extravasation site
Subsecond activation
Adhesion strengthening
Selectin/ligand
GPCR/chemoattractant
Integrin/ligand

Figure 1.7: Leukocyte arrest: Leukocytes patrol blood vessels and exit at sites of infection or tissue injury. First they are slowed down by membrane tethers having adhesion molecules belonging to the selectin family on their tip. After a short rolling phase, integrins become activated and firm adhesion which is followed by migration through the blood vessel is mediated. Adopted from [76] and [56].

Chapter

2

The Immunological Synapse

In the past ten years, advances in high-resolution imaging through confocal microscopy and sensitive cameras have led to the discovery of a specialized protein cluster arrangement called *Immunonological Synapse* or short Immune Synapse (IS) at the interface of T cell and Antigen Presenting Cell (APC) pairs [77–80]. Although the significance of this adhesion inducing structure is not precisely known, its detection has initiated major research efforts to reveal the function, dynamics and related molecular mechanisms of this protein aggregation. Little is known about the underlying biophysics of the IS. It is speculated, that forces play a vital role in activating T cells during T cell-APC adhesion [76]. Specifically, no studies have yet been performed to assess adhesion forces established during these encounters.

2.1 Adaptive immune system

The human body is protected by a genuine immune system, which identifies and eventually destroys infectious microorganisms after their invasion[81]. The immune system responds on several levels: once a foreign pathogen enters our body the first line of response is triggered through the *innate immune system* which is shared by all plants and animals. The innate immune reaction is immediate but non-specific. During evolution, jawed vertebrates developed a second line of defense known as *adaptive immune system.* Whenever microorganisms enter our body specialized cells called Antigen Presenting Cells (APCs) engulf and digest some of these intruders. The expression APC is used to label Dendritic Cells (DCs), B cells and (to some extent) macrophages. The expression originates from the fact that these cells process peptide sequences belonging to unwanted microorganisms and display those on their surfaces using carrier proteins called Major Histocompatibility Complex (MHC).

In a second step, an APC carrying the foreign peptide sequence needs to be detected and identified by a proper T cell. A highly sophisticated recombination scheme allows T cells to randomly generate a vast number of different antigen receptors employing only a small set of genes [82]. These TCRs are unique to each T cell and match exactly a certain foreign peptide sequence, termed *cognate peptide.* The uniqueness of TCRs is responsible for the specificity of the entire system.

T cells patrolling lymphoid and blood tissues scan APCs to determine whether they carry alien peptides on their MHCs. To this end, T cells establish adhesion with APCs and

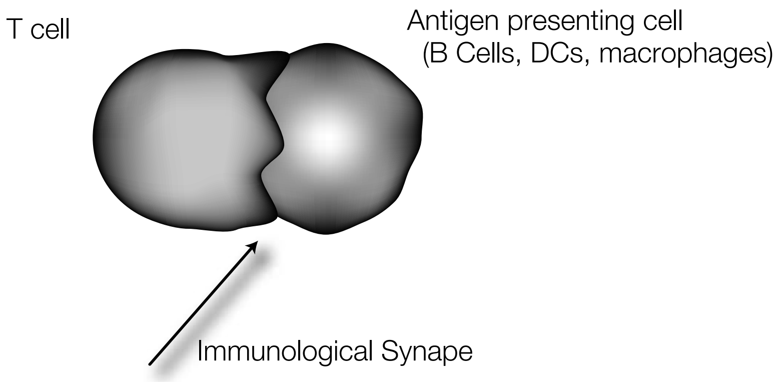

Figure 2.1: T cell-APC contact: A T cell encounters an antigen presenting cell and forms a stable bond to scan for pathogen peptides on the APC surface.

form cell-cell conjugates like in Fig. 2.1. Once a T cell's antigen-specific TCRs recognize cognate foreign peptide on the APC's surface a cascade of defense reactions, including proliferation and activation of other specialized immune cells, is triggered to combat and reverse the infectious microorganism invasion. E.g. macrophages and natural killer cells are activated and thus enabled to destroy intracellular pathogens. A simplified scheme of this combined immune effort is shown in Fig. 2.2. There we have depicted an APC, which carries peptide and another one which does not have foreign peptide on its MHCs. In this work, we will refer to these as **pulsed** and **unpulsed**, respectively, when we later speak about cells used in our experiments.

2.2 Immune synapse formation

During the late 1990's, scientists realized that spatially organized receptor-ligand patterns are established at the contact zone of T cell-APC conjugates [77–79], see Fig. 2.1. These patterns are collectively referred to as IS. The formation of the IS involves the coordinated translocation of two protein complexes: TCR and its ligand MHC, as well as the integrin Lymphocyte Function-associated Antigen-1 (LFA-1) and its ligand Intercellular Adhesion Molecule-1 (ICAM-1). This orchestrated reorganization of membrane proteins involves many cytoplasmic molecules and is presumably dominated by cytoskeletal factors like actin [83]. However, little is known about the biophysics of these cell conjugates and it is debated whether forces play a vital role in this process [76].

In Fig. 2.4 the development of this distinct protein arrangement is illustrated. First, molecules are randomly distributed. After initial contact, the two protein flavors start to separate laterally, through a self-assembly mechanism numerous TCR/MHC microdomains nucleate throughout the contact zone [84, 85]. After 30min active cytoskeletal transport processes create an immune synapse in its final state, termed *mature Immune Synapse* (Fig. 2.4(c)). In Fig. 2.3 a synapse is shown from the side at its final stage. Two Supramolecular Activation Clusters (SMACs) have formed: in the center of the contact zone TCR and MHC form a patch, called center or cSMAC. This cluster is embedded in a ring of LFA-1 and ICAM-1 proteins, forming the peripheral or short pSMAC.

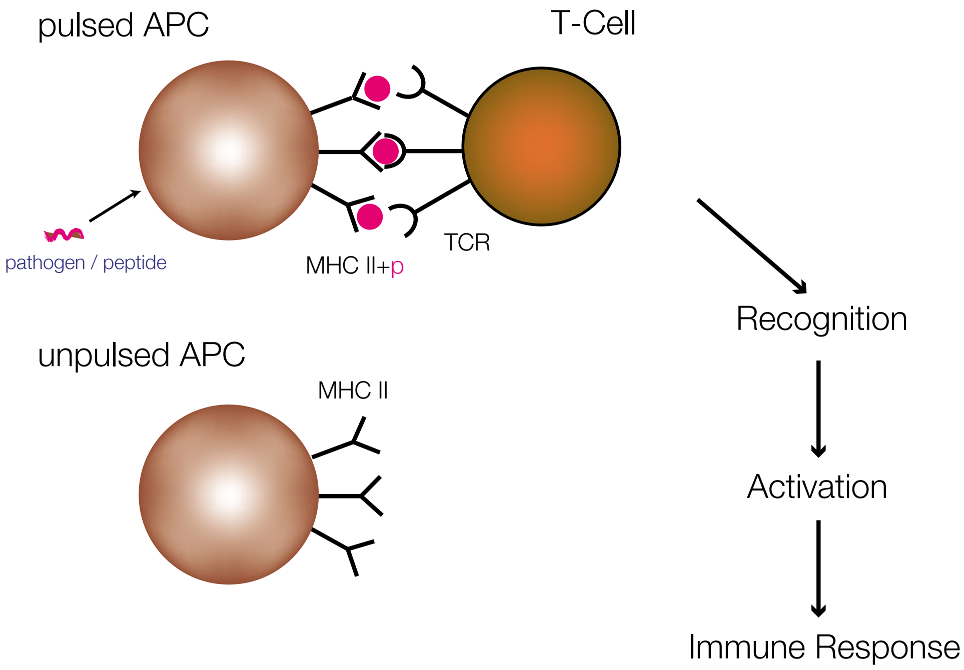
pulsed APC
T-Cell
pathogen / peptide
MHC II+p
TCR
Recognition
unpulsed APC
MHC II
Activation
Immune Response

Figure 2.2: Immune responses are triggered by Antigen Presenting Cell (APC) and T cell contacts. When a T cell with a specific T Cell Receptor (TCR) encounters an APC carrying the corresponding MHC, conjugates are formed, which last for a certain time. Afterwards the cells depart again, and in its aftermath this encounter will trigger an immune response within our body resulting e.g. in proliferation of T-Helper Cells.

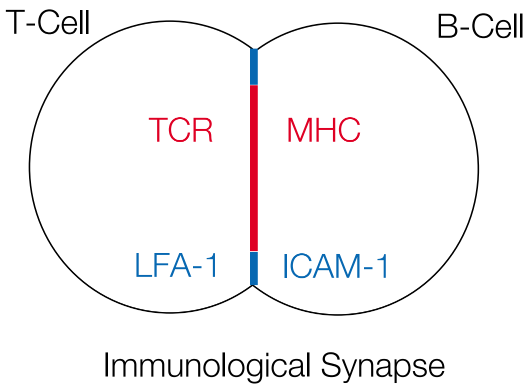
T-Cell
B-Cell
TCR
MHC
LFA-1
ICAM-1
Immunological Synapse

Figure 2.3: Side view of a mature immune synapse: TCR and MHC cluster in the central region, whereas LFA-1 and ICAM-1 aggregate at the periphery.

2.2.1 Sensitivity

The interaction between the TCR and a peptide loaded Major Histocompatibility Complex (pMHC) is one of the most-studied interactions in immunology, but no satisfactory answer has yet been given to elucidate the precise mechanism by which this system operates. E.g.,

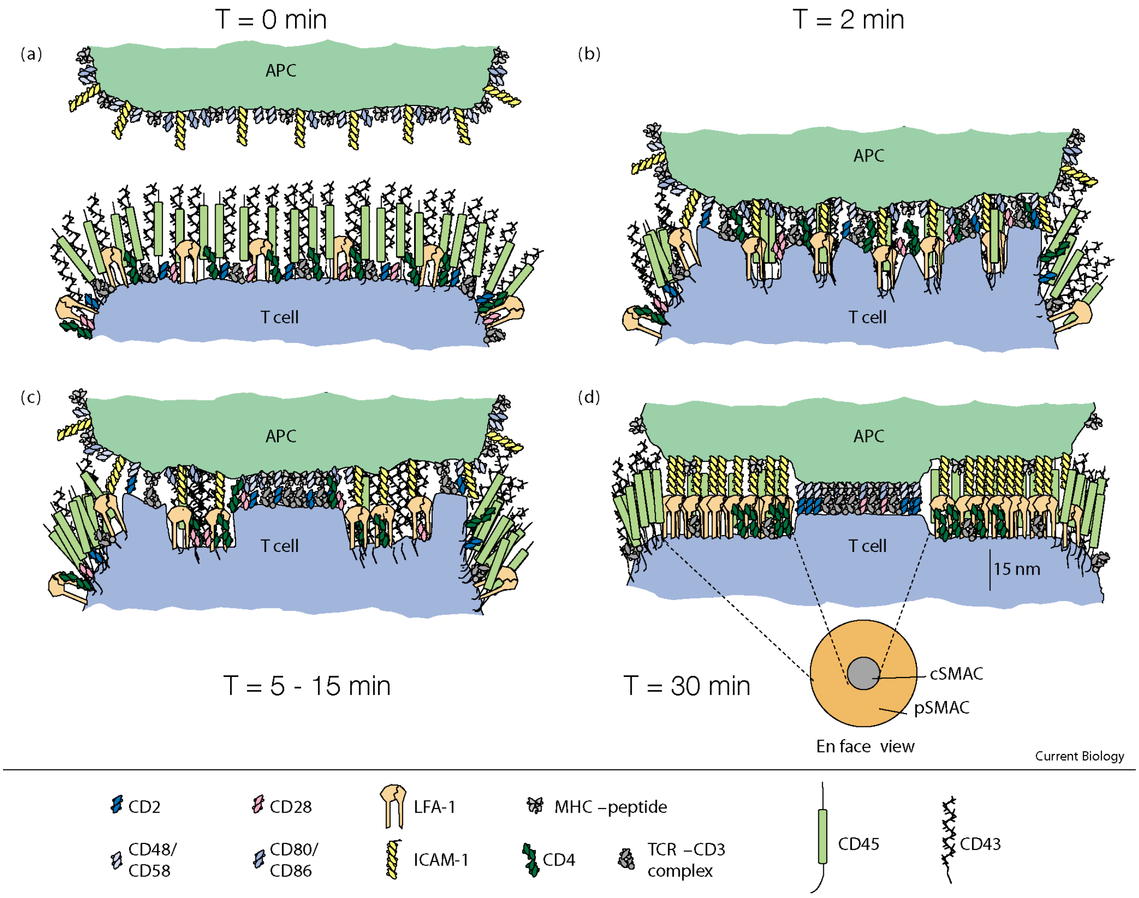
T = 0 min
T = 2 min
(a)
(b)
APC
T cell
(c)
(d)
15 nm
cSMAC
pSMAC
En face view
T = 5 - 15 min
T = 30 min
Current Biology
CD2
CD28
LFA-1
MHC –peptide
CD48/
CD58
CD80/
CD86
ICAM-1
CD4
TCR –CD3
complex
CD45
CD43

Figure 2.4: Formation of an immune synapse over time: (a) Before contact, surface proteins, either single or pre-clustered into lipid-raft domains, are randomly distributed over the cell surface. (b) After a few minutes lateral separation starts and large molecules (like CD43[1]) are pushed out of the interaction region. (c) Active cytoskeleton-directed reorganization gives rise to the cSMAC, which takes several minutes to develop. (d) After, 30min a mature synapse with the pSMAC and the cSMAC is observed: TCR and MHC cluster in the central region, whereas LFA-1 and ICAM-1 aggregate at the periphery. The separation distance in the center is around 15 nm whereas the periphery is separated by 40 nm. Note, that many additional proteins are involved in this translocation. Adapted from [84].

T cells are highly sensitive to antigen, but the exact number of pMHCs that are sufficient to fully activate T cells is still debated and depends on the T cell type [86, 87]. In some cases, the recognition process is extremely specific: changing the antigen sequence by a single amino-acid can inhibit the recognition process.

2.2.2 Thermodynamic segregation

Physically, the spatial patterns observed in T cell-APC conjugates have been attributed to differences in binding length: the recognition TCR/pMHC complex separates the membranes by about 15nm whereas the adhesion pair LFA-1/ICAM-1 is 40nm long, see Fig. 2.4. Through this differential binding lengths several studies have been able to model immune synapse formation *in silico* [85, 88–90]. The theory states, that if different receptor/ligand pairs are in close proximity to each other, the cell's membrane is locally deformed at an energetic cost. Thus, the concentration of recepor/ligand pairs with equal length is energetically favorable. Similarly, the mucin protein CD43 the most abundant membrane molecule on the surface of T cells, is excluded from the IS, which might be due to its large size [91, 92]. In our experiments, we use this fact to attach T cells to the AFM cantilever, cf. Sec. 9.2.

Although these simulations can account for some facets of immune synapse formation and help elucidating certain aspects of protein translocation they are not able to explain many details. E.g., energy minimization seems to be an obvious reason why CD43 is removed from the synapse region but fails to explain why other long proteins are not relocated [91]. From biological studies, it is evident that active transport by cytoskeletal elements cannot be ignored in immune synaptogenesis [83, 93] and CD43 exclusion has clearly been linked to proteins, which couple membrane molecules to the cytoskeleton [94, 95].

2.3 Significance

Although much is known about the structural features of the IS and its formation, the precise function remains illusive and is still debated [96]. Initially, when scientist were overwhelmed and fascinated by its discovery, it was viewed as a uniform activating structure for T cells. Today, however many contact modes and distinct molecular arrangements are known that further complicate this view [97]. Definitely, the IS plays a major role in adaptive immune response by acting as an information transfer structure [80, 84].

Chapter 3

Techniques for Measuring Forces in Living Cells

In 1944 Coman and its co-workers measured separation forces in healthy cell pairs from the lip and cell pairs which were extracted from lip carcinomas [98]. They found that the cancer cells were more loosely bound to each other than the healthy ones. Coman employed two microneedles: a stiff one was used to hold a cell and another flexible one served as force sensor which would bend when the two microneedles were moved in order to separate the two cells. Their simple techniques, which is shown in Fig. 3.1, still resembles the principal investigation method of today's force measurement in cell separation assays: a stiff element is used to hold one cell, while another spring-like element deflects under the applied forces such that by Hooke's law separation forces can be acquired.

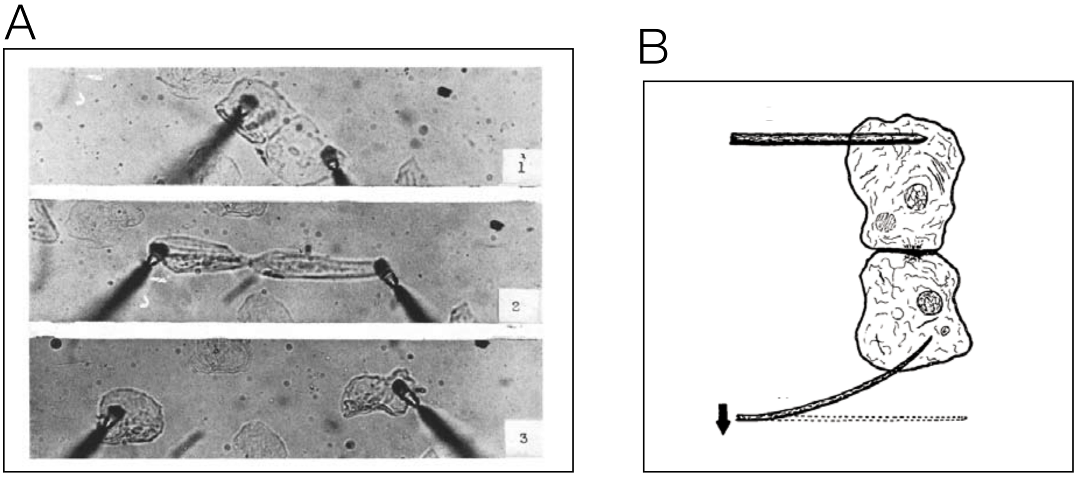

Figure 3.1: First cell-cell separation force measurements performed by Coman and co-workers in 1944. (A) Microscope photographs from an early cell separation experiment. (B) Schematic view of this simple technique: two microneedles are injected into the cells, one of which deflects under force. Adapted from [98] and [99].

In this chapter we will introduce several modern biophysical techniques which are currently employed to investigate cell adhesion processes as well as physical properties of cells.

3.1 Micropipette aspiration

History

The micropipette aspiration technique can be traced back to Mitchison and Swann, who invented their so-called *Cell Elastimer* in 1954 to probe the mechanical properties of the cell surface [100], [101]. They used a simple system depicted in Fig. 3.2: A glass micropipette was immersed into sea-water and connected to a reservoir using a rubber band. The micropipette was then placed close to a sea urchin egg inside the chamber with the help of a micromanipulator. A micrometer screw below the reservoir could be lowered to generate a small suction within the micropipette drawing the egg to the end of the pipette, see Fig. 3.3. The deformation of the cell was then measured as a function of hydrostatic suction and used to compare the internal pressure and the elastic modulus of the membrane of fertilized and unfertilized sea urchin eggs.

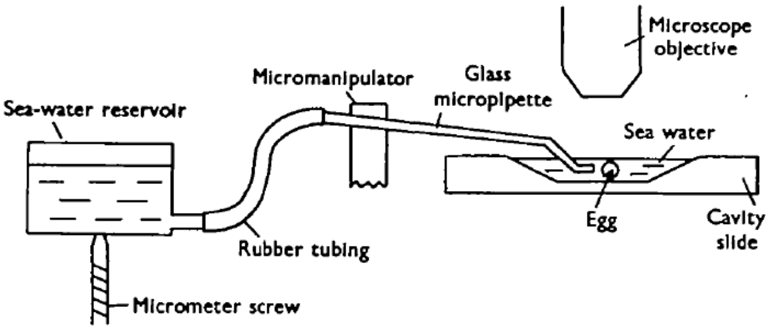

Figure 3.2: General schematic of Mitchison's and Swann's cell elastimer of 1954, which shows basically the same principle as micropipette setups today. A liquid reservoir (sea water in this case) is connected to a hollow glass pipette. The micropipette itself is immersed in an experimental cavity and can be positioned close to a cell using a micromanipulator. Changes in the reservoir level induced by a micrometer screw yield pressure changes inside the micropipette by which the cell can be aspirated into the tube. The deformation or degree of suction can be studied under a microscope as a function of suction pressure and with the help of basic continuum models values for the cell's elastic and viscous properties can be deduced. Adapted from [100].

Probing cellular mechanics

In the subsequent decades this pioneering work was followed by a steady improvement of this technique in several laboratories. Fundamentally, these experiments share three basic elements already present in the 1954 apparatus: micropipettes (hollow glass tubes filled with liquid and immersed in the experimental chamber), micromanipulators (controlling the position of the micropipettes) and manometers (controlling the pressure inside the micropipette). The readout in these setups is the response of the cell to the suction ΔP, measured by the extension of the cell surface into the micropipette L_p, usually normalized by the pipette radius L_p/R_p. In Fig. 3.3 an aspirated cell is shown. Analyzing micropipette aspiration experiments can be a difficult task and sophisticated solutions to describe the cell's deformation during suction were proposed [102, 103]. To start with a very simple approximation let us assume, that a cell behave like a liquid drop. Applying Laplace's law for a drop with constant cortical tension T_c aspirated by a suction pressure of ΔP yields [104]

$$\Delta P = 2\,\tau_c(\frac{1}{x} - \frac{1}{R_c}) \tag{3.1}$$

where τ_c is the cortical tension of the cell, x the radius of the aspirated part and R_c the radius of the cell outside the pipette, see Fig. 3.3. In the case of a hemispherical bulge, meaning that the aspirated cell radius equals the pipette radius ($L_p = R_p$), Eq. 3.1 reads as

$$\begin{align} \Delta P &= 2\,\tau_c(\frac{1}{x} - \frac{1}{R_c}) \tag{3.2} \\ &= 2\,\tau_c(\frac{2\,L_p}{R_p^2 + L_p^2} - \frac{1}{R_p\,R_c}) \notag \\ &= 2\,\tau_c(\frac{1}{R_p} - \frac{1}{R_c}) \tag{3.3} \\ &= \Delta P_c \notag \end{align}$$

since $x^2 = R_p^2 + (x - L_p^2)^2 \Rightarrow x = \frac{1}{2}\frac{R_p^2}{L_p} + \frac{1}{2}L_p$. ΔP_c is called the critical pressure. Cells that behave as liquid drops will freely flow into the pipette if the suction pressure is increased beyond ΔP_c. This way, Evans and Yeung showed that *neutrophil granulocytes* (the most abundant type of white blood cells in humans) behave very much like drops of liquid with a cortical tension of 30 $pN/\mu m$ and a viscosity of around 100 Pa s [105]. In this sense, the micropipette aspiration technique is unique because it can determine whether a certain cell type can behaves like a liquid drop or not.

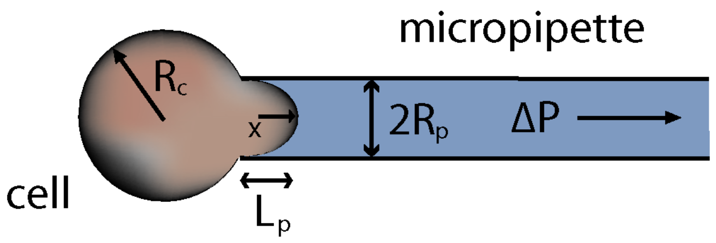

Figure 3.3: Micropipette aspiration technique: A single cell is sucked into a glass tube and deforms under pressure ΔP. R_c is the radius of the cell outside the tube, x the radius of aspirated cell part, L_p the extension length of the surface into the pipette and R_p is the radius of the micropipette.

Cell adhesion assays

Invented as a single cell apparatus to probe the elastic properties of cells the technique was later enhanced with a second pipette to quantify cell adhesion strength [106]. Nowadays, dual micropipette aspiration assays allow for various experimental setups to quantify cell adhesion strength. In Fig. 3.4 three major dual micropipette techniques to measure cell adhesion forces are displayed. In the following paragraphs we will give a short introduction to each of the techniques.

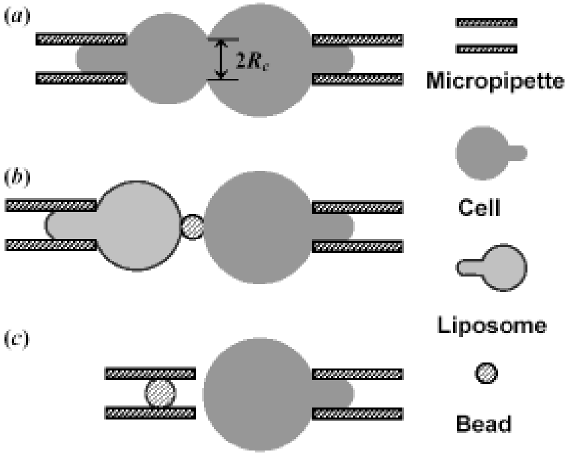

Figure 3.4: Schematic representations of three micropipette-based techniques for quantifying cell-adhesion forces: a) the step-pressure technique, b) the biomembrane force probe, and c) the micropipette-aspiration technique. R_c is the radius of the conjugation interface. All the cells on the right can be replaced with another type of object such as a bead or a flat substrate. Adapted from [106]

Step Pressure Technique (SPT) In Fig. 3.5 and Fig. 3.4a) the procedure of the step pressure technique is displayed. Using two similar micropipettes two cells are brought into close contact by micromanipulators attached to the pipettes. While one of the cells is held by a large suction pressure, the other one is more loosely bound. The two micropipette are positioned at close proximity to each other with micromanipulators such that the cells can form an interface and are allowed to adhere to each other. After a certain time span the micropipette with the smaller suction is pulled away. If the suction pressure was high enough the cells will be separated. If not, the cells will stick together and the micropipette has to re-approach the cell. In this case the suction pressure is increased *stepwise* and the experiment is repeated until cells are detached. The smallest suction pressure required for separation is referred to as the critical separation pressure. Sung et al. pioneered this field in the early 1980s and measured the junction avidity of heterodimeric cell conjugates formed by cytolytic T cells and their target cells to be 6 to 13 times higher than their homodimeric counterparts [107]. Sylvie Dufour et. al. also used the SPT to measure the adhesion strength in cadherin-dependent cell-cell adhesion [108], see Fig. 3.5. Cadherins are transmembrane proteins which play a crucial role in homodimeric cell adhesion, see Chapter 1. In this study they observed that the separation forces between cells increased with the duration of contact and with cadherin levels. Later, the same laboratory investigated how nectins, immunoglobulin-like adhesion molecules involved in cell-cell adhesion, affect the interaction strength of cell doublets [30].

Bio-membrane Force Probe (BFP) While the SPT method yields forces in the order of nN for separating two cells, micropipettes can also be used to measure much smaller

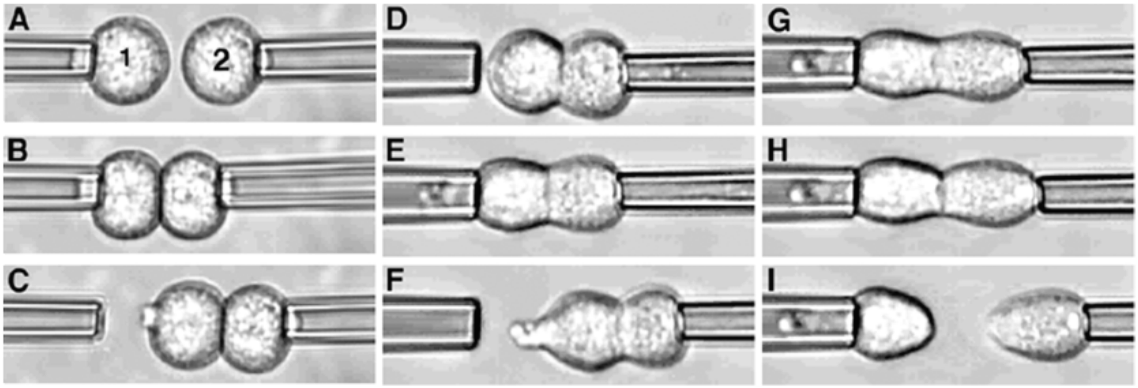

Figure 3.5: Step pressure technique using a dual micropipette aspiration assay: Two cells in suspension (A) are held under weak aspiration by micropipettes, and brought into contact (B). The formation of contact is checked (C) after displacement of the right pipette and the other cell is held by the micropipette with a stronger suction pressure (D). The first cell is held by the micropipette and the suction applied is increased while the right micropipette is displaced (E-I), step by step, until the adherent cells are separated (I). The critical pressure P_c for which cell separation occurs is correlated to the separation force. Note how the cells are deformed inside the pipettes. Adapted from [108]

interaction forces, e.g. the strength of non-covalent bonds, which are in the order of 10-100 pN. Evans and co-workers developed the BFP [109] which is an ultra-sensitive technique to probe adhesion on biological interfaces, like a cell's membrane. Its experimental principle is illustrated in Fig. 3.4b: a pressurized membrane capsule (left) is aspirated by one of the micropipettes and serves as force transducer. The membrane capsule could be a red blood cells or a synthetic lipid bilayer vesicle (liposome). Using a glue which sticks to the membrane capsule but not to the probe's interface, a microbead (Fig. 3.4b) is attached to the membrane to create a surface probe. For adhesion receptors to be probed the bead is additionally coated sparsely with specific ligands. So, the micropipette together with the membrane capsule and its microbead form a force probe which is then approached to the test surface. In many biological applications the test surface simply is another cell immobilized by a second micropipette.

Now, the suction pressure ΔP precisely controls the membrane tension τ_m, which in turn defines the stiffness k_f of the transducer. Considering that ΔP can be controlled up to 0.1 pN/µm, probe displacements of a few nm are easily measured which means that forces as low as $10^{-13} N$ can be detected. A major advantage of this method is the wide range of forces which can be scanned. Since for fluid membrane behavior (e.g. lipid bilayers) Laplace's law is valid we might substitute the membrane capsule radius R_m for R_c in Eq. 3.4 and conclude that the biomembrane's surface tension reads as

$$\tau_m = \frac{\Delta P R_p}{2(1 - R_p/R_m)} \tag{3.4}$$

The spring constant of the force probe k_f can be calculated in first approximation as [109]:

$$k_f \approx \frac{2\,\pi\,\tau_M}{\ln(2R_m/R_p) + \ln(2R_m/r_b)} \tag{3.5}$$

where R_p and r_b are the micropipette radius and the circular radius of the adhesive contact between microbead and membrane capsule. By changing the suction pressure ΔP the spring constant k_f can be adjusted from $0.001 pN/\mu m$ to $10 pN/\mu m$. In [61], Merkel et. al. took advantage of this wide range tuning and explored the energy landscape of the prototype couple the molecules streptavidin and biotin. They probed this special bond over with loading rates over six orders of magnitude and measured de-adhesion forces between 5 pN and 170 pN, showing dramatically how receptor-ligand coupling forces depend on how fast bonds are detached.

Microbead-aspiration technique Another micropipette setup probing membrane tethers, which are formed during cell adhesion, is shown in Fig. 3.4c. A well fitted microbead is placed into a micropipette, another micropipette is used to hold a cell. The microbead is coated with antibodies and serves as a force transducer. The bead movement within the pipette is controlled precisely by the suction pressure ΔP. Initially the bead is moved towards the cell and upon contact it is retracted and a tether is extracted from the cell. Measuring the retraction speed of the bead the pulling force for tether extraction can be calculated, see [110–112].

3.2 Optical tweezers

History

Already in 1619 Johannes Kepler[1] hypothesized in his book „*De cometis libelli tres*" that light could exert mechanical forces on particles. But it was not before 1970 that Arthur Ashkin at the Bell Laboratories [113] used radiation pressure produced by a continouus laser to create a stable optical potential, in which they could trap micron-sized dielectric spheres in suspension. The size d of these particles were in the so-called *Mie regime*, where $d \gg \lambda$, λ being the wavelength of the light, producing these optical traps, which are also commonly referred to as optical tweezers. At that time Ashkin speculated that it should be possible to trap even very small particles in the *Rayleigh regime*, $d \ll \lambda$, by stating that

> [..]*similar accelerations and trapping are possible with atoms and molecules using laser light tuned to specific optical transitions* [113].

In 1997 Steve Chu[2], Claude Cohen-Tannoudji and William Phillips were awarded the Nobel prize for the *development of methods to cool and trap atoms with laser light* [114–116].

Principle

Similar to magnetic tweezers discussed in Sec. 3.3, optical tweezers are employed to manipulate coated beads coupled to proteins [117, 118] or cells [119]. The way optical traps achieve control over beads is shown in Fig. 3.6. An object with higher diffractive index than its surrounding medium is illuminated by a beam of light.

---

[1] German mathematician, astronomer and astrologer, ⋆1571 - †1630

[2] Chu met Arthur Ashkin 1983 at Bell Labs who had tried to trap atoms there, but couldn't proceed with his studies due to funding cuts. Later, Chu became a professor of Physics at Stanford in 1987 and completed Ashkin's work there.

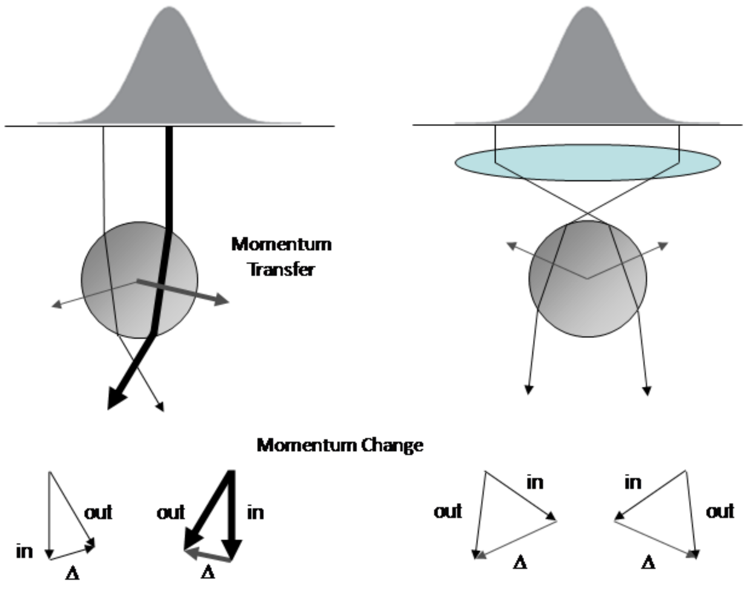

Figure 3.6: Illustration of optical tweezers. Light transfer creates an momentum which pulls the bead towards the center of the beam. Courtesy of Kai Uhrig.

The refraction of the rays by the object changes the momentum of the photons, proportional to the change in the direction from the input to the output rays. Due to the momentum conservation theorem, an equal, but opposite momentum must be transferred to the object. Two cases are illustrated in Fig. 3.6: On the left, there is a beam with a Gaussian profile and a bead with higher refractive index than the medium. The bead is placed slightly shifted to the left of the beams center. Photons hitting the bead on the left side are deflected to the right; the ones on the right side are deflected to the left. Due to the Gaussian profile of the beam, more photons are present in the center of the beam (right side of the bead), which is depicted by the thicker arrow in the sketch. So the resulting momentum transfer to the bead (grey arrows) will point to the center of the beam and downstream of the photon flux. To achieve stable 3D trapping, a focused light beam is necessary. This situation is shown in the right part of the drawing. The photons of a tightly focused beam will gain momentum in the downstream direction of the beam when diffracted by the object. This results in a net force on the bead towards the beams focus. The radial momentum components will cancel each other out if the bead is in the beams axis. Otherwise a force component to the beams central axis, according to the left drawing will result. Combining the two situations one can understand, that in a stable optical trap the forces on the object will always point to the place of the highest light intensity, i.e. the focus. Scattering forces on the object (not depicted here) will shift this stable trapping point downstream from the focus. Since the momentum of photons is very small, high light intensities and gradients are required. This is why laser light and high NA (numerical aperture) objectives are used in optical trapping.

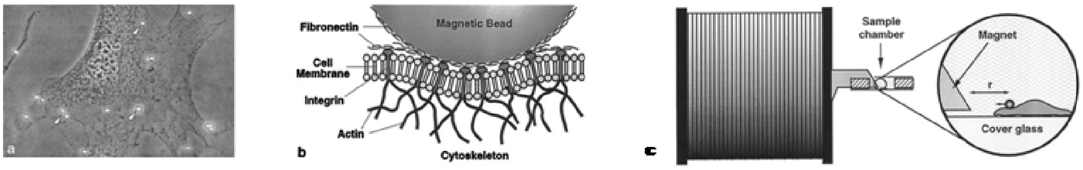

Figure 3.7: Magnetic Tweezers Setup: (a) Magnetic micro-sized beads distributed on a 3T3 fibroblast, which are coated with fibronectin (b) to ensure coupling to the cytoskeleton through integrins. (c) Schematic view of the magnetic tweezer central unit. The magnet has to be placed close to the cell to ensure high forces. Adapted from [125].

Applications in biophysics

The high sensitivity of optical traps ideally suits them to perform force measurements on the molecular level. Optical tweezers have been used extensively in the past to study motor proteins like kinesin [117], [120] and myosin [121]. An online search at pubmed.org yields more than 600 papers related to optical tweezers. On the other Hand, Optical Tweezers have successfully been used to trap viruses and small bacteria [122] and to stretch human red blood cells [123] but they are not a feasible choice for measuring forces on a cellular level. Even though an entire cell can be trapped, the applicable force range is quite low in nature, usually less than 200pN. E.g., Thoumine et. al. studied the study short-term binding of fibroblasts on fibronectin coated surface [124]. But they were not able to measure forces higher than a couple of 10 pN, which occur when cells are allowed to adhere longer than just a few seconds. There is, however, an optical method inspired by optical tweezers which is able to stretch entire cells. We will discuss this *optical stretcher* in the Sec. 3.4.

3.3 Magnetic tweezers

Magnetic tweezers are used to manipulate paramagnetic, ferromagnetic or ferrimagnetic beads on the cell surface. These magnetic beads are usually functionalized with proteins like fibronectin coupling to integrins, which in turn are connected to the cytoskeleton. Using a single or multiple magnet setup, these beads can either be pulled by the application of magnetic pulses in a gradient magnetic field $\vec{B}(t)$

$$\vec{F} = (\vec{m}\vec{\nabla})\vec{B}$$

or be twisted to gain a oscillating torque in a twisting field $B_z = |B|\hat{e_z}\cos\phi(t)$, see Fig. 3.7. Sackmann et. al. used the gradient field to measure local viscoelastic parameters, like the shear elastic modulus and the effective viscosity by analyzing the creep response of the beads in terms of mechanical equivalent circuits [125, 126]. In these experiments a constant force is applied to the beads by the external field $\vec{B}$ and their displacement is observed by simple particle tracking. In the case of oscillating fields the technique is usually referred to as *magnetic twisting cytometry.* The beads are rotated back and forth and the amount of bead rotation and their relaxation is measured by magnetometers to gain insight in the mechanism of frictional energy loss and elastic energy storage in living cells [127, 128].

Recent development in this field has resulted in the successful application of magnetic tweezer in measuring cell-substrate unbinding forces and the nanomanipulation of bead inside cells [129, 130].

3.4 The Optical Stretcher

Jochen Guck et. al. invented a device (Fig. 3.8) capable of deforming living cells by two counterpropagating divergent laser beams [131]. With this label-free setup they could measure a cell's elasticity without high power absorption since the to beams need not be focused on the cell. The basic principle is based on one-beam gradient traps discussed in Sec. 3.2.

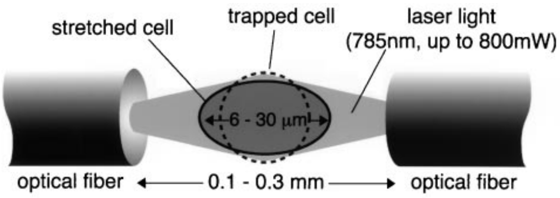

Figure 3.8: Scheme of the optical stretcher device. A cell in suspension is trapped and then stretched by two counterpropagating divergent laser beams emitted through optical fibers. The degree to which a cell is stretched can be correlated to its elasticity and this in turn to a malignant state. Using a flow perpendicular two the beam axis, cells can be trapped and stretched in a high-throughput fashion. Adapted from [131].

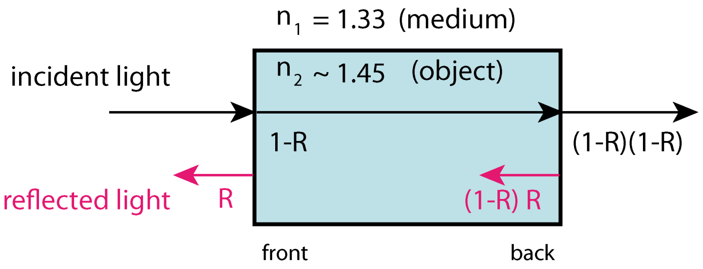

Figure 3.9: Momentum transfer on a dielectric object due to an incident laser beam. A fraction R = 0.2% is reflected on the interface of medium and object. When the light beam leaves the object a fraction of R is again reflected back. By summation of all terms a scattering force can be calculated which cannot be neglected for small objects and high beam power.

Consider a cubic object resembling a cell with a refractive index n_2 which is larger than the refractive index n_1 of its surrounding medium (see Fig. 3.9). At the medium-object interface the fraction $R \approx 0.2\%$ of a laser beam with an incidence angle of $\alpha = 0$, which in turn means that the portion $(1 - R)$ of the original beam keeps on travelling after entering the object. Upon leaving the object another beam fraction R is reflected on the second interface. Since the lasers employed in these kind of experiments have wavelengths of $\lambda \approx 780$ nm, which is significantly smaller than the radius of the cell, $R \approx 10\mu m$, it is feasible to use ray optics to calculate momentum transfers. Thus, we can assume that the momentum of the incident ray inside the object is given by

$$p_2 = n_2\, E/c \tag{3.6}$$

according to Minkowski[3][133], [134]. Considering that momentum is conserved, the forces exerted on the front and back-side of the cubic object in Fig. 3.9 are given by

$$F_{front} = [n_1 - (1-R)n_2 + Rn_1]\ P/c \tag{3.7}$$

$$F_{back} = -\,[n_2 - (1-R)n_1 + Rn_2]\,(1-R)\,P/c \tag{3.8}$$

where P is the power of the laser beam. Note that the forces point away from each other and so a value of $500mW$ for the laser power P will yield a total force value of $F_{total} \approx 20pN$. This *scattering force* acts on the center of mass of the object and is 10 times lower than F_{front} and F_{back}. If a second beam is incident from the opposite side of the object (see. Fig. 3.8.), the total force upon the center of mass will vanish $F_{total} = 0$. However, the forces exerted on the front and on the back surfaces of the object will add up and hence equal

$$F_{surface} = F_{front} + F_{back} \approx 400pN. \tag{3.9}$$

Therefore, contrary to intuition, an elastic object like a cell will be *stretched* rather than *compressed* in a double laser trap like in Fig. 3.8. A Young's modulus of $E = 100N/m$ will thus yield a deformation of $\Delta l = l\sigma/E \approx 400nm$ considering that $\sigma \approx 400pN/(10\mu m)^2$ for a cell having a radius of roughly $10\mu m^2$. Combined, these divergent laser beams will act as a trap since a displacement from laser axis breaks the symmetry of the force distribution and, thus, result in a net restoring force perpendicular to the axis.

Guck et. al. integrated their optical stretching/trapping setup later into an microfluidic device, where a high number of cells could be passed between the two laser beams, turning the machine effectively into a high-throughput setup [135]. This way many cells per minute can be screened for optical deformability which is a relatively high number compared to other techniques. In [135] Guck et. al. were able to show that the optical stretcher can be used

- to sort cells, since different cell lines will have different optical deformability
- to distinguish between normal, cancerous and metastatic cells, since their elasticity and hence their optical deformability would increase, respectively

The ultimate goal is to turn this device into a label-free, high-throughput cell analysis method for cancer diagnosis and stem cell sorting.

---

[3] The question how much momentum a beam of light transfers to a material with a refractive index of n through which it passes is being debated for a century now. Hermann Minkowski published a paper in 1908 saying that the reduced speed of light c/n in media leads to a higher momentum of $p = nE/c$. In a rivaling paper Max Abraham postulated a year later that $p = E/(nc)$, since $E = mc^2$ and thus $p = E/c^2\, c/n$. Although these momenta differ by a factor of n^2 no experiment could proof any of two assumptions definitely and it seems as if the two assumptions hold in the case of light viewed as wave or as particles, respectively [132]. Since our object is significantly larger than the beam and we do not include interference effects it seems to be fair to use the Minkowski momentum.

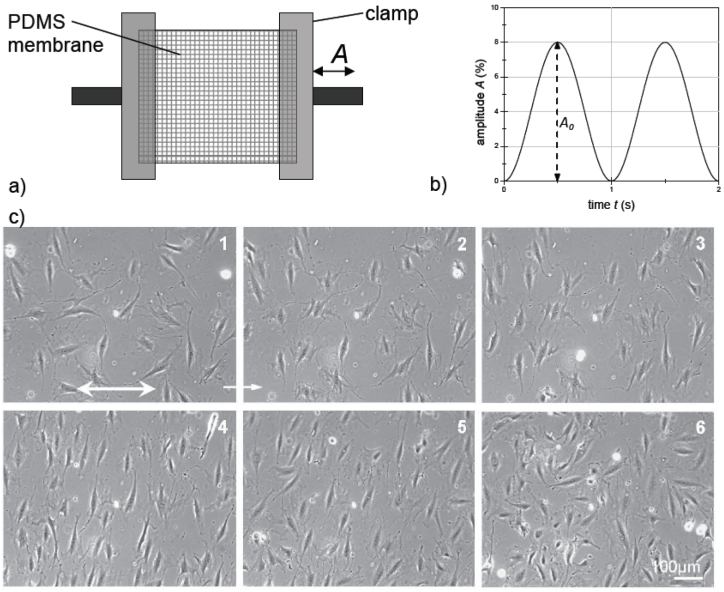

Figure 3.10: Uniaxial substrate stretching device. A PDMS membrane is uniaxially strecthed by attached step-motors. Cells placed on that substrate adapt to the external stress. Adapted from [136]

3.5 Substrate Stretcher

We will briefly introduce a machine, which does not measure mechanical properties of cells, but rather induces mechanical strain upon a large number of cells. Here, a flat elastomeric membrane which serves as cell culture substrate is periodically stretched with the help of two brushless servo motors, see Fig. 3.10. The membrane is made of Poly(dimethylsiloxane) (PDMS) and has usually an elastic modulus of about 1 MPa. The setup used by Jungbauer et. al. in our lab [136] is a uniaxial device, i.e. the substrate can be stretched in one direction. $A(t)$ is the substrate's elongation in the stretching direction and is given by the simple relation

$$A(t) = A_0\,(1 + \sin 2\pi\nu\, t)/2,$$

where A_0 is the maximal amplitude and ν the frequency of the applied strain.

The setup can either be used to quantify the effect of mechanical stress on gene expression [137], [138] and stem cell differention [139]. Also, if the device is placed under a microscope, reorientation and adaption of the cells due to the applied stress can be measured quantitatively. Jungbauer et. al. showed that the mean cell orientation of rat embryonic and human fibroblast changes exponentially with characteristic time of 1-5 hours, depending on the frequency with which the strain was applied [136].

Part II

Experimental Measurement Techniques

Chapter

4

The Cell Stretcher and its Applications

The so-called *uni-axial cell stretcher* is a microplate-based single-cell manipulation system. This technique is fairly new and was introduced in the late 1990's by Olivier Thoumine and Albrecht Ott [140]. Microplates are thin glass needles pulled from rectangular borosilicate bars. Two of these microplates are implemented in each setup: a rigid one holding the cell, and a flexible one serving as force sensor[1].

4.1 Introduction

In Fig. 4.1 the technique's principle is shown: A cell is placed between the two microplates of which the rigid one can be moved along the x-axis of the system using a Piezo actuator. The flexible microplate will bend under the exerted force and by Hooke's law its position can be correlated to the force: $F = -k\,\Delta x$, where k is the force constant of the flexible microplate. The bending of the flexible plate is measured using an optical fiber attached to its backside, see Fig. 4.1, and a photo-sensitive quadrant diode. We will discuss this in more detail in Sec. 4.3. The technique has been steadily enhanced over the past decade to facilitate experiments. In this work, our setup was improved to measure fluorescence and was employed to measure cell separation forces for the first time. Also, the requirement to employ optical fibers in force measurements was removed.

Relevant studies

The technique has been established over the past decade by relevant physiological studies relating malignancy to physical properties of cells [123, 141] and biophysical advances on the other hand [142–144]. In an outstanding publication from Prof. Spatz's Lab, A. Micoulet could measure that Sphingosylphosphorylcholine (SPC), a naturally occurring bioactive lipid, induces a perinuclear reorganization of intact keratin filaments and this, in turn, increases cellular elasticity [141]. Since SPC blood levels of patients with ovarian cancer are higher than normal it is reasonable to assume that this reorganization may facilitate biological phenomena that require a high degree of elasticity. Thus, this mechanism might allow cells to squeeze through membranous pores during metastasis. See [145] for a comprehensive report.

---

[1] In this section when talking about a flexible microplate we refer to a microplate which force constant is such that it will bend under forces exerted by single cells on a micrometer scale. Single cell forces are in the range of nano-Newtons, so force constants are in the order of 0.01 N/m = 10 nN/µm.

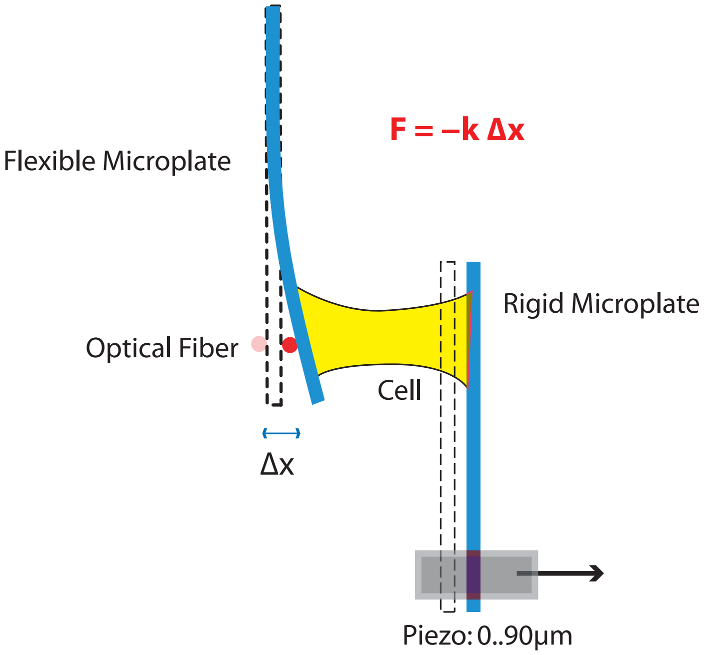
Flexible Microplate
F = −k Δx
Rigid Microplate
Optical Fiber
Cell
Δx
Piezo: 0..90µm

Figure 4.1: The cell stretcher device: A living cell is placed between two glass microplates of which one is rigid (right) and the other is so flexible that it will bend under forces applied by a single cell. The rigid microplate can be moved by a piezo actuator and the deflection Δx of the flexible cantilever, measured by an optical fiber, is used to calculate the applied force using Hooke's law: $F = -k\,\Delta x$. The microplates can be functionalized individually to provide adhesive surfaces to the cell.

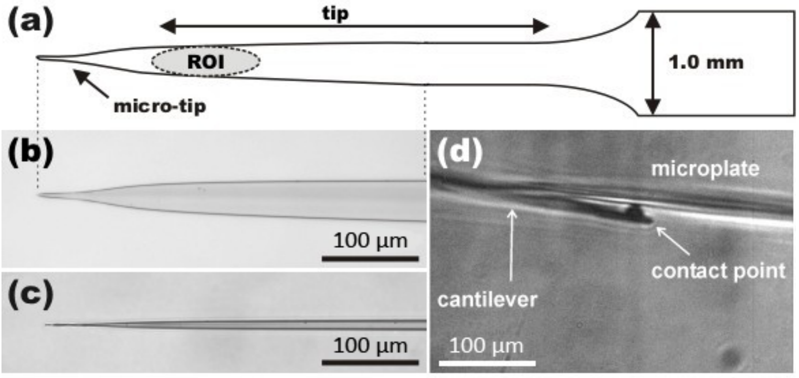
(a)
tip
ROI
micro-tip
1.0 mm
(b)
100 µm
(c)
100 µm
(d)
microplate
contact point
cantilever
100 µm

Figure 4.2: (a) Schematic representation of a microplate; tip and region of where cell adhesion takes place (ROI) are indicated. (b) & (c) top and side view of a microplate, respectively; (d) Calibration of a flexible microplate with an AFM cantilever of known stiffness. The cantilever contacts the microplate at the cantilever ROI. Adapted from [145].

4.2 Experimental setup

The setup used in this work has been described exhaustively in [146]. The device is home-made and was built from scratch in our lab. In Fig. 4.1 the basic principle of the uni-axial cell stretcher is shown. Two microplates (Fig. 4.2), one rigid the other one flexible, are fixed to separate microplate holder and dipped into the liquid container where the cells with medium are located and experiments are performed, see Fig. 4.4. The microplate holders are attached to a micromanpulation system and placed on a metal solid block to reduce thermal vibrations. The holders and thus the microplates can be positioned by optimized micrometer stages (Physik Instrumente, Karlsruhe, Germany) in the x-y plane. Their z-position can be controlled quite accurately by a rotating wheel fixed to the solid block. Additionally, the block holding the rigid microplate can be translated 90 μm with a piezo element attached to the micrometer stage. The manual microscrews are used to position the microplates initially, the piezo actuator to perform experiments. The entire system is mounted on an AxioVert 135 upright microscope (Zeiss AG, Göttingen, Germany) which is placed inside an experimental chamber made of styrodur and plexiglas at the front side to ensure thermal insulation. The chamber itself is set-up on an anti-vibration table mounted on two piles of styrofoam to minimize environmental vibration. Inside the chamber the temperature is kept constant at 37° C by electric heat wires regulated by two temperature controls, which are connected to two separate thermometers inside the chamber. CO_2 level is kept at 5% by a home-made controller.

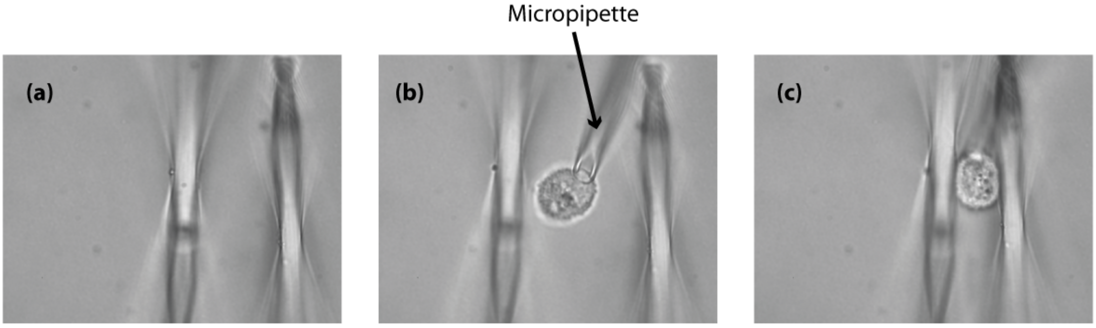

Figure 4.3: (a) Two microplates are positioned parallel to each other. (b) A cell which was previously captured by a micropipette on the bottom of the liquid container is placed between two microplates. (c) Once adhesion between the microplates and the cell is accomplished, the micropipette is retracted and force measurements can commence.

4.2.1 Experimental procedure

To perform single-cell experiments the liquid container is filled with cell medium and the microplates are positioned to be parallel, see Fig. 4.3. Cells are injected with a pipette close to the glass bottom of the liquid container. After cells have sedimented on the bottom, one can be captured with a micropipette and placed between the two microplates. After a certain time span the cell will adhere to the plates and the micropipette will be retracted slowly. This is a critical step and has to be performed with great care. After the micropipette is fully retracted, experiments can be performed.

4.2.2 Microplate production and calibration

Microplates were produced using a modified micropipette puller (P-2000, Sutter Instruments, USA). A 10cm long borosilicate ribbon is melted by a CO_2 laser and stretched to create two heterogeneous microplates: one rigid, the other one flexible. Flexible microplates were calibrated according to [146]. A Si_3N_4 AFM cantilever with a force constant of about $k_{\mathrm{AFM}} = 0.05$ N/m is placed under the microscope. The cantilever was previously calibrated at the AFM, cf. Subsec. 9.2.4. Using the piezo element, the microplate is moved against the cantilever which was fixed by a custom made holder[2]. Both, microplate and cantilever are deflected when pressed together. Plotting cantilever against microplate deflection will yield the flexible microplate's force constant k, since by Hooke's law

$$k \cdot d = k_{\mathrm{AFM}} \cdot d_{\mathrm{AFM}},$$

where d and d_{AFM} are the deflection of the flexible microplate and the AFM cantilever, respectively. Since this procedure is time-consuming microplates were only calibrated after successful experiments.

4.3 Enhanced experimental setup

4.3.1 Fluorescence

The setup described in [145] was enhanced by implementation of an Orca-AG CCD camera (C4742-80-12AG, Hamamatsu GmbH, Germany). The camera is cooled by a Peltier element resulting in low dark noise. The native resolution of 1344x1024 (1.37 million pixels) was usually reduced to 672x512 by 2x2 binning of the pixels since the optical resolution was limited by the microscope. This way, frame rate and sensitivity increased 4-fold, which is important for fluorescent applications.

A six position excitation filter wheel (Ludl Electronic Products Ltd., New York) was mounted to the back side of the microscope to filter the wavelength before it enters the microscope. A dual excitation filter set for GFP (470nm ± 20nm, excitation) and mCherry (572nm ± 18nm, excitation) was installed together with a X-Cite 120PC illumination system (EXFO Life Sciences, Canada) which uses a 120-watt metal halide lamp to deliver spectral excitation with a uniformly illuminated field of view.

4.3.2 Microplate detection

In our setup, the deflection of the flexible microplate was measured by tracking a 685nm laser light spot emitted through an optical fiber glued to the backside of the flexible cantilever [146]. The movement of the fiber was detected by a photo-sensitive quadrant diode. Unfortunately, using an optical fiber for force measurements has several drawbacks: Preparation of the optical fiber is fairly complex. Initially, a fiber without cladding material has a diameter of around 125µm which is too large since its rigidity will alter the flexible cantilever's force constant k. To ensure that the fiber will not interfere with

---

[2] Kindly prepared by Thomas Kriesche

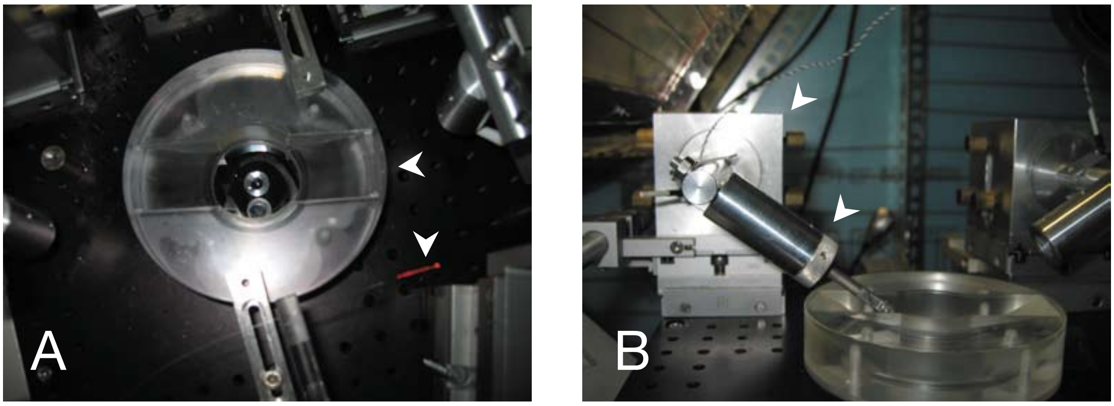

Figure 4.4: (a) Top view into the experiment chamber. Top white arrow denotes the liquid container where cells and medium are placed. Lower arrow depicts etched glass fiber with laser beam. (b) Top arrow: solid block holding microplate holder immersed in medium (lower arrow).

the measurements it has to be etched down to a diameter of around 6-8 µm. This is accomplished by dipping the glass fiber into hydrofluoric acid, which is a highly corrosive contact poison, hence, extremely dangerous to handle. Besides, the procedure is poorly reproducible since etching rates increase with lower diameters and, thus, a few seconds can result in diameters which are too small. Also, small impurities on the fiber can add up causing inhomogeneities which, in turn, result in poor light transmission, high-angle scattering at the glass-liquid interface and subsequently faulty position detection. After a fiber has been successfully etched down to an acceptable diameter and checked for effective light transmission it can be stored in water to be used in a later experiment. To this end it has to be glued to the backside of the flexible microplate introducing another difficult step: the thin optical fiber of 6-8 µm diameter has to be dipped into Polydimethylsiloxane (PDMS) for a few seconds and then be placed on the backside of the microplate pretty fast since the PDMS will cross-link and not glue anymore. Handling of the fibers was not easy since they would rip easily when put in and out of the experiment chamber. Moreover, an intact fiber can only be used once since PDMS residues prevent further experiments. In Fig. 4.4 the liquid chamber and an optical fiber before attachment are shown.

To overcome these problems, we evaluated the ORCA camera's image with an edge-detection algorithms. Hence, we could measure the microplate position quite accurately and avoid using an optical fiber, and thus facilitate experiments tremendously. We will discuss this in the following section.

4.3.3 Integrated LabVIEW control program

LabVIEW[3] (National Instruments, USA) is a platform and development environment for a visual programming language used for data acquisition, instrument control, and analysis and signal processing, in both, industrial and scientific applications. To control the entire setup a customized LabVIEW program was developed from scratch. In Fig. 4.5 the main window of the program is displayed. It was programmed to access the shutters of bright and fluorescence illumination, the filter wheel's position, the camera properties like shutter time and sensitivity and to control the position of the piezo and, hence, the position of the rigid microplate. Moreover, the control program can record time and z-stack images utilizing a 80µm pifoc (Physik Instrumente, Karlsruhe, Germany), on which the microscope objective was mounted. Integrating the experiment's entire control into one program with a user-friendly interface facilitated measurements. Finally, the position of the two microplates is detected now digitally evaluating the camera's image with built-in edge-detection algorithms from the NI-Vision package included in LabVIEW, see Fig. 4.5 (a) and (b). The force can thus be calculated in real-time and be displayed in the *force window*. Another window was used to show the distance of the two microplates. Using a feedback algorithm, which measures the deflection of the flexible cantilever and controls the piezo, it is possible perform measurements at constant force or constant deformation.

---

[3] LabVIEW is short for Laboratory Virtual Instrumentation Engineering Workbench

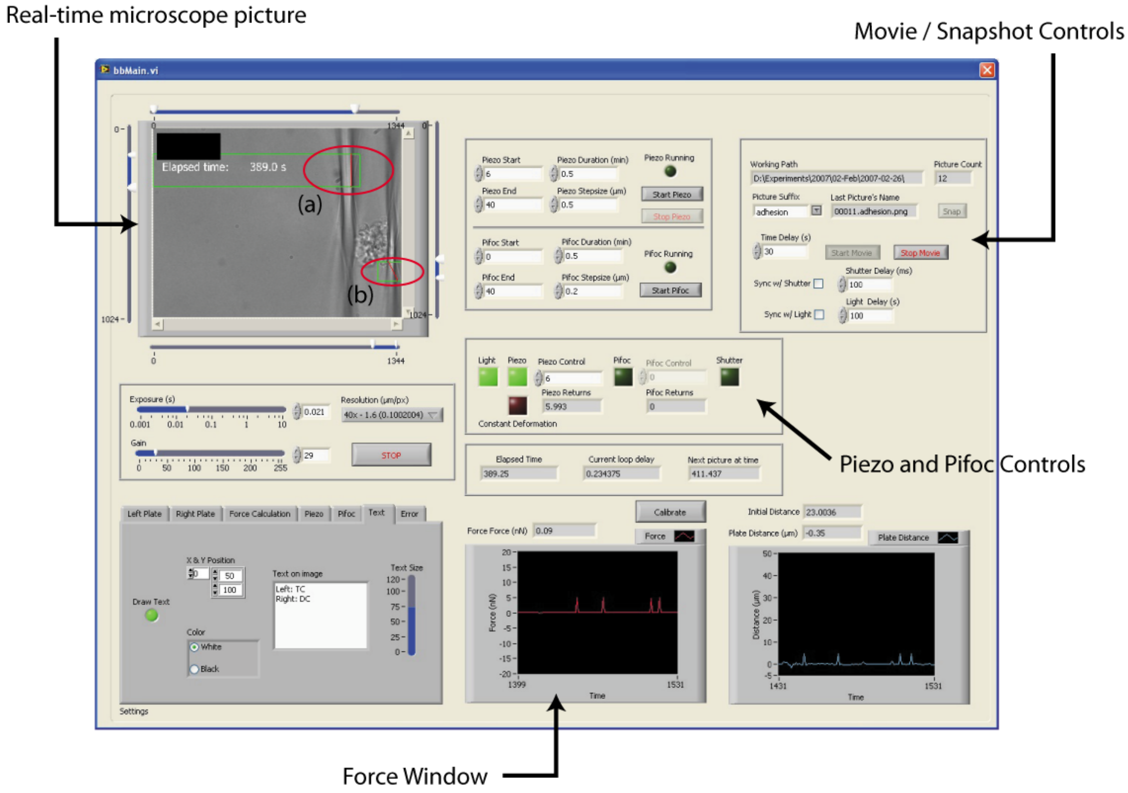
Real-time microscope picture
Movie / Snapshot Controls
Piezo and Pifoc Controls
Force Window

Elapsed time: 389.0 s
Piezo Start 6
Piezo Duration (min) 0.5
Piezo End 40
Piezo Stepsize (µm) 0.5
Pifoc Start 0
Pifoc Duration (min) 0.5
Pifoc End 40
Pifoc Stepsize (µm) 0.2
Working Path D:\Experiments\2007\02-Feb\2007-02-26\
Picture Count 12
Picture Suffix adhesion
Last Picture's Name 00011.adhesion.png
Time Delay (s) 30
Sync w/ Shutter ☐
Shutter Delay (ms) 100
Sync w/ Light ☐
Light Delay (s) 100
Exposure (s) 0.021
Resolution (µm/px) 40x - 1.6 (0.1002004)
Gain 29
Piezo Control 6
Pifoc Control 0
Piezo Returns 5.993
Pifoc Returns 0
Elapsed Time 389.25
Current loop delay 0.234375
Next picture at time 411.437
Force Force (nN) 0.09
Initial Distance 23.0036
Plate Distance (µm) -0.35
X & Y Position 0 50 100
Text on image
Left: TC
Right: DC
Color ● White ○ Black

bbMain.vi
(a)
(b)
0
1344
1024
Start Piezo
Stop Piezo
Piezo Running
Start Pifoc
Pifoc Running
Snap
Start Movie
Stop Movie
Light
Piezo
Pifoc
Shutter
Constant Deformation
0.001
0.01
0.1
1
10
0
50
100
150
200
255
STOP
Left Plate
Right Plate
Force Calculation
Piezo
Pifoc
Text
Error
Draw Text
Text Size
120
100
75
50
25
0
Settings
Calibrate
Force
Plate Distance
20
15
10
5
0
-5
-10
-15
-20
Force (nN)
1399
1531
Time
50
40
30
20
10
0
-5
Distance (µm)
1431
1531
Time

Figure 4.5: LabVIEW multi-functional control program.

4.4 Adhesion contrast

The cell stretcher is in an ideal tool to study cells that adhere to the ECM, like fibroblasts or epithelial cells. In order to study cells as physiological as possible it is necessary to embed them in their native environment, see Chapter 1. So, cell adhesion involves specific recognition events between individual cell-surface receptors and proteins in the environment of the cell.

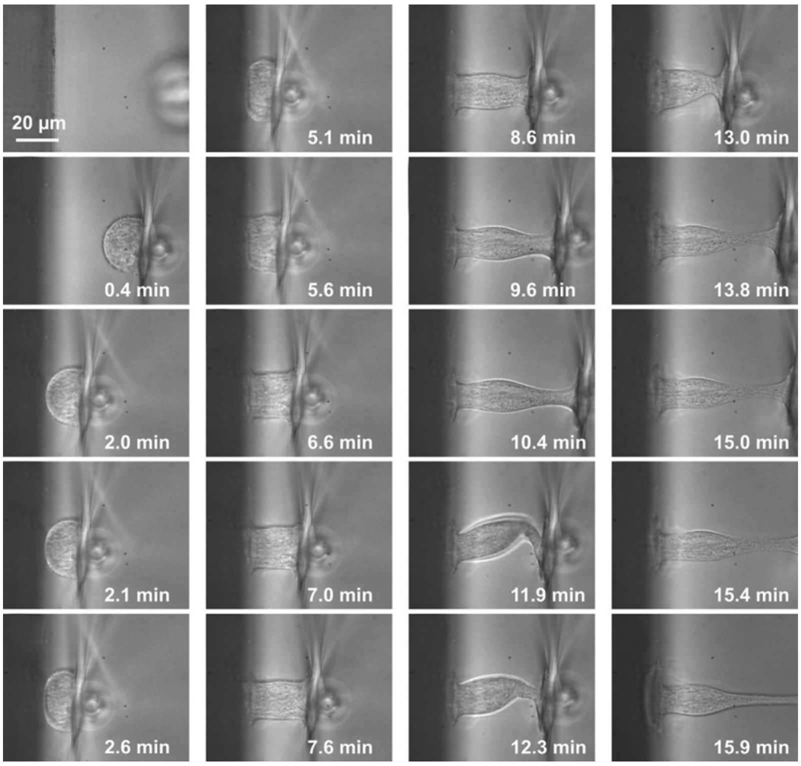

Figure 4.6: Time series of images of an cell stretching experiment: attachment of the cell to a microplate (b), cell compression after the contact with the borosilicate microplate (c)-(f), cell stretching (g)-(m), cell compression (n)-(p), cell stretching (q)-(t). Adapted from [147].

The ECM can be mimicked to a certain degree by functionalizing substrates, e.g. glass, with proteins extracted from the ECM, like fibronectin or its functional peptide RGD[4]. Another way to induce adhesion is by attaching the cell non-specifically to a surface. We will call such a non-specific binding *passive* adhesion, whereas an specific adhesion which is mediated through an ECM protein will be called *active*. Since the cell stretcher apparatus provides two different surfaces for cell adhesion, it is suited to measure effects of adhesion upon a single cell. We investigated the effect of active and passive coatings on the single cell level. In [147][5] we discussed an experiment shown in Fig. 4.6. A single cell is first attached through a passive coating to the right microplate. In this case, the microplate was first functionalized with amino-silane and subsequently with glutaraldehyde ($C_5H_8O_2$) to ensure adhesion of the cell to the microplate. One of its -CHO groups couples to the amino-silane, the other one to the cell's membrane proteins yielding a stable, covalent bond between cell and surface. The attached cell was then allowed to adhere to an active surface coated with fibronectin. The asymmetric surface adhesion, or adhesion contrast, induced an inhomogeneity in the subsequent cell stretcher experiment in Fig. 4.6. We employed a nonlinear elastic finite element method on tetrahedral grids to analyze this asymmetry which showed that the cytoplasm stiffness in the cell area attached to the fibronectin-coated microplate is significantly higher in comparison to the biologically neutral glutaraldehyde side [147].

---

[4] RGD is the main integrin binding motif of fibronectin and other ECM proteins.

[5] E. Gladilin and A. Micoulet and B. Hosseini and K. Rohr and J. Spatz and R. Eils, **3D Finite Element Analysis of Uniaxial Cell Stretching: From Image to Insight**, *Phys. Biol.*, 2007(4)

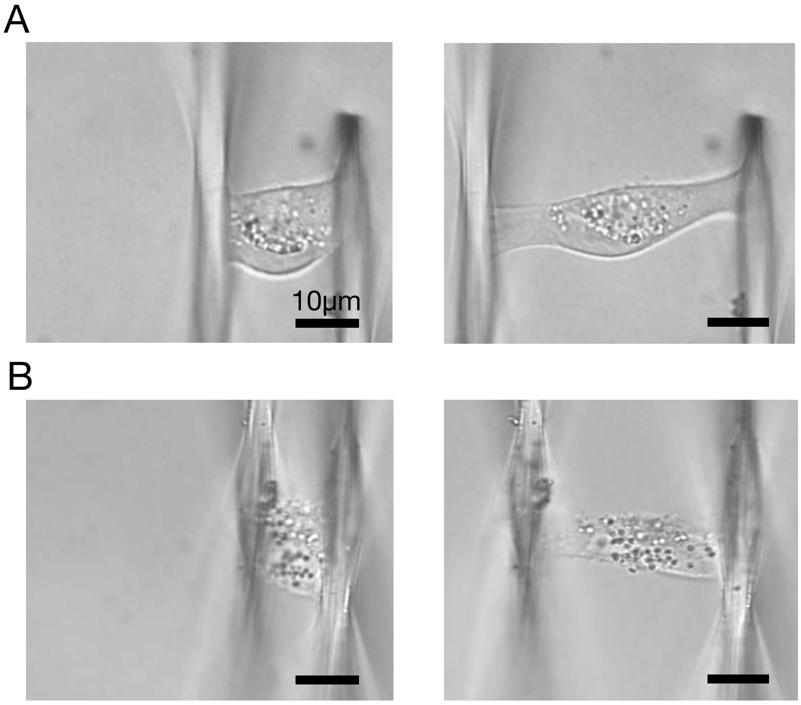

Figure 4.7: Passive vs. active functionalization of microplates: Internal compartments are displaced as MDCKII cells are stretched. We used Concanavalin A as passive (A) and fibronectin (B) as active adhesive on both microplates.

We continued to investigate effects of adhesion contrast on Madin-Darby Canine Kidney Cells II (MDCKII). We coated two microplates with Concanavalin A (ConA), a lectin protein, which binds specifically to various carbohydrates on the cells membrane. ConA is often employed to attach single cells to AFM cantilevers [148]. Analogous to glutaraldehyde, ConA glues the cell to the microplates, but triggers no adhesion signal. Therefore, cytoskeletal proteins are not recruited and the cell is thus not reinforced. In contrast, cells spreading on fibronectin establish cell adhesion, which allows the cell to adapt to its environment. To quantify the effect of adhesion contrast, we adapted an idea of Wang et. al. [149] who used mitochondria that were fluorescently labeled by as fiducial markers to measure changes in internal cell structure that resulted from stress transmitted to integrins through a micromanipluator. Similarly, we used internal compartments within the cell to study the effect of different microplate coatings, see Fig. 4.7. We plated MDCKII cells between two fibronectin and two ConA coated microplates, respectively. After an incubation time of 30min cells were stretched by the piezo and consecutive image sequences were recorded. Using ImageJ[6] we performed an edge detection algorithm to dissect the internal compartments, see Fig. 4.8. Individual compartments, the cell membrane and the microplate edges are clearly visible. On each image we marked the left miroplate edge and compartments that were in the plane of observation throughout the image series. Then a threshold was introduced to mask everything else out so that only the markings were left, Fig. 4.8 (C) and (D). In Fig. 4.9 the microplate displacement is plotted against the displacement of the compartments for ConA and fibronectin coatings. Similar to [147] an actively adhered cell is closer attached to its surrounding than a passively glued cell. Since the compartments are usually attached to the cytoskeleton (see [149]) and the cytoskeleton in turn connects to integrins in adhesion processes.

---

[6] ImageJ is a powerful image processing program developed at the National Institutes of Health: http://rsb.info.nih.gov/ij/

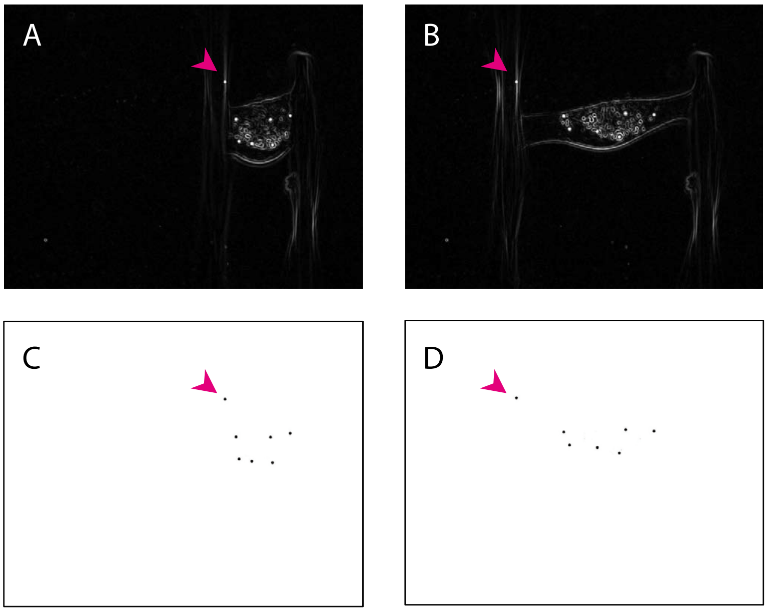

Figure 4.8: Cell stretcher experiment analyzed by image processing. Employing an edge-detection algorithm microplate edges and internal compartments are visualized, A and B. Revealed edges are used mask out other image parts so that microplate and compartment movement can be traced, C and D.

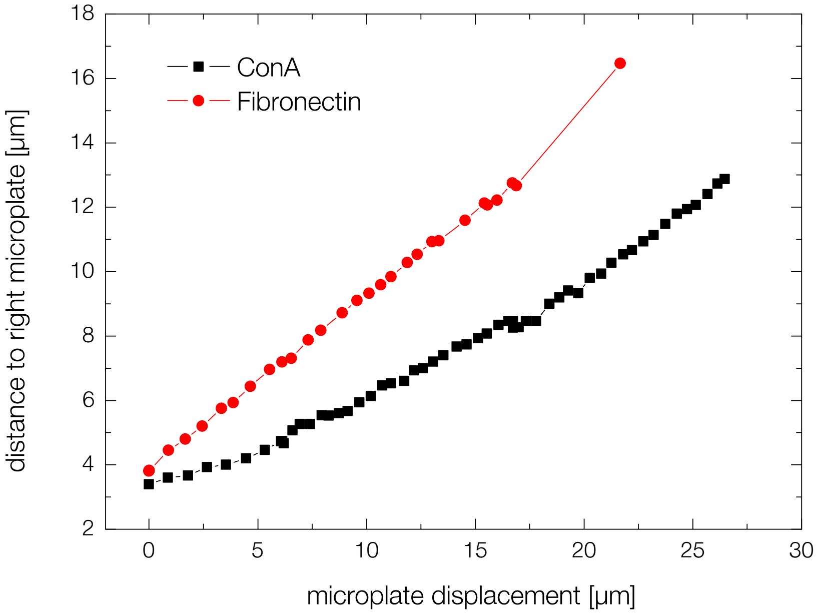

Figure 4.9: Compartment displacement plotted as function of microplate displacement. Red circles denote fibronectin, black squares ConA experiments.

Chapter

5

The Atomic Force Microscope

The Atomic Force Microscope (AFM) was invented during the first half of the 1980's [150] by Gerd Binnig et. al. at the University of Stanford and IBM Labs in Zürich. It was designed as an extremely sensitive device to probe and image the surface of a specimen. Its working principle is fairly simple: a tiny cantilever with a sharp tip fabricated from silicon or silicon nitride is mounted onto a piezo element, which can be moved along the vertical axis of the surface. When the very soft cantilever is elastically deformed due to external forces, e.g. interaction with the probe's surface, its deflection Δx can be measured. If coupled to a lateral scanning device the height information gained by the cantilever bending can be collected to create a two-dimensional image of the surface. Moreover, since cantilever stiffness can be measured the deflection Δx translates into force by Hooke's law:

$$F = -k\Delta x. \tag{5.1}$$

The first AFMs had a Scanning Tunnel Microscope (STM) mounted on top of the cantilever (Fig. 5.1) to measure the bending. In today's setups a laser beam is focused on the cantilever's back-side and reflected towards a quadrant photo diode, which in turn measures the deflection of the beam (see Fig. 5.2).

5.1 Introduction

Even though its inventors created the AFM to scan the surface of specimen they stated in their seminal paper

> *"We envision a general-purpose device that will measure any type of force."* [150].

Since that time, Atomic Force Microscopy has evolved into a highly versatile, multi-purpose machine [151] and can be employed for many applications in material science [152] as well as in biophysics [153], like high resolution surface imaging, single-molecule manipulation [154], measuring the bending energy of DNA [155], nanoscale functional imaging of live cells [156], and single-cell force spectroscopy [157], just to name a few.

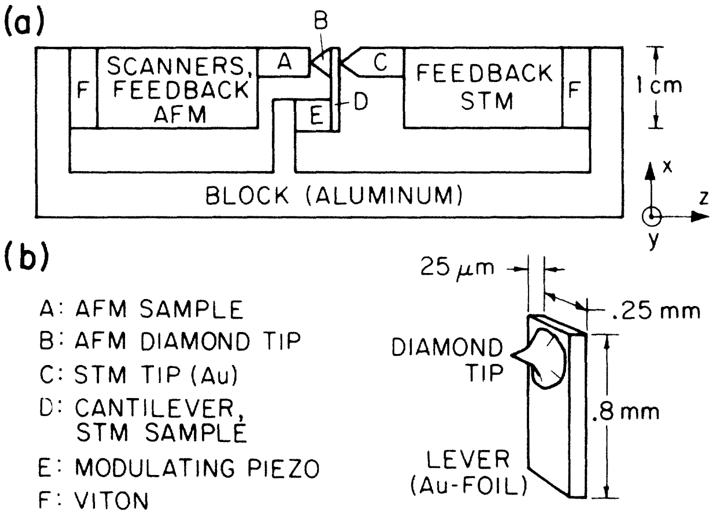

Figure 5.1: (a) First AFM Setup by Binnig and co-workers. A STM was used to measure the cantilever deflection. (b) Cantilever with sharp diamond tip to scan the specimen surface. Adapted from [150].

5.2 Applications

5.2.1 Single-Cell Force Spectroscopy

The term Single-Cell Force Spectroscopy (SCFS) has recently been introduced for experiments, where forces between cells and substrates or another cell are measured [158]. Hermann Gaub and co-workers were the first to use the AFM for measuring forces between single cells in the late '90s [157, 159]. The basic principle of Single-Cell Force Spectroscopy (SCFS) is illustrated in Fig. 5.2. The surface of a tipless cantilever is functionalized with an adhesive to immobilize one of the cells. Another cell sitting on the surface is approached from the top to allow for cell-cell adhesion. After a certain contact time T_C the cells are detached and the force required for separation is recorded.

In Fig. 5.3 a typical AFM force curve for SCFS is displayed. The diagram should be read from left to right starting with the upper red line. First, the piezo is fully retracted and then commences to approach the surface. During this approach the cantilever moves freely, i.e. no forces are applied, and thus the deflection recorded by the photo diode is zero. Once the cell on the cantilever comes into contact with the cell on the bottom the cantilever starts bending and force is applied (Fig. 5.3a). The piezo keeps moving until a force threshold, called *setpoint*, is reached. After this, the Cantilever will not move for the adhesion time T_C and then start retracting. The deflection during this backward motion is shown in Fig. 5.3 as black line. The total separation force is defined as the difference between the lowest point in the spectrum (Fig. 5.3b) and its value when the piezo is fully retracted (Fig. 5.3c).

Another hallmark of this kind of diagram is visible in the enlarged inset of Fig. 5.3 shown in Fig. 5.4: separation steps corresponding to rupture events. These single rupture events correspond to sequential unbinding events, which can are reflected in AFM spectra

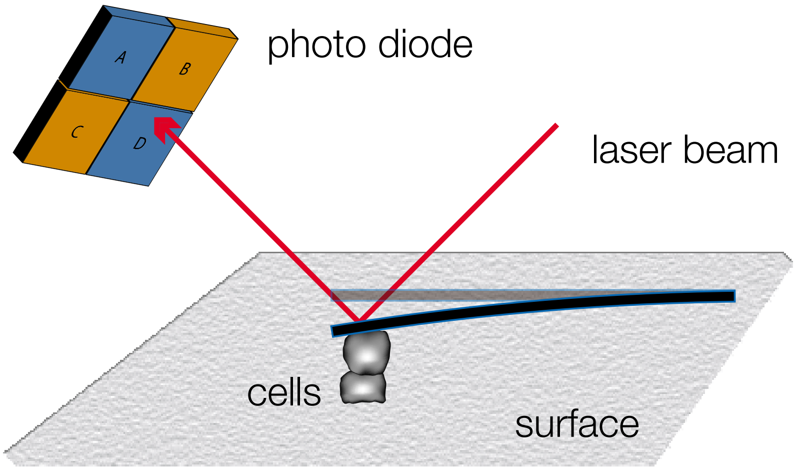

Figure 5.2: A typical AFM SCFS experiment: A cell attached to the surface is approached from top by another cell on a tipless cantilever. Under cell-cell adhesion forces the cantilever is deflected and, during retraction, this deflection is recorded. Using Hooke's law, deflection data is translated into force.

as single step like structures. These steps can be characterized by three values: length of step, step size and slope. If the slope is almost zero, like the events in Fig. 5.3 these events are called *t-events* in contrast to *j-events*, which have a negative slope and thus resemble the shape of the letter **j**. T-events are associated with viscous tethers, which are pulled out of the cell membrane and usually occur at the end of the spectrum. Tethers are pulled out of the membrane by one or several adhesion proteins at the tip. Tethers are pulled at $r_f = 0$, i.e. zero slope, and are thus easily characterized and spotted in force spectra. These tethers are visible with the cell stretcher. Since tethers are pulled away from the cell for many microns, adhesion proteins at their tip cannot be reinforcement by cytoskeleton molecules. Hence, t-events can help to elucidate how many molecules are present at the tip of a tether.

J-events on the contrary, occur in the middle section of spectra and have a short breakway. In contrast to the pure viscous tether, j-events are viscoelastic and probe the stiffness of bond and its environment. They have a negative slope k_j which is directly correlated to the loading rate $r_f = k_j\, v$, where v is the retraction velocity of the cantilever. These events yield insights into how well surface molecules are attached to the cytoskeleton.

The AFM was used in this study for SCFS. We will explain our adjusted experiment scheme in detail later (see Sec. 9.3) and look at t-events and j-events, which occur in our adhesion experiments.

5.2.2 Force Mapping

Another AFM application widely used in biophysics is *force mapping*, which creates a 2-dimensional elasticity map of an adhered cell. To this end, uncoated cantilevers are employed like the one shown in Fig. 5.5.

The thin tip on the cantilever is used to scan adherent cells in a petri dish. Local viscoelastic properties of the cell are determined through indentation and subsequent Hertz

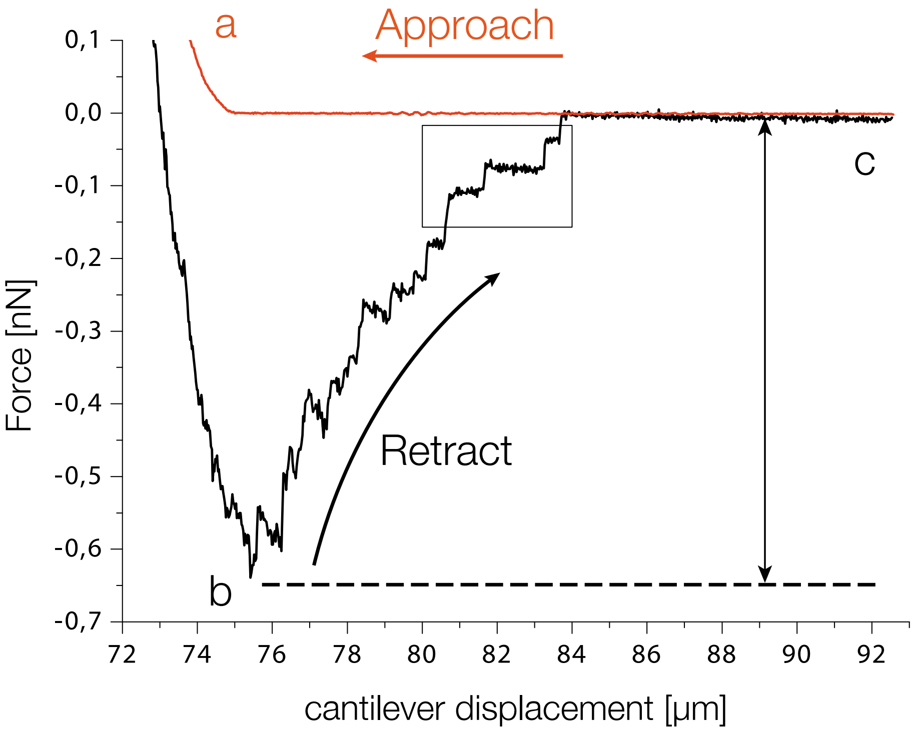

Figure 5.3: Typical AFM force spectrum for SCFS experiments: The upper red line shows how the cantilever approaches the surface, no deflection is measured since no force is applied. When the upper cell is pressed against the cell on the bottom, the cantilever starts to bend until a certain setpoint is reached (a). The black line denotes the retraction phase, where the piezo retracts the cantilever and the separation force is measured, defined as difference between the lowest point of the spectrum (b) and the value when the piezo is fully retracted (c). The rectangular region is enlarged and displayed in Fig. 5.4.

fit to the indentation curve [160–164].

5.3 Setup

In this section, we will describe the specific AFM setup which was used in this study and explain details concerning measurements and data handling.

5.3.1 AFM Head and Microscope

Our setup consists of a ”Nano-Wizard I” AFM head complemented by a CellHesion module (JPK Instruments AG, Berlin, Germany) mounted on an upright Zeiss AxioVert 200 microscope (Carl Zeiss MicroImaging GmbH, Göttingen, Germany). The microscope is placed on an anti-vibration table (TS-150, Table Stable Ltd.) to damp vibrations and noise from the environment. Around the microscope a special incubator (EMBL GPI68

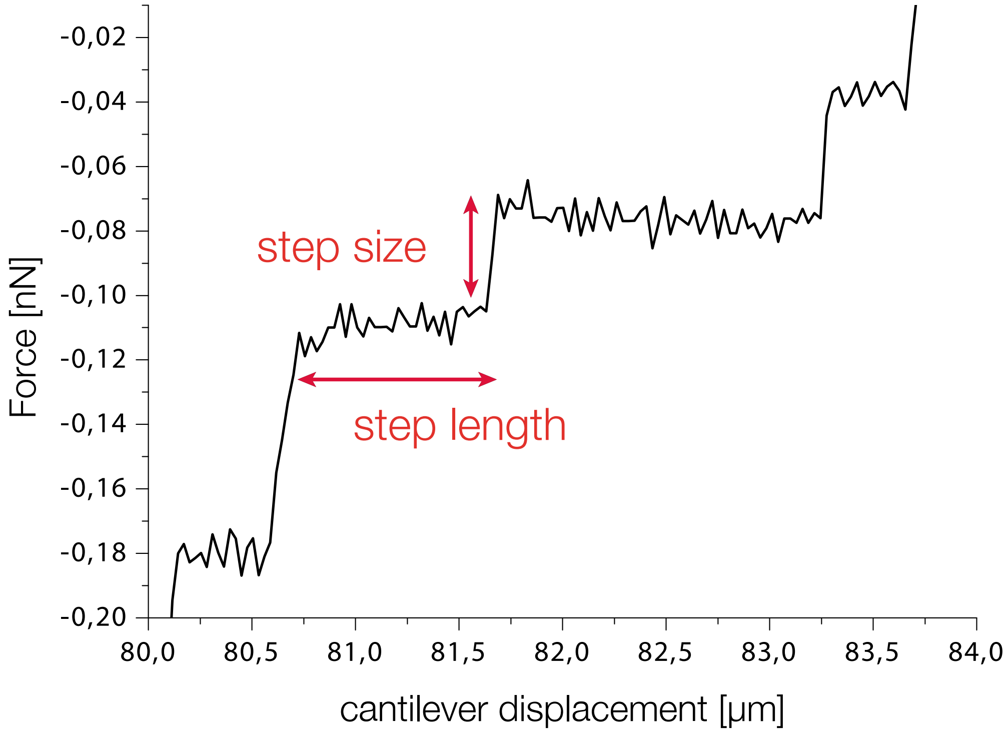

Figure 5.4: Separation steps in SCFS experiment: The AFM spectrum exhibits separation steps, which can be correlated to single rupture events. These steps can be characterized by three values: step size [nN], step length [µm] and slope or stiffness [nN/µm].

IV) is installed to provide physiological conditions (37°C , 5% CO2). AFMs employed in surface scanning applications typically use piezo elements of 15µm of travel. Since cells have diameters of around 10µm, usually 15µm are not enough to separate to cells from each other. Therefore, the attached CellHesion module provides a piezo length of 100µm.

5.3.2 Calibration of Force Constants and Sensitivity

Cantilevers are fabricated photolithographically which leads to sub-micrometer precision in their length and width but variations in the cantilever thickness are very well possible. Because of this variance every cantilever has to be calibrated individually to obtain characteristic force constants. In our setup, soft cantilevers like the ones we used in our experiments can be calibrated quite easily by analyzing the power spectrum of thermal noise fluctuations of the cantilever [165]. Additionally the sensitivity has to be measured as well every time the cantilever chip is placed in and out of the AFM or after the position of the laser on the cantilever was changed. The sensitivity S is the proportionality factor expressed in m/V which translates the photo diode's voltage U into cantilever's deflection d. It is measured by pressing the cantilever onto the glass surface, which yields a linear

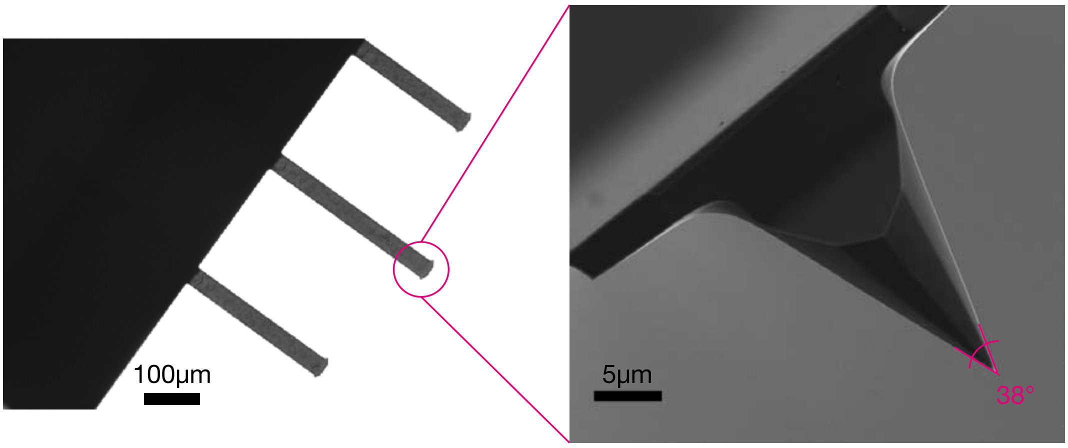

Figure 5.5: Scanning electron micrograph of an AFM cantilever with a sharp tip. These kind of cantilevers are used in scanning experiments, where local viscoelastic properties of cells are determined through indentation and subsequent Hertz fit to the indentation curve. We used tipless cantilevers in separation experiments.

height deflection curve (see Fig. 5.6). A fit to this linear slope delivers the sensitivity S:

$$d = S \cdot U.$$

To calculate the force we measure U_0, which corresponds to the cantilever in a relaxed state. Usually U_0 is set to 0 by guiding the laser reflection right in the middle of the quadrant photodiode (see Fig. 5.2). Thus, the force is finally calculated by

$$F = -k \cdot \Delta x = -k \cdot (d - d_0) = -k \cdot S\,U. \tag{5.2}$$

5.3.3 Data Processing

Using a homemade MatLab program, final force curves were corrected for cantilever drift and for different support positions. In SCFS experiments, the cantilever is loaded with a cell. Thus, a small deviation from Eq. 5.2 will occur, because the cell does usually not sit at the very end of the cantilever but somewhere between laser spot and cantilever edge (see Fig. 5.7). Hence, the load of the cantilever is not at the tip during experiment, but instead a few µm away from the edge. Therefore a correction factor c_f needs to be calculated for each experiment [166]:

$$c_f = \frac{1 + 2l_C}{L_0 - 2l_C + l_L},$$

where L_0 is the cantilever length (well defined by the manufacturer) and l_C and l_L are the individual cell's position and the position of the laser l_L on the cantilever, respectively. The positions were measured by calibrating images taken right before the experiment, like the one shown in Fig. 5.7. Finally, our MatLab program was used to evaluate single rupture events (force steps, see Fig. 5.4) and total adhesion forces from each (see Fig. 5.3) force-distance spectrum.

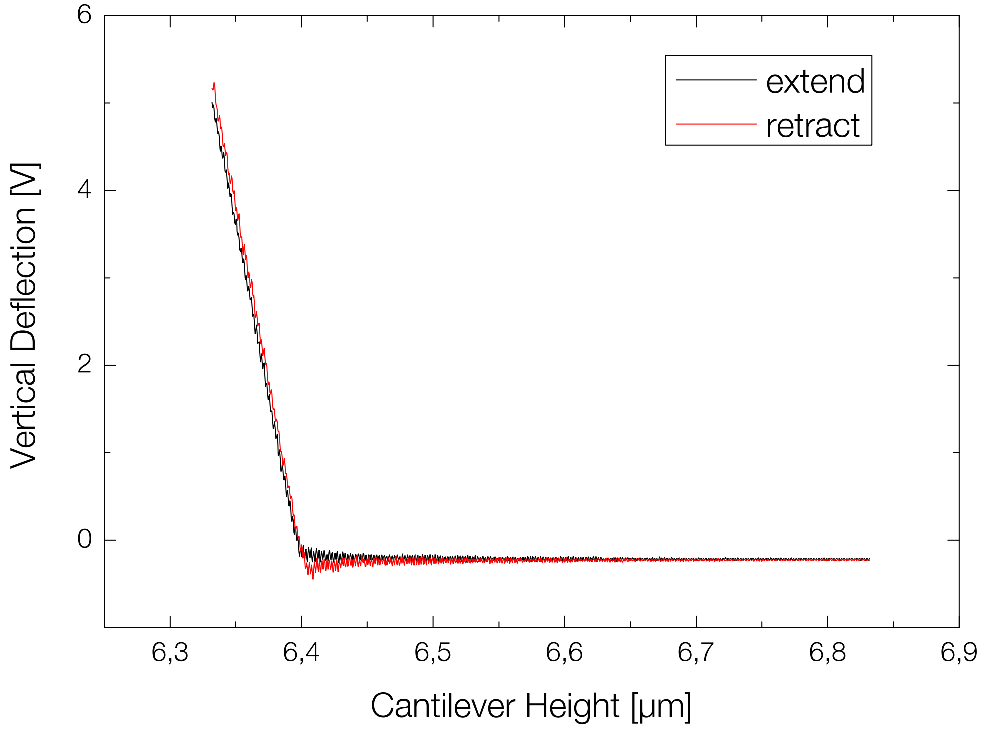

Figure 5.6: Approach (black line) and retraction (red line) curve of an AFM cantilever pressed onto on a glass surface. Fitting a line to the left slope will yield the sensitivity S.

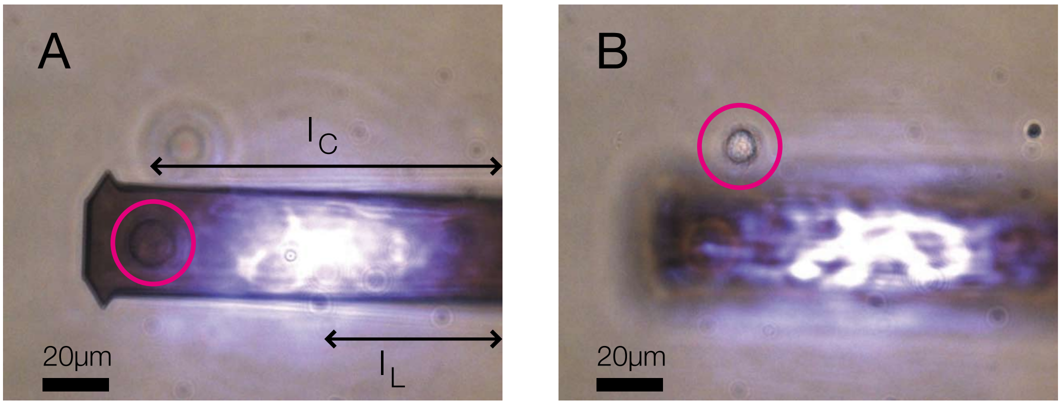

Figure 5.7: (A) 3B11 T cell attached to the bottom side of a cantilever (red circle). The cell is visible because the cantilever is semi-transparent. (B) LK35.2 B cell on the petri dish bottom (red circle). Cantilever carrying T cell is out of focus since it hovers above the surface. The bright spot on both pictures is the laser beam.

Chapter

6

Fluorescent-activated Cell Sorting

Fluorescent-Activated Cell Sorting (FACS), also known as Flow Cytometry (FC), is a technique for the analysis of multiple parameters of individual cells within heterogeneous populations. This analysis is accomplished by passing thousands of cells per second through a beam of laser light and analyzing the forward and side-ward scattered light, as well as, fluorescence emitted by the cells. In Fig. 6.1, a schematic overview of a FACS apparatus is given. First, a cell population is feed into the FACS. By hydrodynamic focusing the fluidics system generates a stream of single cells, which pass by a laser beam. For each cell, scattered light and fluorescence is measured by the detectors.

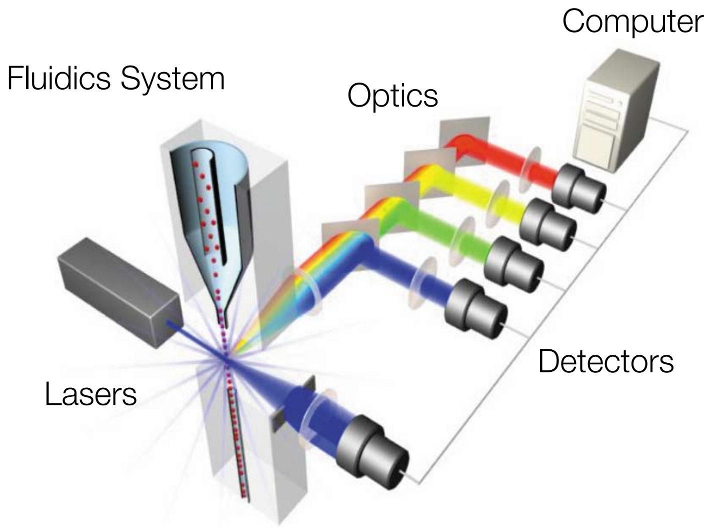

Figure 6.1: Schematic of a FACS machine: a cell population in solution is turned into a stream of individual cells by the fluidic system and then screened by a laser beam. The amount of forward, side-ward scattered and fluorescent light emitted by the cell is collected by special detectors and processed by an attached computer system. Adapted from http://www.invitrogen.com.

An attached computer system collects and saves the data. Thus, a huge number of cells can be analyzed by this method. In advanced setups sub-populations of cells can be sorted out. There, an additional fluidic system, vertically aligned to the original stream, is triggered every time a cell passes by having a fluorescent signal above a specified threshold.

In this study, we used FACS to sort cells extracted from mice for primary cell experiments: particular fluorescent markers couple to membrane proteins specific for a sort of cell only.

Another application is displayed in Fig. 6.2. To test whether CD43-antibody is a good choice to specifically attach 3B11 T cells to AFM cantilevers (see Chapter 9) we performed FACS analysis of these cells. Fig. 6.2 shows two typical FACS diagrams. Every dot represents an individual cell. The diagram is divided into four regions and the entire population is evaluated based on this division. The x-axis represents the fluorescent signal of an Alexa-488 conjugated anti-CD43-antibody by a biotin-streptavidin sandwich which in turn binds to the membrane receptor CD43. The y-axis is not evaluated in this experiment. It is obvious, that for 3B11 T cells the entire population is shifted towards the right, which means that the cells feature a high number of CD43 on their membrane. In contrast, the LK35.2 B cells are mostly aggregated in the lower left quadrant which means that very few anti CD43-antibodies could couple to the cells, thus, yielding a lower fluorescent signal. Hence, B cells do not carry many CD43 membrane proteins. This results is integrated in the right diagrams, where control experiments without CD43 antibody and the actual experiment are plotted. Clearly, for the 3B11 cells the population is shifted if the antibody is introduced, but for the LK35.2 B cells control and experiment show no difference. Thus, 3B11 T cell can be attached to cantilever coated with anti CD43-antibodies, which is essential for the AFM experiments. Moreover, the absence of CD43 on the B cells guarantees that no B cell is accidentally picked up during AFM measurements.

LK35.2 B cells

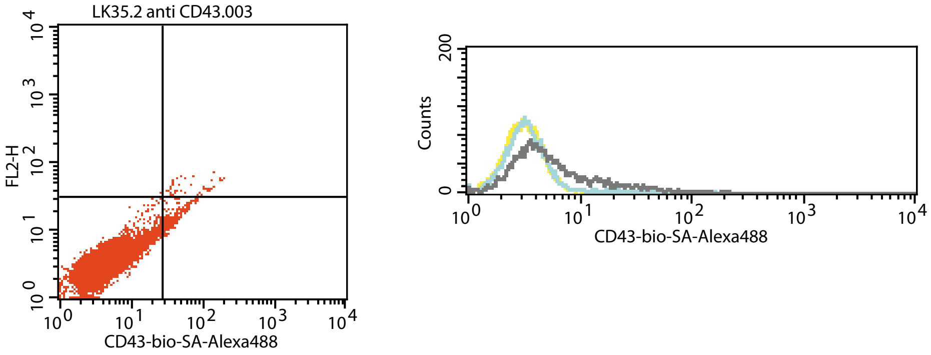

3B11 CD4+T cells

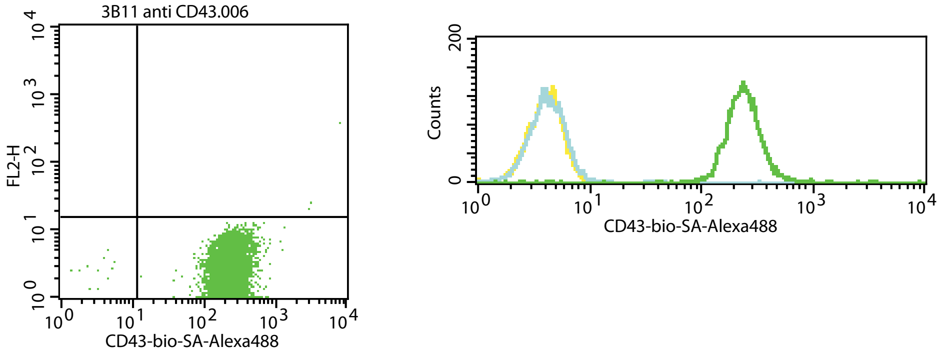

Figure 6.2: FACS data for 3B11 and LK35.2 cells: Left side - FACS data is usually displayed in a four segment diagram. Every dot represents a single cell. x- and y-axes correlate to fluorescent signals. Here, only the x-axis is relevant since we were interested in the amount of anti CD43-antibodies bound to the cells. It is visible that almost every measured LK35.2 cell is in the lower left quadrant whereas the 3B11 cells are in the lower right quadrant, which means that the former exhibit low and the latter high number of CD43, respectively.

Part III

Separation Experiments

Chapter

7

Motivation

In Chapter 2 we have learned that an effective immune response requires a specific cell-cell contact between T cells and Antigen Presenting Cells (APCs). This interaction is highly sensitive and only a few peptides associated with MHC molecules on the APC are enough to trigger the formation of an Immune Synapse (IS) and subsequent immune response. Recent studies have shown that actin as well as many signaling proteins [94, 95] play a crucial role in peptide recognition and the establishment of a pronounced cell-cell adhesion which is characterized by an orchestrated protein re-localization that results in large clusters of ICAM-1/LFA-1 and TCR/MHC. This transient cell-cell contact and the associated information transfer can take up to several hours depending on cell type [78, 167]. But in the end cells will depart from each other and go separate ways.

The questions that arise from this observation are: How can cells that usually float in our blood stream establish firm adhesion to one-another? How big are adhesion forces between in T cell/APC conjugates? What enables cells to control their adhesion propensity?

Force as facilitator?

A model, which is based on *inside-out signaling* and *integrin activation* is displayed in Fig. 7.1. The interface of a T cell/APC conjugate is shown. When the T cell begins to scan the APC for foreign antigen, its LFA-1 integrins are in a non-activated, or *non-primed* state, which means that the binding-affinity to their ligand receptor ICAM-1on APC side is rather low. Once the T Cell Receptor recognizes the peptide associated to the MHC complex of the APC and inside-out signal is triggered which drives LFA-1 into an intermediate affinity state. Inside-out signifies that the affinity state of the surface receptor was changed from the inside: the cytoplasmic tail domain of the transmembrane protein is modified such that the integrin opens up, just like a switchblade, to reach an intermediate affinity state where it can bind to its ligand [19, 27, 168–170]. This process is accompanied by the association of actin cytoskeleton to LFA-1. In Fig. 7.2 this amazing transformation is depicted by schematic drawings and scanning electron micrographs. Finally, motor proteins mediate a cytoskeleton contraction exerting low forces on LFA-1 to induce full integrin activation and to finally arrest the two cells for adhesion. This force has to be counterbalanced on the APC side.

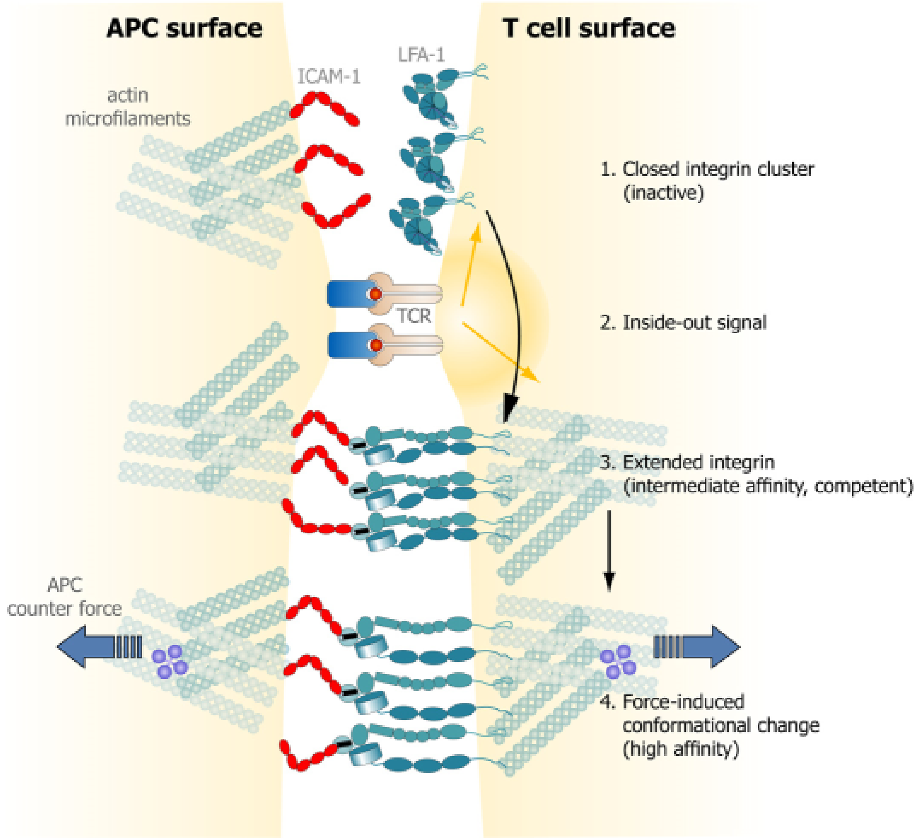
APC surface
T cell surface
ICAM-1
LFA-1
actin microfilaments
1. Closed integrin cluster (inactive)
TCR
2. Inside-out signal
3. Extended integrin (intermediate affinity, competent)
APC counter force
4. Force-induced conformational change (high affinity)

Figure 7.1: Proposed Role for Internal, Cytoskeleton-Driven Forces in the Interactions of TCR and Integrin Clusters the Immunological Synapse. Adapted from [76].

We can test this model by creating predictions that can be falsified. If we were to measure forces between T cells APCs we would expect that:

1. There is no, or little force, if no peptide is present. Since then, integrins are not activated and subsequent force induced adhesion are is not triggered.
2. If there is peptide present, forces will increase overtime because integrins become more and more activated (affinity regulation) or because more integrins gather at the contact site (valency regulation).
3. Consequently, forces should decrease again at later times since these cells contacts are transient in nature and the T cell has to detach again.

Therefore, we want to measure separation forces in T cell/APC conjugates in the presence and absence of cognate peptide. Note, that forces required to separate cell pairs represent a measure for the strength of cell-cell adhesion and not associated with the free energy of this binary system. The main objectives of this work are thus to

- Establish an appropriate technique capable of measuring separation forces on the cellular scale for contact times T_C in the range of 0-2 hours and to compile a protocol which makes experiments comparable.

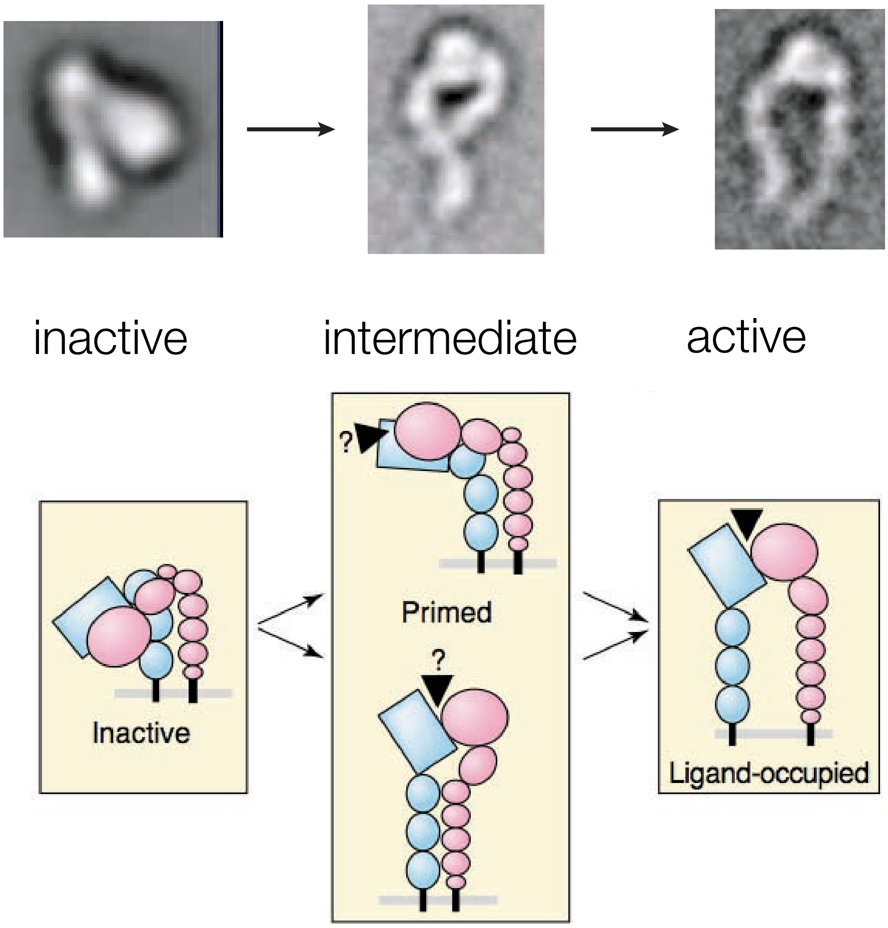
inactive
intermediate
active
Primed
?
?
Inactive
Ligand-occupied

Figure 7.2: Integrin activation, switchblade model. Upper panel shows electron micrographs of an integrin in its various activation states. Lower panel: respective schematic drawings illustrating α and β strands. Adapted from [27, 168].

- Find an adequate cell pair that allows for easy and reliable handling.
- Identify the right time-scale during which alterations in separation force values are expected.
- Measure a reasonable number of cell pairs to generate a reliable statistics of total separation forces.

Chapter

8

Qualitative Observations - Cell Stretcher

Since our objective was to measure the force between cells in T cell/APC conjugates, we employed the cell stretcher differently than described in chapter in Chapter 4. We modified the cell stretcher in such a way that an individual cell could be placed onto the flexible and rigid microplate, respectively. To our knowledge, this is the first time that a microplate based device is employed to study cell-cell adhesion. We measure separation forces and visualize the adhesion process. Cells are mounted onto the microplates by "fishing" them on the glass bottom. After placing the plates parallel to each other, the cells are brought into contact and left to adhere for a certain time period. Cells are then separated by moving the piezo transducer for 80 µm at a speed of 1 µm/s. The cell stretcher device is not an appropriate choice for measuring many cell conjugates which is required for scanning a range of adhesion times. Since only a single cell pair could be measured per day we decided to use the cell stretcher to gain qualitative information about the system. These experiments helped us later to interpret data acquired with the AFM, which is discussed in the next chapter.

8.1 Modified cell stretcher

We modified the cell stretcher apparatus to perform cell-cell adhesion experiments. In Fig. 8.1 the experimental procedure is shown. One cell type was introduced at very low concentration into the liquid chamber. After a short sedimentation time, one microplate was introduced and rotated by 90° to be parallel to the glass bottom of the liquid chamber, see Fig. 8.1A. Then, by slowly retracting the cantilever in a parallel movement to the bottom, a cell was slowly picked up from the ground, Fig. 8.1B. Then, the microplate was moved upwards and re-rotated by 90°. Afterwards, the second cell type was injected. To avoid that the first type was grabbed by the second cantilever, the second cell type was injected at a significantly higher concentration and sometimes labeled with a dye. Finally, the second microplate was loaded with a cell of the second type just like the first one, retracted, rotated and placed in such a way that the cells on the two microplates faced each other, see Fig. 8.2.

The cells were then moved by the micromanipulators, brought into contact and separated after a contact time of T_C. Images and force curves were recorded during contact and subsequent separation of the cells.

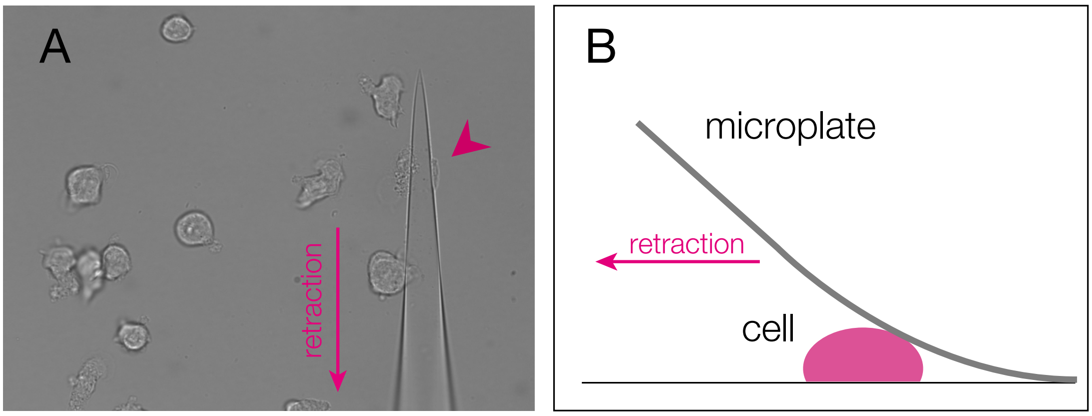

Figure 8.1: Collecting Cells on the Bottom with the Cell Stretcher: Microplates are rotated by 90, lowered to the glass bottom until they slightly bend. By slow retraction a cell is loaded onto the microplate. (A) Microscope image of dendritic cells with a microplate approaching the cell marked by an arrow. (B) Schematic diagram of cell collection process.

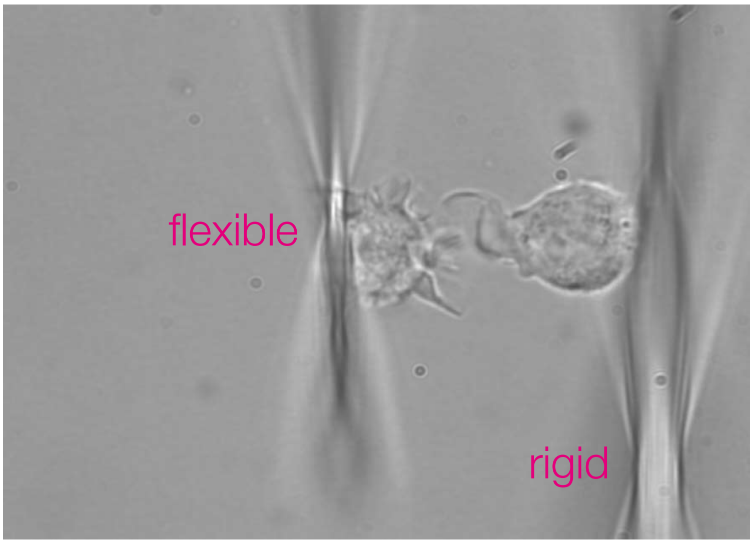

Figure 8.2: Cell Stretcher Used a Single Cell Spectroscope: Two cells of different type facing each other and awaiting experiment. Flexible microplate on the left and rigid microplate on the right carry a T cell and a B cell, respectively. These were collected from the ground before.

Disadvantages

Collecting cells on the microplate is a complicated endeavor: to provide firm adhesion, microplates need to be rotated and pressed onto the glass bottom to create a surface which is more or less parallel to the glass in order to establish an interface between cell and microplate. On the one hand, this may lead to the destruction of the microplate if pressure forces are too high, on the other hand there is no way to tell how much force was applied when the microplate was pressed against the cell. Because of that, cells adhesion to the microplates was often very heterogeneous and not reliably reproducible. Some cells were too flat because the applied force was too high, other cells too loosely bound. Another problem stems from the fact, that the microplate could never be entirely parallel to the bottom, see Fig. 8.1 B, which allowed it to slip away. The contact angle between microplate and glass bottom was roughly 35°, clearly higher than the contact angle in the AFM (see Chapter 5) of 15°. These problems are inherent limitations to the technique. In Atef Asnancios' lab an enhanced cell stretcher was built, which has microplates that are parallel to the bottom [144]. But this setup cannot be turned into a cell-cell adhesion measuring device since it is not possible to rotate the microplates to pick up the cells. Also, no microplate based setup is able to measure contact forces in cell collection from the glass bottom since forces are measured in x-direction (see Fig. 4.1) and not in z-axis.

8.2 Experiment preparation

Experiment chamber

50mm^2 diameter round cover slips were cleaned in Piranha solution (1:3 mixture of H_2O_2 and concentrated H_2SO_4) for at least 30min and washed three times in Milli-Q™ water.

Cell culture

Cells were maintained in RPMI 1640 culture medium (Gibco, 31870) containing 10% heat inactivated Fetal Calf Serum (FCS), 1% L-Glutamine (Gibco, 25030), 1% Pen-Strep (Gibco, 4160). For 500ml culture medium, 3.5ml HEPES buffer and 0.5ml β-mercaptoethanol were added. Cells were cultured at 37°C and 5% CO_2 in a Heraeus incubator. For the experiment, we added 1µg/ml propidium iodide (PI) to discriminate live from dead cells. PI is a fluorescent molecule that penetrates dead cells and intercalates their DNA, which results in an increase of their fluorescence by a factor of 20-30. Hence, dead cells can be identified and excluded from experiments.

Antigen loading of APCs

We used the hybridomal B cell line LK35.2 [171] and primary B6 cells as APCs in cell stretcher experiments. These cell were loaded with a cognate peptide recognized by an appropriate T cell. LK35.2 were incubated with 100-200µM Hen Egg Lysozome (peptide 34-45) (HEL_{34-45}) for 2h at 37°C (HEL_{34-45} was purchased from DKFZ Peptide Synthesis Unit, Dr. R. Piepkorn), and then washed three times with culture medium. Similarly, B6 cells were incubated in 200nM peptide, OVA-derived epitope SIINFEKL (S8L), which is recognized by B3Z T cells.

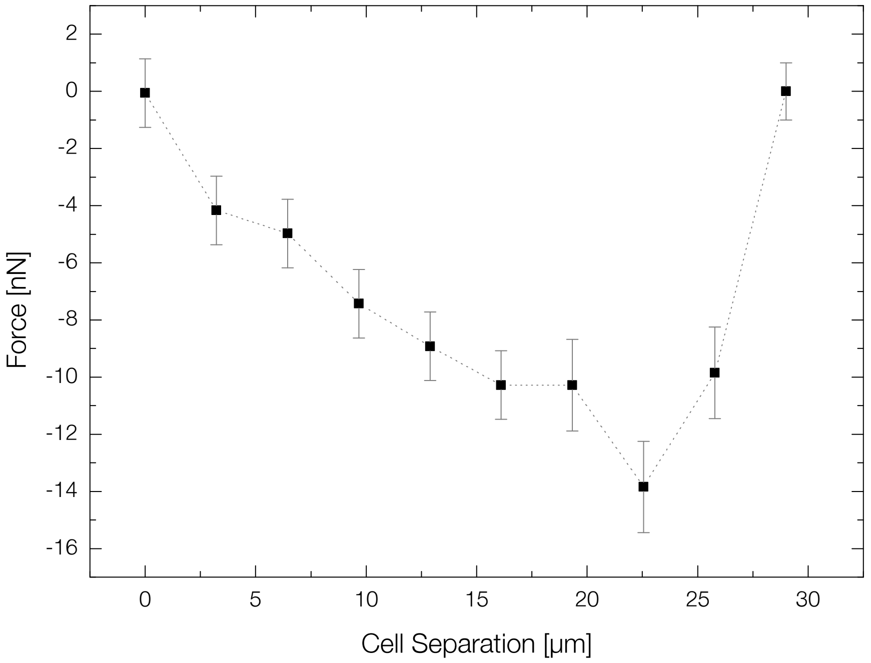

Figure 8.3: Representative Force in Cell-Cell Separation Experiment: The maximum deflection at 22µm cell separation was defined as separation force. Each point was obtained by averaging 30 consecutive raw data points.

Microplate preparation

Microplates were also cleaned in Piranha solution, then functionalized with adhesive coatings. We used Concanavalin A and Poly-L-Lysine (PLL) for most experiments. In the first experiments, glutaraldehyde was employed to fix cells on the microplates. But this was not feasible since cells would stick too strongly on the microplates, resulting in low adhesion propensity with other cells.

Cell fishing

Cells were collected onto the microplates by the method described in Sec. 8.1. The cells were then brought into close contact and left to adhere for a certain time. In cell stretcher experiments we choose T_C =45min as arbitrary adhesion time since this seemed to be a reasonable time after which high cell-cell adhesion forces were to be expected [30, 85, 172].

Separation forces

After a certain adhesion time, cells were separated, and the bending of the flexible microplate was recorded during de-adhesion. After the cells were entirely disengaged, the flexible microplate relaxed and the maximal deflection during separation was taken as sep-

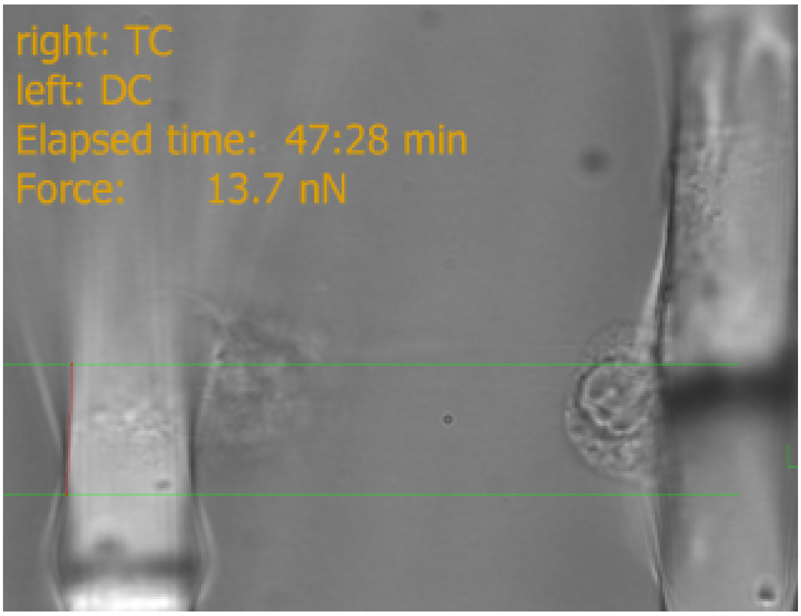

Figure 8.4: Cell Conjugate Separation with the Cell Stretcher: The deflection of the microplate correlates to $\approx$ 13nN. The automatic edge detection mechanism is visible on the left microplate as thin red vertical line. Although hard to see, tethers are formed between the two cells.

aration force. A cell pair, which is being separated is shown in Fig. 8.4. A representative force curve is displayed in Fig. 8.3.

8.3 Experiments

A separation experiment is shown in Fig. 8.6. The cells were left in contact for 45 minutes. During adhesion time environmental variables like temperature and CO_2 level were kept constant. Thermal drift was minimized by the chamber construction and vertical drifts were avoided since microplate holders were each fixed with three screws. We performed several experiments with and without peptides on the APC. After T_C = 45min pulsed cell pairs showed multiple tether formation like displayed in the bottom picture of Fig. 8.6.

Table 8.1: T cell/APC experiments with the cell stretcher

T cell	adhesive	APC	adhesive	peptide	T_C [min]	Force [nN]
B3Z	PLL 0.1%	B6 DC	ConA	OVA-S8L	45	3–6
A6B3	PLL 0.1%	LK35.2	PLL 0.1%	HEL_{34-45}	45	10–14

Tether formation was an indication of strong adhesion since unpulsed pairs did not show tether formation, or if any, just a single tether was found. Forces were in the range of 10-20nN and below 5nN for pulsed and unpulsed cell conjugates, respectively. Since cell stretcher experiments were intended to provide qualitative information about the cells and their behavior we did not calibrate the microplates, but estimates forces using usual

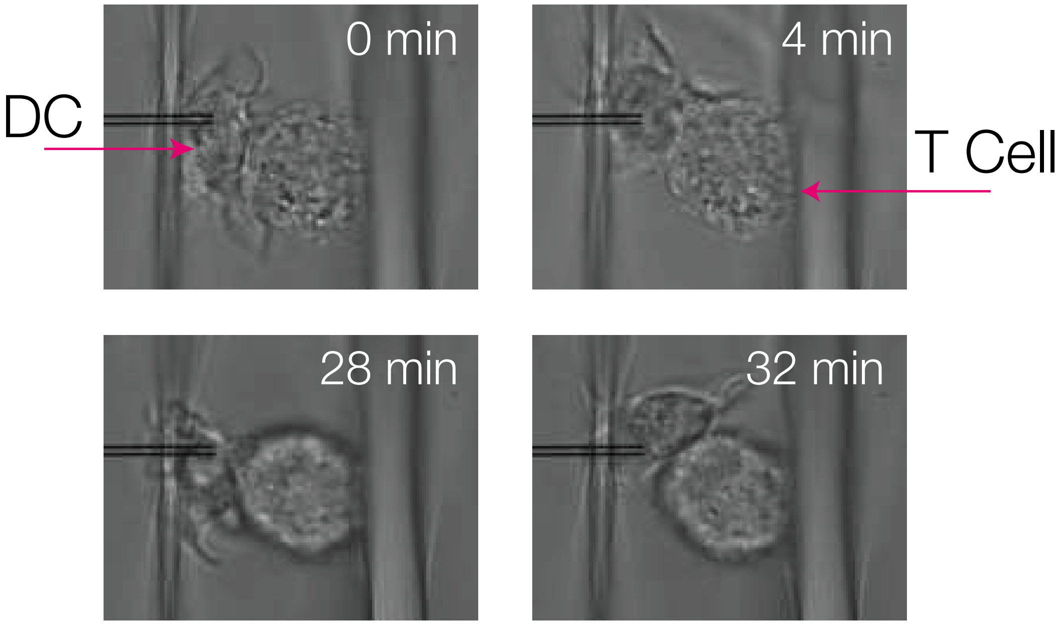

Figure 8.5: An unpulsed DC scans T cell constantly during recognition process. No adhesion was achieved in this experiments. Note the slight focus shift after 30min. (Black parallel lines are a built-in positioning system of the microscope.

microplate force constants.

In Table 8.1 cell stretcher experiments are summarized. We used the OVA-S8L specific T cell hybridoma line B3Z against freshly isolated primary B6 DCs. The primary cells were used at day 7 through 12 in their development. B3Z and B6 cells were attached using PLL and ConA, respectively. We observed tether formation in the pulsed case, whereas no cell-cell adhesion and, thus, no tethers were seen in the unpulsed case. In contrast to many examples of T cell/APC interaction [97, 167] we observed that the DCs were highly active and motile during experiments and scanned the T cell constantly like shown in Fig. 8.5.

Since the DCs were quite difficult to extract and to prepare for experiment we decided to continue using cell lines, which are much easier to handle. Also, the high motility of the DCs did not allow for long term adhesion measurements. Thus, as a second pair we tested two cell lines: HEL_{34-45} specific A6B3 T cell hybridoma [173] and LK35.2 B [171] cell hybridoma as APC. For measurements, LK35.2 were pulsed with HEL_{34-45} before the experiments. Again, we observed many tethers and very few or no tethers in the case of pulsed and unpulsed APC, respectively. Scanning activity was reasonably lower in the second cell pair. Separation of an A6B3/LK35.2 cell conjugate is shown in Fig. 8.6. The exact number of tethers is not easy to tell in cell stretcher experiments, since only one focus plane is imaged during separation. This is due to the fact that shifts in focus will yield jumps in the force and displacement measurement, because the edge detection algorithm will find the microplate edges wandering left and right even though the microplate did not move. The reason for this is that the microplates are introduced at a 35° angle into the experiment chamber and are thus not parallel to the bottom. Hence, the exact number of tethers could not be observed without disturbing the force measurement significantly. Nevertheless, we scrolled through multiple focus planes in a few experiments to see that around 10–15 tethers formed in the pulsed case.

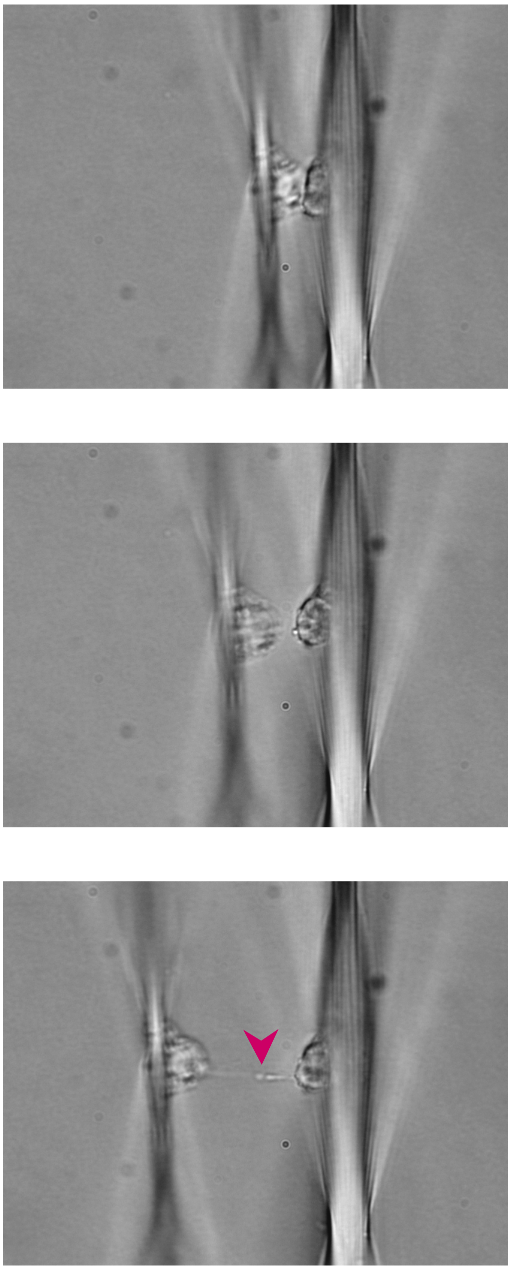

Figure 8.6: Series images showing tethers in cell separation: A cell conjugate is separated with the cell stretcher. A pronounced tether is formed and clearly visible. Breaking of the tether is visible with the cell stretcher, but not measurable. In contrast, with the AFM tether breaking can be measured quite exactly but not visualized, see Chapter 9.

8.4 Conclusion

Preparing cell stretcher experiments involves some crucial steps. Actually, many hours of work can be wasted if one of the microplates loaded with a cell is destroyed through little inattention. The cell stretcher is a good tool for phenomenological cell-cell studies. The technique is similar to micropipette aspiration (cf. Chapter 3) but does not damage the cells through aspiration and is rather suited for cell types that require adhesion since both microplates can be functionalized. Nevertheless there are several problems inherent to this device, some of which we discussed in Sec. 8.1 already. The two major drawbacks of this technique can be summarized:

Sensitivity

In Fig. 8.3 a typical cell stretcher force curve is shown. The piezo retracted over a range of 30µm and highest plate deflection is detected at around 22µm. Afterwards the cells seemed to be separated, even though in this particular experiment, the cells were still attached by several membrane tethers, like the on shown in Fig. 8.6. This shows that the microplates are not able to measure single tether retractions which are usually in the sub 100pN domain [110, 112, 174]. Employing the AFM we could detect single tether ruptures.

High-throughput

Using the cell stretcher only one cell conjugate could be measured per day, mainly because the preparation of the experiment takes a long time. When discussing the next steps in our research program we concluded that we need around 150-200 single conjugate measurements to obtain reasonable statistics.

These two points were the main reason to perform quantitative measurements using the AFM and to measure adhesion forces for a range of adhesion times in the unpulsed and pulsed situation. We will discuss the results in the following chapter.

Chapter

9

AFM Separation Experiments

Here, we summarize the first long time adhesion experiments in cell-cell interaction measured directly by Atomic Force Microscope (AFM). Experiences gained with the cell stretcher helped us to establish experimental conditions that allow to study contact times that are longer than just a few minutes. We could measure the time dynamics of T cell/APC adhesion over the range of 60 minutes and found that pulsed[1] B cells, acting as APCs, yield stronger adhesion in T cell/B cell interactions compared to unpulsed B cells. We will first elucidate how we chose the right cell pair for our measurements, then introduce experiment preparation and procedure and finally discuss the results.

9.1 Characterization of 3B11/LK35.2 conjugates

We used 3B11 [175] as T cell and the B cell line LK35.2 [171] as APCs. Both cell types, 3B11 and LK35.2, are hybridoma cell lines, which means that they were produced by fusing a tumor cell line with a T cell and a B cell, respectively. These resulting hybrid cells (termed hybridomas), are immortal, i.e. multiply infinitely, because of the tumor cell. Subclonal expansion, i.e. the amplification of a certain sub-population of cells, ensures that the T cell line recognizes only a specific antigen. In the case of 3B11 this is Hen Egg Lysozome (peptide 34-45) (HEL_{34-45}), which we introduced before.

9.1.1 Selection of 3B11 cell line

When performing measurements with the cell stretcher we noticed that a rather high number of A6B3 cell died during experiments, which we attributed to the PLL coating of the microplates. That was one of the reasons to switch to anti-CD43 antibodies for T cell adhesion on the cantilever. We further checked several cell lines for survival rates on PLL by simply plating cells on PLL coated dishes and counting the fraction of dead cells using Propidium Iodide (PI). Even though T cells were now attached using anti-CD43 we tried to ensure that T cells were not harmed when in contact with the PLL coated petri dish. This situation is not too far fetched since cells moved quite a bit sometimes, scanning each other constantly. Thus, we tested viability of several hybridoma T cell lines on PLL coated substrates. The results are displayed in Fig. 9.1. Under the same conditions, only

---

[1] Again, pulsed refers to APCs, which carry foreign peptide, whereas unpulsed refers to APCs without peptide.

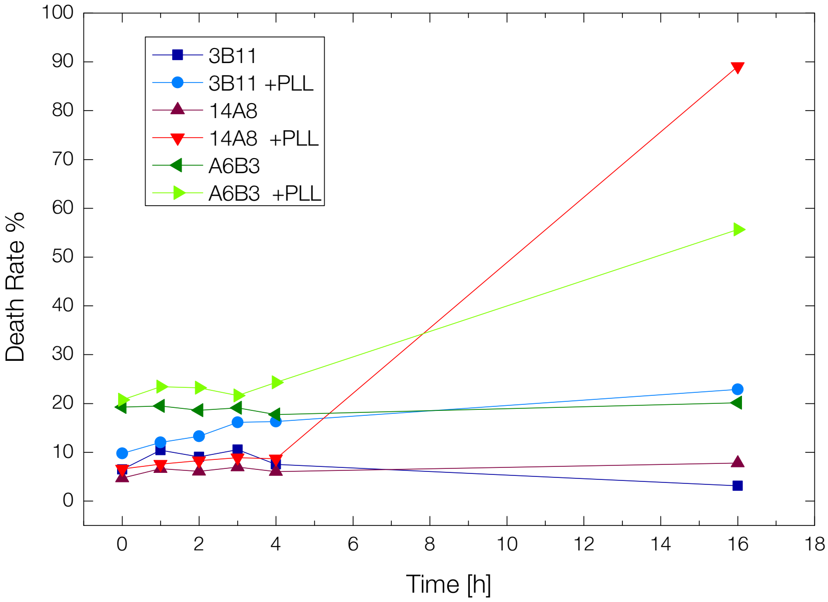

Figure 9.1: Survival of CD4+ T cell hybridomas on PLL coated versus uncoated glass slides over time.

a fraction of cells die in the first few hours, but survival rates deviate strongly afterwards. Even though we intended to limit contact time to a couple of hours, we decided to use 3B11 for AFM experiments since they were affected the least by PLL and survived best on both, untreated and PLL coated surfaces.

9.1.2 IL2 assay, immune synapse formation and conjugate formation

To find optimal concentration for peptide loading we performed an Interleukin-2 (IL-2) assay. IL-2 is a soluble mediator of the immune system and usually produced by the body during immune responses. To measure the response of T cells to antigen loaded B cells, secretion of IL-2 was measured at different peptide concentrations. The results are displayed in Fig. 9.2A. Since IL-2 segregation was the highest at 100µmol/ml HEL_{34-45} we used this concentration in AFM measurements.

Also, we showed that these cells actually do form an Immune Synapse (IS). In Fig. 9.2B we show sample conjugates for unpulsed and pulsed LK35.2 cells. In presence of the peptide an IS is clearly formed, whereas in absence of HEL_{34-45} we did not observe IS formation. Conjugate formation was additionally checked by FACS analysis, see Fig. 9.3. Only very few conjugates were present for unpulsed cells, whereas in the pulsed case conjugates are clearly detectable in the FACS machine.

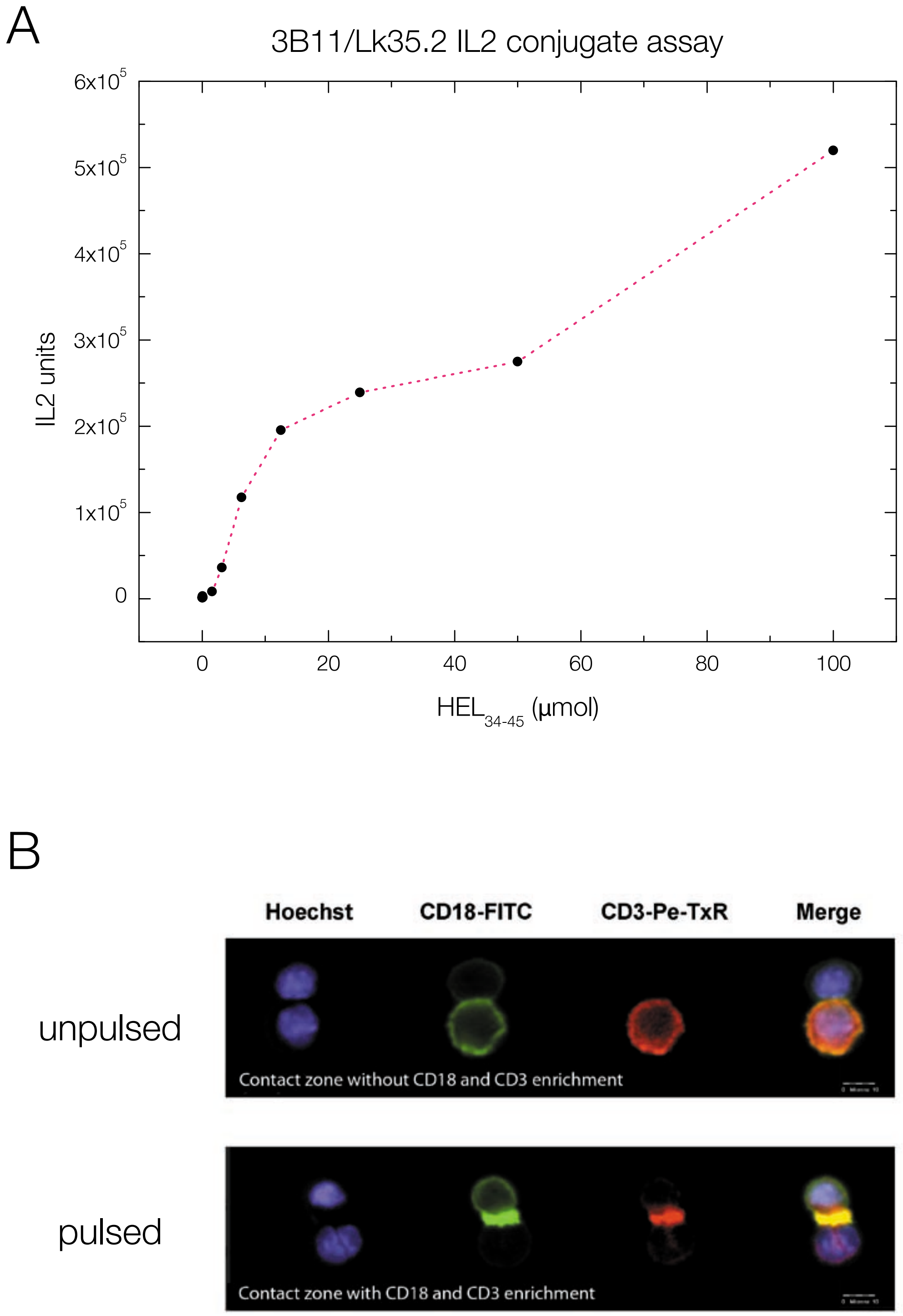

Figure 9.2: **A**: IL2 production 311/LK35.2 pairs as a function of HEL$_{34-45}$ peptide. Courtesy of Prof. Hämmerling, DKFZ. **B**: Pulsed and unpulsed cells pairs were stained for LFA-1 (CD18-FITC, green), CD3-PE-TexasRed (red) and the cell nucleus (Hoechst, blue). A total number of 20,000 events were acquired per sample. Shown are representative pictures of T cell-B cell conjugates with (lower panel) and without (upper panel) an enrichment of CD18 and CD3 in the contact zone. See Sec. A.3 for details of image acquisition. Courtesy of Guido Wabnitz, Uni Heidelberg.

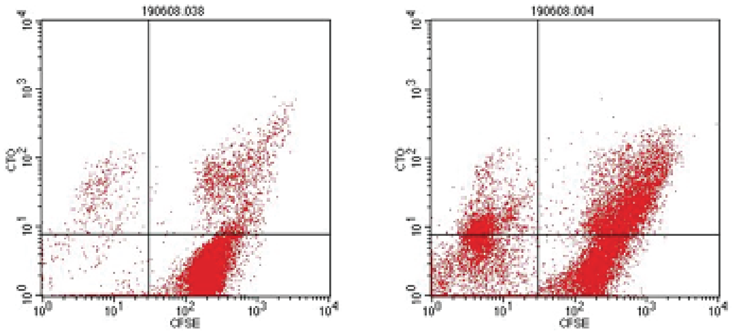

unpulsed pulsed

Figure 9.3: FACS data for 3B11/LK35.2 conjugate formation. Unpulsed and pulsed cell pairs were probed in FACS study. No conjugates are formed for unpulsed cells (left), whereas in the pulsed case (right) conjugates are formed and the population is thus shifted to the left. Note that here, only 33% of cells form a pair. The majority of cells do not form a pair and stays on the right side of the spectrum. Courtesy of Prof. Gunzer, Magdeburg.

9.2 Experiment preparation

9.2.1 Sample surfaces

In SCFS experiments one cell population needs to be fixed to the surface whereas the other has to be collected easily onto the cantilever from the bottom. This requires a dual surface, which supports adhesion on one domain and inhibits it on the other. To this end, we produced modified glass cover slips. First we cleaned the cover slips in Piranha solution (1:3 mixture of H_2O_2 and concentrated H_2SO_4), leaving the glass surface negatively charged and receptive for surface functionalization agents. To separate the $50mm^2$ diameter cover slips into two domains, we applied silicon glue (Twinsil, Picodent, Wipperfürth, Germany). To create the domain where cell could adhere, we covered one side with Poly-L-Lysine (0.01% in PBS), which immobilizes negatively charged cells. The other side was coated with poly(-L-)lysine-grafted-Poly-Ethylene-Glycol (PLL-g-PEG) copolymers, which form a protein-repellent layer that suppresses cell adhesion.

A modified glass cover slip is shown in Fig. 9.4. The protein-repellent side covered with PLL-g-PEG is marked with an **X**. The glass domains were incubated with PLL and PLL-g-PEG for 40min, respectively, and then dried for another 30min at 65°C in an oven. Note that liquid drops spread easily on the PLL-g-PEG but not as much as on the PLL coated side, because of their different hydrophobicity. This behavior was used as a simple test to check whether preparation of the glass cover slips was successful. The blue barrier was not only important for functionalization, it was also used to separate the two cell populations physically during experiments. The glass cover slips were glued to the bottom of perforated plastic petri dishes to create the experiment container. This modified petri dish was kept under argon atmosphere, which ensured stability of the surface functionalization over a couple of weeks.

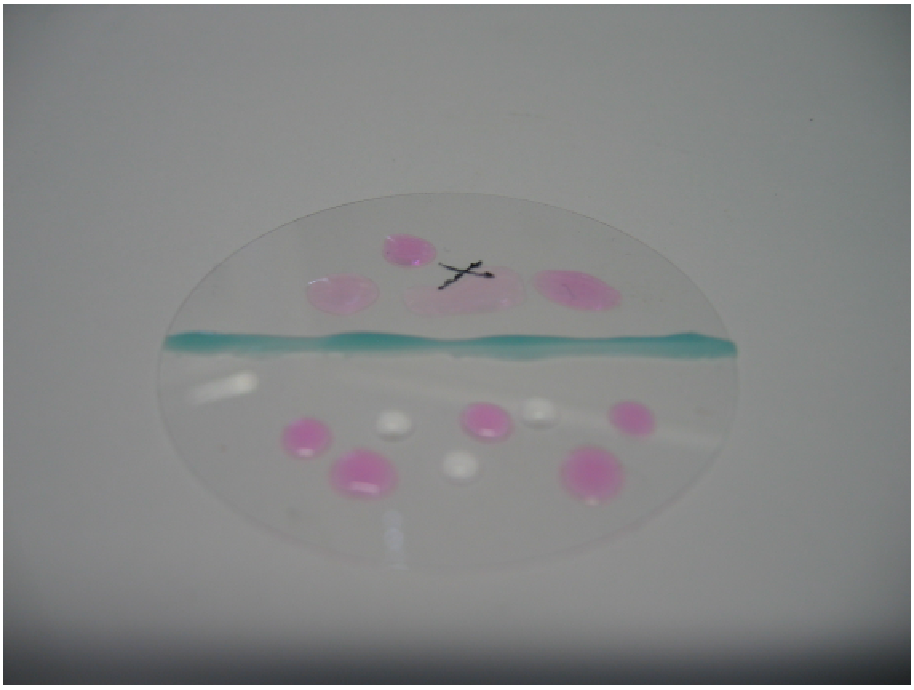

Figure 9.4: Modified Glass Cover Slip: Upper side marked with an **X** is functionalized with PLL-g-PEG to prevent cell adhesion. The lower side is coated with PLL a positively charged peptide immobilizes cells, which are negatively charged.

9.2.2 Cell culture

Cells were usually maintained in RPMI 1640 culture medium (Gibco, 31870) containing 10% heat inactivated Fetal Calf Serum (FCS), 1% L-Glutamine (Gibco, 25030), 1% penicillin/streptomycin (pen/strep) (Gibco, 4160). For 500ml culture medium, 3.5ml HEPES buffer and 0.5ml β-mercaptoethanol were added. Cells were cultured at 37°C and 5% CO_2 in a Heraeus incubator. For the experiment, we added 1µg/ml propidium iodide (PI) to discriminate live from dead cells. PI is a fluorescent molecule that penetrates dead cells and intercalates into their DNA, which increases its fluorescence by a factor of 20-30. Thus, dead cells can be identified and excluded from experiments.

9.2.3 Antigen loading of APCs

We pulsed APCs with a T cell cognate peptide like described in Sec. 8.2. Particularly, our major APC line, LK35.2 B, was incubated with 100µmol/ml HEL_{34-45} peptide for 2h at 37°C (HEL_{34-45} was purchased from DKFZ Peptide Synthesis Unit, Dr. R. Piepkorn), and then washed three times with culture medium. Subsequently, cells were stained cytoplasmatically with 0.25µM carboxyfluorescein succinimidyl ester according to the manufacturer's guidelines (CFSE, Molecular Probes, Karlsruhe, Germany) and washed three times with PBS (5min, 1500rpm).

9.2.4 Cantilever preparation

Silicon nitride, tipless cantilever chips (NSC 12 NoAl, mikro-masch, Tallinn, Estonia) were used in all experiments. Each chip carried three individual cantilevers. This way three experiments could be performed without changing the cantilever chip. Force constants ranged from 0.05 to 0.50 N/m determined by individual calibration of the cantilever with the thermal noise method [165]. Calibration was performed in air before before each experiment. Prior to functionalization cantilevers were cleaned in cold piranha solution for 30min, rinsed extensively with sterile Milli-Q water and then dried under nitrogen. Finally, we incubated the cantilevers in 10μg/ml streptavidin (Sigma-Aldrich, 85878) for at least one hour and later in 10μg/ml biotin-conjugated rat anti-mouse CD43 monoclonal antibody solution (BD Biosciences, 553269), also for 1h hour.

9.3 Experimental procedure

Experiments were performed in special petri dishes described in Subsec. 9.2.1 to separate T cells from B cells. The B cells were plated on the PLL coated side of one these petri dish at least 15 min before the experiment to ensure firm attachment of the cells to PLL. Then, an antibody coated cantilever chip was mounted on the AFM head. By approaching the protein repellent side, sensitivity was measured as specified in Subsec. 5.3.2. Next, T cells were injected into the petri dish. After a short sedimentation time of roughly one minute cells could be picked up from the bottom and be moved to the other, PLL coated, side. This procedure is outlined in Fig. 9.5. First, a T Cell was gently collected onto the cantilever. To this end, the cantilever was hovered above a T cell and then slowly approached until contact was established, Fig. 9.5 A-B. Since binding of the T cell to the antibody coated cantilever is firm and instantaneous, only small pressure forces of 1-2nN were required to establish solid adhesion. T cell viability was checked by PI just before it was picked up. Subsequently, the cantilever carrying the cell was retracted at least 2000μm to guarantee that the border line separating the two petri dish domains was not hit during movement, Fig. 9.5 C-D. Finally, cantilever and T cell were placed right above a B cell resting on the PLL coated bottom, which was also checked for viability with PI before. At last, at a speed of 1μm/s the cantilever slowly approached the resting B cell until contact between both cells was established, Fig. 9.5 E. Again, we used setpoints between 0.5 and 2nN to press the two cells together. Note, that due to the viscous properties this pressure is pretty soon dispersed throughout the cell. After a given contact time T_C the two cells were separated from each other by retracting the cantilever over a range of around 90μm, Fig. 9.5F. The force required to separate the two cells was measured and represents the interaction strength between a cell conjugate.

9.4 Total separation force dynamics for 3B11/LK35.2 pairs

We performed over 300 3B11/LK35.2 cell-cell separation experiments at the AFM. Such a high number of experiments is not achievable with the cell stretcher. More than half of these experiments failed because of technical errors and motility of the cells. Especially at later time points, 30 and 60 minutes, experiments were difficult to perform and fail rates grew with longer contact times. Cells started to move, separate or slided into a

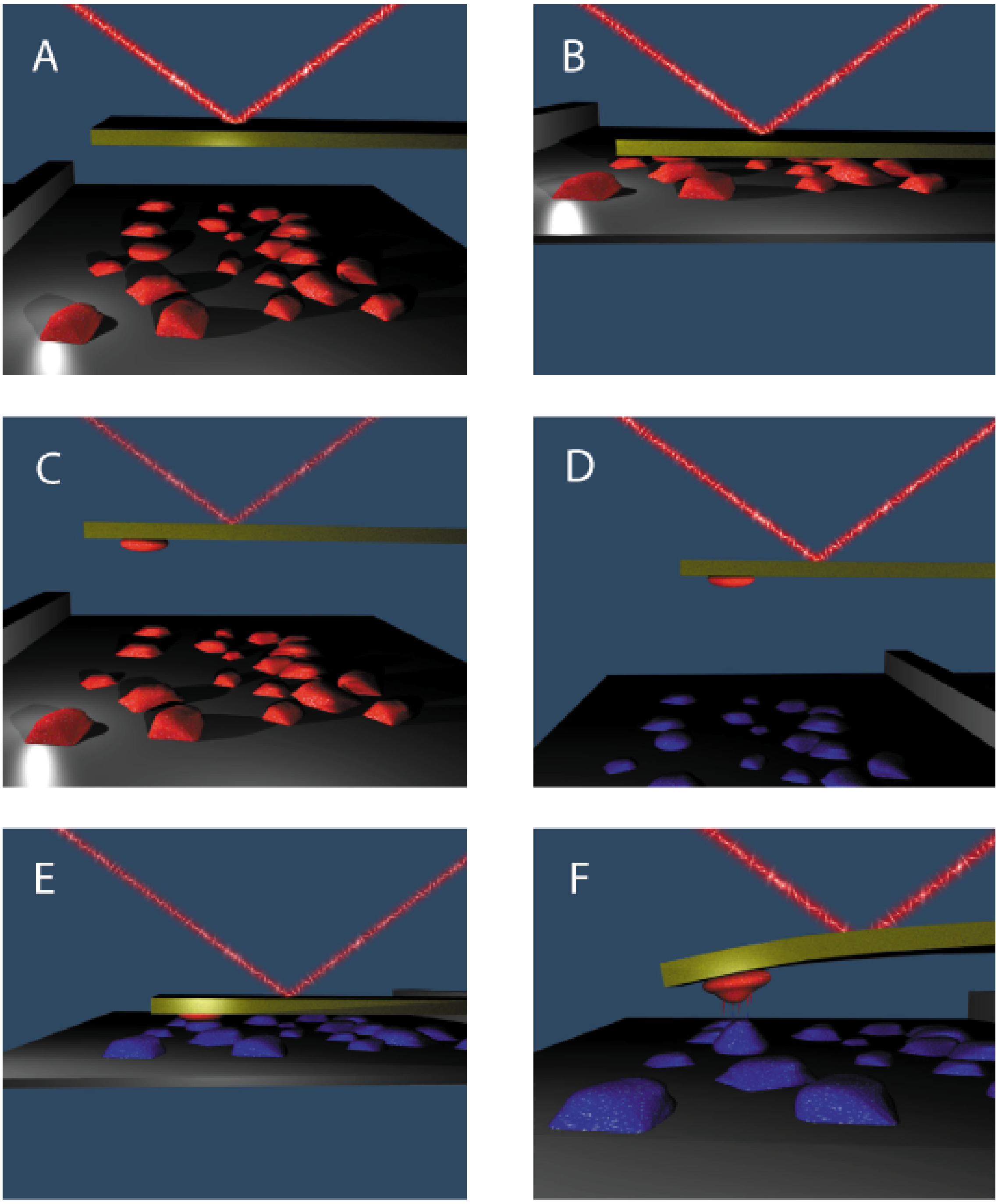

Figure 9.5: Illustration an AFM Cell Separation Experiment: A T cell is approached and picked up by the cantilever (A-C). The cantilever is then moved to the petri dish side where the B cells were placed before. Afterwards, T cell and cantilever are moved on top of an isolated, non-dead B cell, which is then approached until contact between the two cells is established. After a certain contact time T_C the cells are separated and a force curve is recorded.

parallel position, such that the AFM cantilever touched both cells. In some cases, cells were not separated but instead lifted from the petri dish in pairs. In other cases the T cell detached from the cantilever and stayed coupled to the B cell. Moreover, we used T cells coupled to the cantilever only for a single adhesion experiments. Many studies [157, 159, 176–178] engage cells for several subsequent measurements. The reason for this is quite simple: placing a cell onto a cantilever is a difficult task and thus many studies are performed using the same cell over and over again. We doubt that this is a good idea. In cell stretcher experiments we see that the cell membrane is damaged during separation. Even a recovery time of a few minutes, employed in many studies, might not be long enough to reestablish the pre-experimental situation, which is necessary if measurements ought to be comparable. Moreover, we often observed that the cell died soon after the experiment. Thus, we used cells only once.

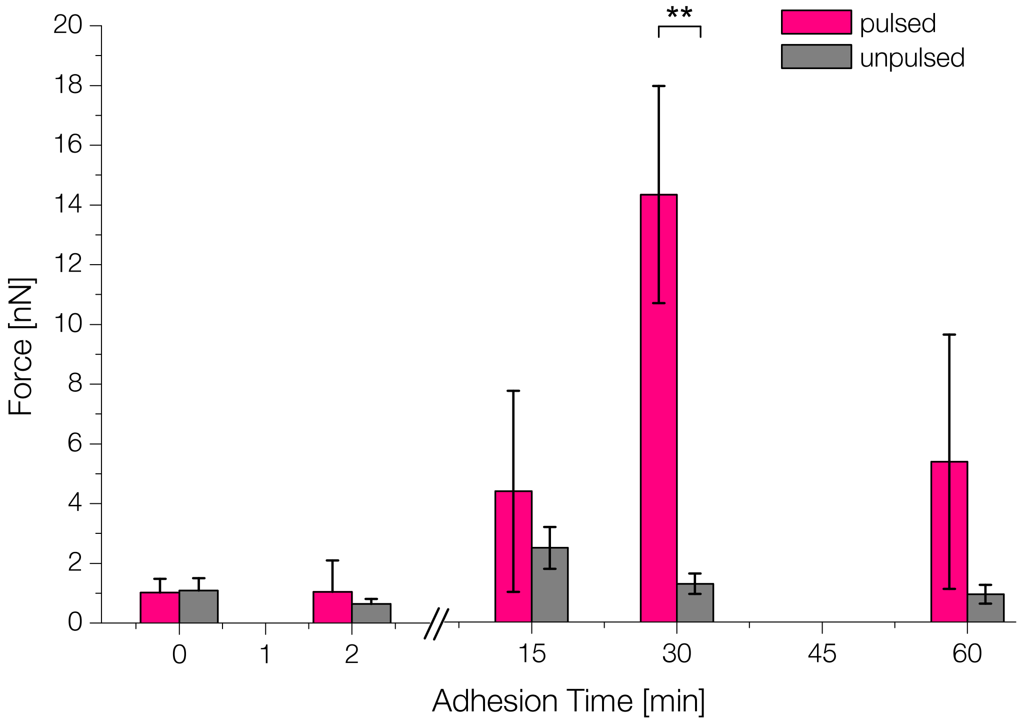

Figure 9.6: 3B11/LK35.2 Separation Force Dynamics: We measured separation forces in 3B11/LK35.2 cell conjugates for contact times between 0–60 minutes with pulsed (pink) and unpulsed (grey) LK35.2 cells. Forces to separate the cell conjugates are comparable in the first few minutes but start deviating at later time points. Error bars denote SD of mean.

In Fig. 9.6 the time dynamics of 3B11/LK35.2 cell conjugate experiments is shown. We measured pulsed cell pairs, i.e. where antigen was presented on the B cells and as control experiment we measured the same cells without peptide on their MHCs. We usually performed pulsed and unpulsed experiments on the same day for a specific contact time T_C to obtain comparable results. That said, we did not observe any deviation of force values depending on the day of experimentation. The graph in Fig. 9.6 includes 92 successful measurements in total. The results are also summarized in Table 9.1. At $T_C =$ 0 min, cells were pressed against each other until the setpoint was reached and separated right after. This allowed the cells to be in contact for around 1-3 seconds. Separation forces calculated as standard mean over all 0 min experiments yield similar values for pulsed and control cell pairs, 1.018 ± 0.458 pN and 1.083 ± 0.829 pN (Standard Deviation (SD)), respectively. Results are similar after 2min of contact. After $T_C = 15$ min, both, the pulsed and control pairs showed higher separation forces at, 4.379 ± 3.368 pN and 2.48 ± 1.710 pN, respectively.

Table 9.1: 3B11/LK35.2 experiments with the AFM.

Contact Time [min]	**Mean separation force and SD** [nN]	
	pulsed	unpulsed
0	1.018 ± 0.458	1.083 ± 0.829
2	1.042 ± 1.048	0.642 ± 0.746
15	4.379 ± 3.368	2.48 ± 1.710
30	14.312 ± 3.636	1.280 ± 0.902
60	5.365 ± 4.254	0.935 ± 0.543

At $T_C = 30$ min we observe a mean separation force of 14.312 ± 3.636 pN for pulsed pairs, which represents a more than 10-fold increase compared to 1.280 ± 0.902 for control pairs. Significance levels are high, a Student's t-test yields $p < 0.0001$ for the null hypothesis. After an hour, pulsed values drop to 5.365 ± 4.254 pN and unpulsed to 0.935 ± 0.543 pN. In a few experiments with pulsed B cells we observed forces, which were even higher than 20nN, but we could not resolve these measurements since the T cell was ripped from the cantilever during separation.

In Fig. 9.7 scatter plots for $T_C = 15$, 30 and 60 min are shown in the pulsed and unpulsed case. At 15 min and 60 min wee see a mixed picture. In pulsed experiments, some cells started to adhere quite strongly after 15 min, and some were still strongly attached even after 60 min. But averaging over all experiments, the increase and subsequent decrease in total adhesion forces for pulsed cells prevails. In the unpulsed case, forces remained low over the entire time spectrum, although we see a slight increase after 15 min, which is not significant. In Fig. 9.8 a histogram is shown, which includes every control (unpulsed) experiment.

We measured contact zones in pulsed and unpulsed conjugates with MIFC[2], which combines the advantages of a FACS and a fluorescence microscope [179], see appendix for details. In this assay a high number of the two cell populations are mixed and then analyzed in the FACS after a certain time. Note, that this mixing time cannot be compared with our contact time T_C in AFM measurements since we do not know when conjugates start to form. The results are shown in Fig. 9.9. Contact zones are roughly 10 µm in diameter for pulsed and unpulsed cells. However, a slight difference of 6% is seen between the two populations. A length of 10 µm translates into a radius of 5 µm, since in MIFC experiments a side view projection of the interface is seen, like in Fig. 9.2. Notably, the contact zones sizes remain constant over a long period of time for both populations. Using these contact zone length sizes and cell sizes obtained before and after every experiment

---

[2] Experiments were kindly performed by Guido Wabnitz, Uni Heidelberg.

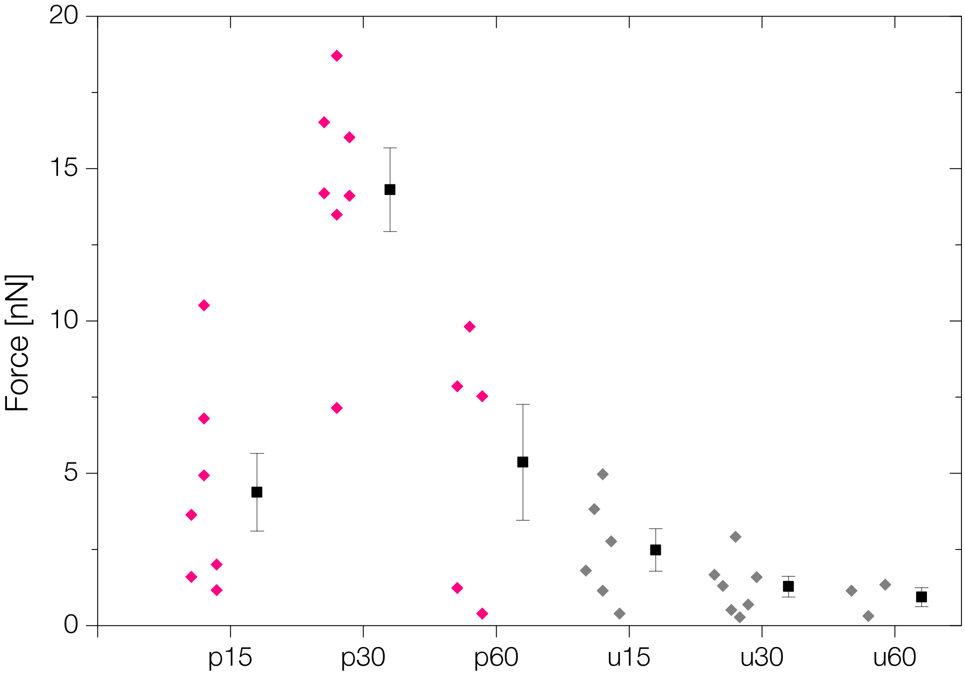

Figure 9.7: Scatter plots for 15, 30 and 60 min experiments, pulsed and unpulsed, including mean and SE of mean. Note, that not every experiment is displayed, since some data points overlap. p15, p30 and p60 denote pulsed experiments (pink diamonds) at 15, 30 and 60 min, respectively. Similarly for unpulsed experiments (gray diamond) used u15, u30 and u60.

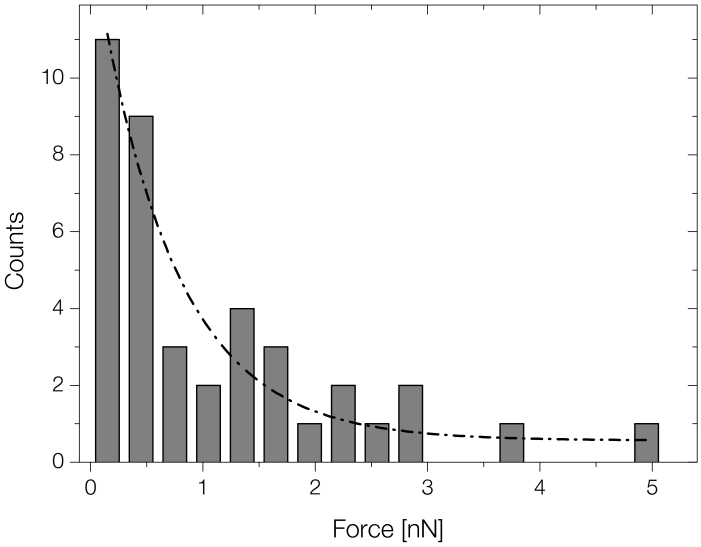

Figure 9.8: Histogram showing all experiments performed with unpulsed B cells. A simple exponential decay is fitted through the data.

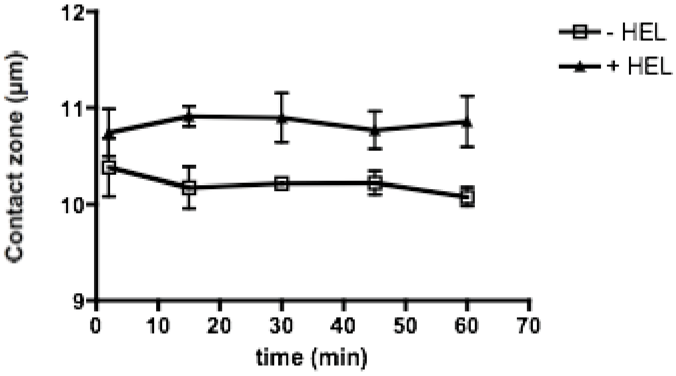

Figure 9.9: Contact zone of 3B11/LK35.2 conjugates over time: we analyzed cells couples using Multispectral Imaging Flow Cytometry (MIFC), which combines the advantages of a flow cytometer and a fluorescence microscope. Here, contact zones were defined as mature synapses if both CD3 and CD18, the β-subunit of LFA-1, were enriched in the contact zone, see Fig. 9.2. Courtesy of Guido Wabnitz, Uni Heidelberg.

we can estimate the force area after 30 min in the pulsed case as

$$\sigma = \frac{F_{pulsed}(30\mathrm{min})}{\pi(5\mu\mathrm{m})^2} \approx 0.18\,\mathrm{nN}/\mu\mathrm{m}^2. \tag{9.1}$$

9.4.1 Discussion

Comparing our results, we conclude that the range of the measured forces agrees pretty well to previous studies. Most total adhesion experiments, including long-time adhesion assays, have been performed by micropipette aspiration. The underlying reason is that the cells are held tightly and cannot escape when they are partly aspirated. On an AFM cantilever however, cells can move rather freely and might migrate away.

In micropipette experiments, Sylvie Dufour and co-workers have shown that tight cell-cell junctions require up to 400 nN to be separated, which build up over the course of 60 min [108]. Considering that tight-junctions are among the strongest and longest interaction between cells, e.g. for cells in tissues, 20 nN as order of magnitude seem reasonable for a transient cell-cell bond like a T cell/APC conjugate. Short-time AFM studies yield similar results in the low nN range [177, 180] and AFM studies with a cell and a layer of cells yield values in the 20 nN range [176]. But it is difficult to compare these results with our measurements since the cell types differ vastly.

Much closer to our system, Sung K. et. al. measured the junction avidity of cytolytic T cells (F1) and their target cells (JY), also employing micropipettes. They obtained a value of $\sigma = 1.5 \times 10^4$ dyn/cm^2 for F1/JY pairs, which is 1.5 nN/µm^2 converted to our scales. Even though it is not perfectly possible to measure the interaction surface of the cells during AFM measurements, we can roughly estimate the surface by observations of the MIFC analysis as explained above. Thus, we obtain a value of $\sigma \approx 0.2$nN/µm for pulsed pairs, which an order of magnitude below what Sung measured. Their simple control experiment with JY/JY couples resulted in $\sigma = 1.2 \times 10^3$ dyn/cm^2, which is also 10-fold larger than our control. This might indicate that we overestimate contact areas. Assuming a radius of roughly 2.0µm yields very good agreement of our studies. 2.0µm is a radius which correlates very well to IS sizes measured before [78], see Fig. 9.16. An overestimation is not unlikely, since in MIFC we examine cell conjugates from the side, which allows for a rough estimate only. Also, there we took the sum of pSMAC and cSMAC surface areas, which definitely contribute differently to overall adhesion strength.

Of course, another reason for discrepancy might be that cytolytic T cells require stronger adhesion in order to perform their cytotoxic function.

9.5 Single rupture events

We evaluated single rupture t-events and j-events for in 3B11/LK35.2 separation measurements. We introduced these AFM force spectra features in Sec. 5.2.

9.5.1 t-events

T-events are rupture events in the force spectrum, which are purely viscous in nature: their stiffness or slope is zero ($k = 0$), cf. Sec. 5.2 and Fig. 5.4. These t-events correspond to the tethers observed in the cell stretcher device like the one shown in Fig. 8.6. In contrast to the cell stretcher, the AFM is able to resolve the rupture of such membrane tethers. These are viscously pulled out of the membrane resevoir during the last part of separation measurement, which means that these ruptures most likely occur between proteins which are not coupled to the cytoskeleton: otherwise these ruptures would be have a negative slope and resemble *j-events*. In contrast to other studies we see differences in the most probable rupture forces after 30 min of contact time [174], which we will now explain in more detail.

Table 9.2: 3B11/LK35.2 t-events.

$\mathbf{T_C}$ **[min]**	**Most probable rupture force f* [pN]**[a]				**Significance**[b]
	events	pulsed	events	unpulsed	(t-test p-value)
0	18	38.4 ± 19.1	33	45.8 ± 56.0	
2	171	50.9 ± 90.3	92	52.6 ± 36.7	
15	62	118.3 ± 88.5	68	116.7 ± 89.0	
30	69	143.8 ± 100.4	61	41.3 ± 24.8	** ($p < 0.001$)
60	36	114.7 ± 81.6	18	45.4 ± 32.5	** ($p < 0.001$)

---

[a] and SD

[b] Here, we compare pulsed to unpulsed populations at the same contact time.

The number of t-events for each contact time and the respective most probable rupture forces f^* including their standard deviation are summarized in Table 9.2. In Fig. 9.10 histograms of all force steps in t-events for $T_C = 2$ min and $T_C = 30$ min are shown. We observe a big overlap between pulsed and unpulsed tether rupture forces after 2 min of contact time. The most probable rupture forces f^* obtained as mean value are 50.9 ± 90.3

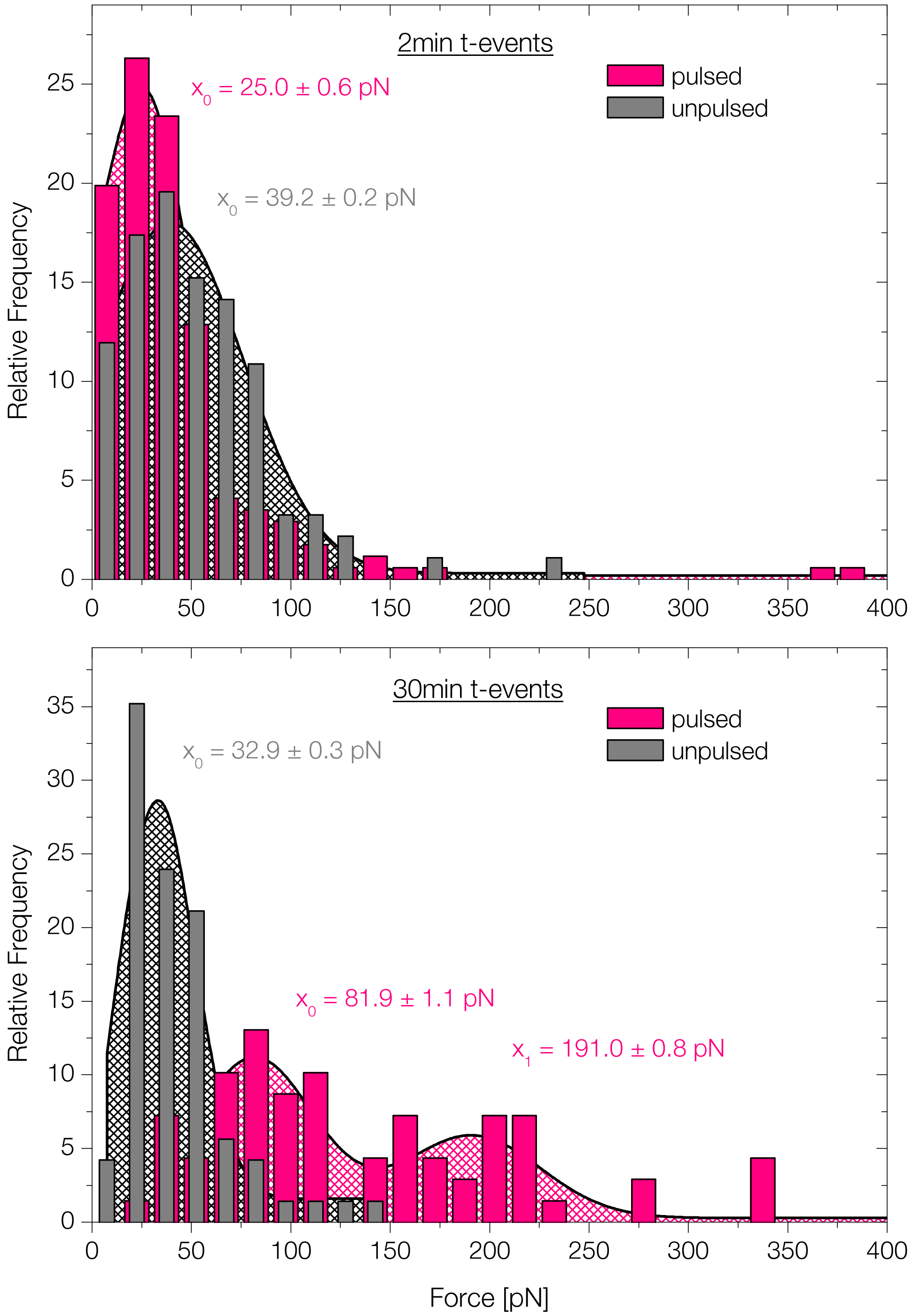

Figure 9.10: Single rupture t-events for 2 and 30 minutes of adhesion: After 2 min both, pulsed and unpulsed, t-events show similar most probable mean rupture forces. A different picture is seen for $T_C = 30$ min. There, rupture forces increase in pulsed experiments but remain low for unpulsed. A Gaussian distribution fits the 2 min events and 30 min unpulsed, whereas a double Gaussian was used in the 30 min pulsed case.

pN and 52.6 ± 36.7 pN, respectively. Likewise, a Gaussian curve to these distributions yields values of 25 pN for pulsed and 39 pN for unpulsed values. This corresponds very well to other studies, which have found similar values around 30-50 pN for t-events [66, 157, 174]. But, unlike other studies we evaluated t-events after contact times larger than 2 min, which yields very interesting results. In both cases, pulsed and unpulsed, we see a significant increase in mean rupture forces after a contact time of $T_C = 15$ min up to 118.3 ± 88.5 pN and 116.7 ± 89.0 pN, respectively. After 30 min we observe a significant decrease for the unpulsed population and an increase for the pulsed population, which is almost significant (p = 0.064). Going towards 60 min we observe a that both populations, pulsed and unpulsed, do not differ significantly from their 30 min mean rupture force values. We interpret the increase of mean rupture forces for tethers as increases in number of bound adhesion complexes per tether, i.e. an increase of valency.

For tethers, association to the cytoskeleton can be neglected since tethers are very long structure detached from the inner core of the cell. Another indication that the cells use valency regulation is seen dramatically in Fig. 9.10. There, we plotted histograms for $T_C = 2$ min and 30 min for pulsed and unpulsed t-event rupture forces. In contrast to $T_C = 2$ min rupture forces differ significantly after contact times of 30 min. A double Gaussian can be fitted to the pulsed values at 30 min, indicating that we measured double ruptures.

In Fig. 9.11 we have plotted all t-events distributions and their respective means including the error of the mean (standard error). There, we use p0, p2, p15, p30, p60 and u0, u2, u15, u30, u60 to indicate pulsed and unpulsed at the various contact times T_C.

9.5.2 j-events - dynamic force spectroscopy

In contrast to t-events, j-events are viscoelastic in nature and are used to probe the stiffness of a bond, see Sec. 5.2. They are well described by Bell's theory and as a corollary to his equation (Eq. 1.1) the probability of unbinding of an adhesion complex as a function of pulling force f is given by [53]

$$P(f) = k_{\mathrm{off}}^{0} \exp\left(\frac{f\,\rho}{k_B T}\right) \exp\left(\frac{k_{\mathrm{off}}^{0} k_B T}{\rho\, r_f}\left[1 - \exp\left\{\frac{f\,\rho}{k_B T}\right\}\right]\right). \tag{9.2}$$

By differentiation it follows that the most probable unbinding force reads as

$$\begin{aligned} f^* &= f_0 \ln\left(\frac{r_f}{k_{\mathrm{off}}^{0} f_0}\right) \\ &= \frac{k_B T}{\rho} \ln\left(\frac{\rho}{k_{\mathrm{off}}^{0} k_B T}\right) + \frac{k_B T}{\rho} \ln(r_f), \\ &= a \cdot b + a \ln(r_f) \end{aligned} \tag{9.3}$$

where $f_0 = k_B T/\rho$, like introduced in Subsec. 1.5.1. We evaluated j-events and plotted rupture forces against $\ln(r_f)$, which we calculated by the slope of each single j-event. The result is shown in Fig. 9.12. Two distinct regimes are recognized and fitted to Eq. 9.3 to obtain the parameters ρ and k_{off}^{0}. Bell model parameters are compiled in Table 9.3. The two regimes indicate that separation requires overcoming at least two activation potential barriers which can be related to the slow and fast loading rate regime, respectively [53].

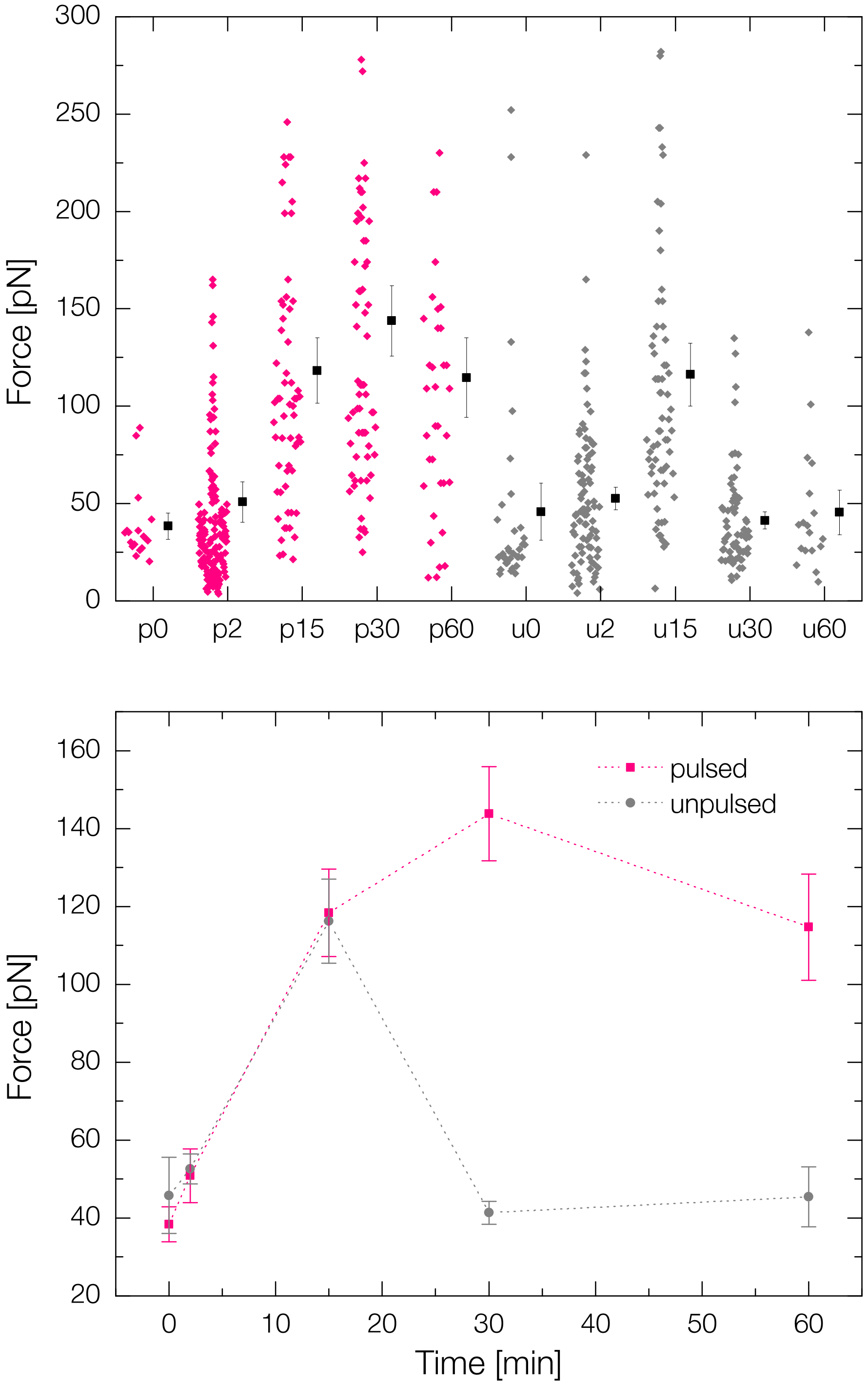

Figure 9.11: Upper panel: Rupture force distributions of all t-events in 3B11/LK35.2 AFM experiments plotted as scatter diagram. Each diamond represents a t-event. p0, p2, p15, p30, p60 and u0, u2, u15, u30, u60 indicate pulsed and unpulsed at the various contact times T_C, respectively. Lower panel: Most probable rupture forces plotted over contact time T_C. Note, that the connecting lines are meant to be a guide to the reader's eye, only.

Table 9.3: Bell model parameters for j-events 3B11/LK35.2 obtained from fit and their respective SE.

slow regime (1-100 pN/s)			**fast regime** ($>$ 100 pN/s)		
ρ	$=$	$6.80 \pm 1.30\,\text{Å}$	ρ	$=$	$0.41 \pm 0.04\,\text{Å}$
k^0_{off}	$=$	$0.20 \pm 0.05\,s^{-1}$	k^0_{off}	$=$	$0.80 \pm 0.33\,s^{-1}$

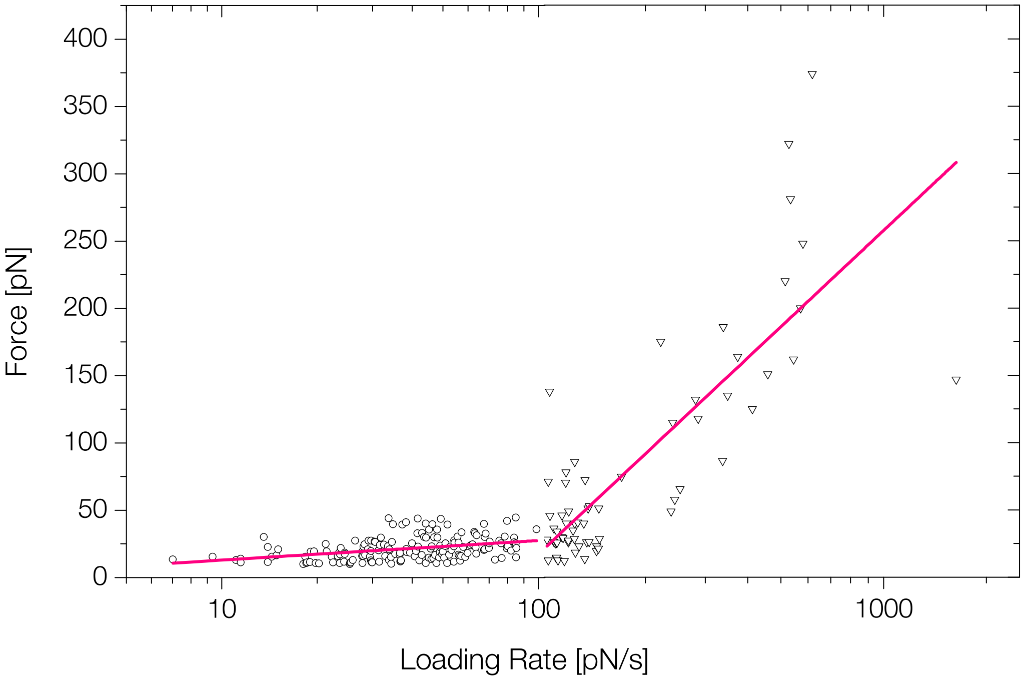

Figure 9.12: We plotted all j-event rupture forces as function of $\ln(r_f)$. Two linear regimes, slow and fast loading, are visible.

Several things have to be noted: we did not calculate mean rupture forces for individual loading rates, but rather plotted every data point we had for fitting which was due to the number of force curves available. So, we plotted every data point and fitted $\ln(r_f)$ plots through the data cloud. Still, the fitted curves work quite well and show two distinct loading rate regimes, 1-100 pN/s and above 100 pN/s. By far the most interesting observation is shown in Fig. 9.13: the high loading rate regime is populated almost entirely by pulsed measurements after $T_C = 2$ min. This shows that single molecule rupture events gain in strength over time and that experiments that concentrate on very short contact times (below 1 s) will ignore effects which obviously appear in long time adhesion.

The loading rate numbers we achieve are remarkably low for AFM measurements and are not well accessible in studies, which employ hybrid experiments [62, 181, 182]: cantilevers carrying a cell approach a ligand coated surface and subsequently retract. Although, in

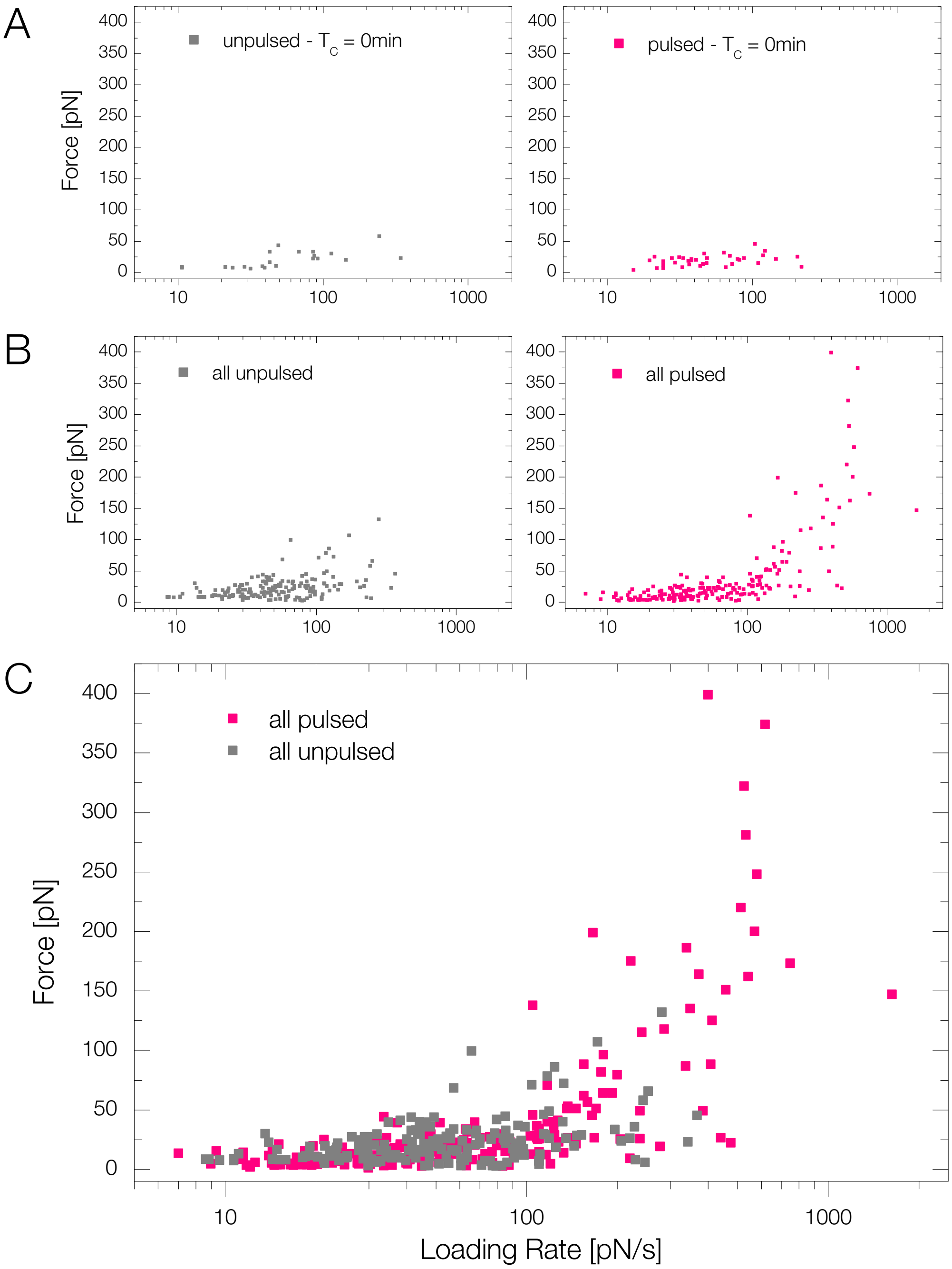

Figure 9.13: j-events plotted over loading rate r_f for unpulsed and pulsed experiments. (A) j-events for $T_C = 0$ min in unpulsed and pulsed experiments. (B) All unpulsed and pulsed j-events. (C) Combined graph, which shows that the high loading rate regime is populated almost entirely by pulsed measurements.

these experiments the interaction is well defined. In our case we are not certain which receptor-ligand pair is responsible for the loading rate dependent increase in rupture forces. Zhang et. al. measured forces between LFA-1 expressing T cell hybridoma (3A9) attached to an AFM cantilever and a surface coated with ICAM-1. They identified regimes that are different from ours: 20 pN/s – 10^4 pN/s and 10^4 pN/s – 5×10^4 pN/s. We are inclined to think that their loading rates might be too high for the lower regime that we measure. Also, the observation that only pulsed measurements after 2min populate the higher regime indicates the activation of the integrins. Thus, measuring cell/cell interactions allows us to study proteins in their native environment and at loading rates on scales which are not accessible in hybrid experiments, where one cell is replaced by a surface. Even worse, these setups might measure mainly interactions of activated proteins since loading rates and respective forces measured there are mostly higher than 1000 pN/s. Whereas loading rates in cell/cell setups are lower like in our experiment and in [157]. This is attributed to the damping effect the cell as a whole has. Our maximal loading rates calculate as $r_f = k_{\text{cantilever}} \times v \approx 10^5$ pN/s, which is much higher than loading rates we observe in the spectra. Simply, speaking the cell, which is attached to the pulling cantilever damps the loading rate and, hence, bonds at the cell-cell interface break at slower rates. Moreover, in our case the ligand is on a cell as well, not on a stiff surface, which represents another viscoelastic element that damps r_f. Hence, we believe that our method measures protein interaction in their native environment and at loading rates observed in nature.

9.6 1934.4/L cells experiments

Separation forces for another pair of cells were measured: We used L cells, which are a cultured line of C3H mouse fibroblast, as APC and 1934.4 CD4+ [183] as T cells. These L cells do not express ICAM-1, which is shown by FACS analysis, displayed in Fig. 9.14. L cells were pulsed for 2 hours with 1mg/ml Q-MBP peptide, which is specifically recognized by 1934.4 T cells.

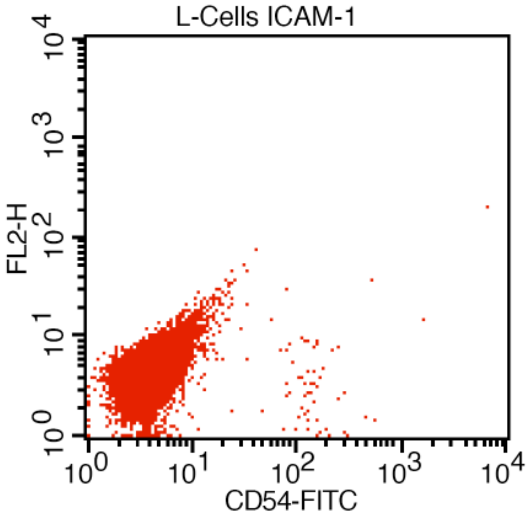

Figure 9.14: ICAM expression in L cells measured with FACS: L cells do not express the Intercellular Adhesion Molecule-1 (ICAM-1), which is also known as CD54.

We did not perform long-time contact measurements since without ICAM-1 no increase in adhesion like in the case of 3B11/LK35.2 is expected. We compared pulsed and unpulsed L cells with an adhesion time of 2 min and obtained separation forces of F = 1.166 ± 0.085 nN and 0.392 ± 0.273 nN, respectively. The measurements are summarized and visualized in Fig. 9.15. In comparison to the first couple 3B11/LK35.2 the distributions for L cell/1934.4 pairs is rather narrow and not as spread. Even though the mean separation force in pulsed 3B11/LK35.2 experiments with $T_C = 2$ min is slightly larger compared to unpulsed experiments (1.042 ± 1.048 nN vs. 0.642 ± 0.746 nN), statistically these two populations are not distinguishable. Not so in the case of 1934.4/L cells: The difference is visually (see Fig. 9.15) and statistically distinct (p-value < 0.001).

This clearly indicates that the main contribution of adhesion, even at $T_C = 0$ min and 2 min, is contributed by LFA/ICAM interactions in the case of 3B11/LK35.2 couples, where the APC expresses ICAM in contrast to the L cells. An interesting future experiment would involve L cells transfected with ICAM to measure the exact contribution of ICAM to adhesion.

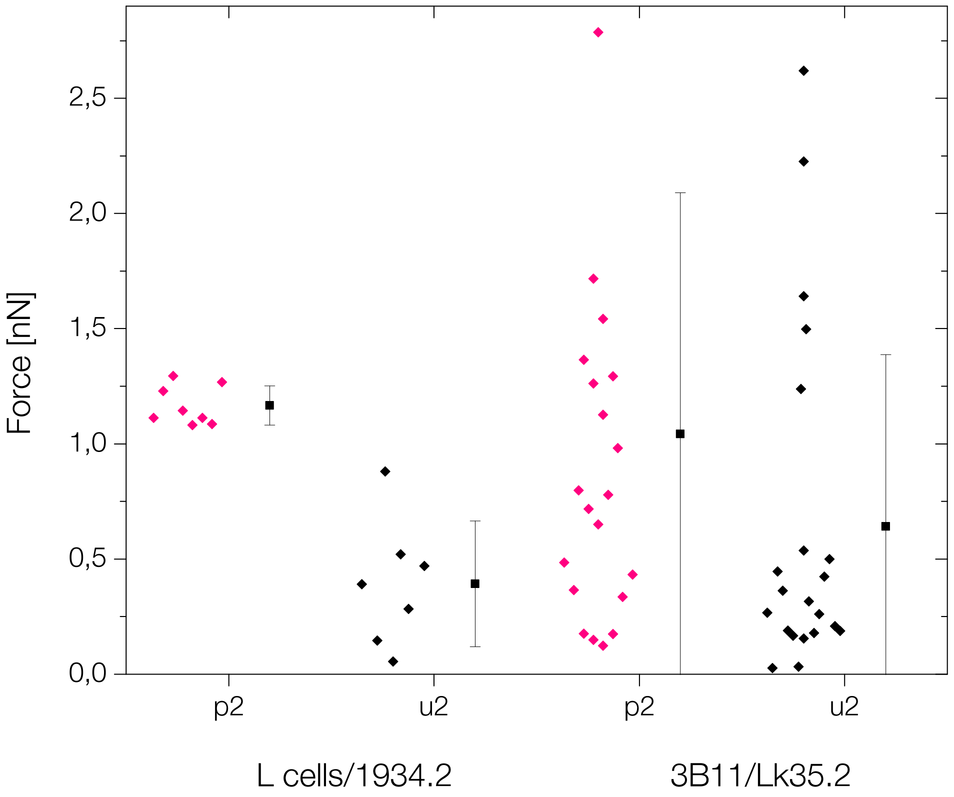

Figure 9.15: 3B11/LK35.2 compared to 1934.4/L cell experiments for $T_C = 2\text{min}$. Compared to 3B11/LK35.2 experiments, mean values and populations are quite distinct in pulsed and unpulsed 1934.4/L cell measurements. Since L cells are ICAM-1 deficient this could indicate that the significant difference in separation force results stems from the specific peptide on the L cell's MHC, which binds to the 1934.4 T cell receptor.

9.7 Discussion

We have successfully measured the dynamic separation forces in T cell/APC conjugates with AFM. Using single rupture events we shed light on the underlying protein interactions in cell-cell adhesion, which helped us to gain more information than just evaluating total adhesion forces.

Before, people have proposed that AFM is not an appropriate tool to investigate long time adhesion since cells are motile and drifts prevent experimental stability. In 2002, Benoit and co-workers stated

> *“Due to these drift effects of the force detection system the duration of controlled contact between cells is limited to a few minutes.”* [159]

We showed that, still, atomic force microscopy is capable of measuring long-time adhesion forces and their effects: a single measurement yields total adhesion forces as well as molecular features of the interaction. Our results show, that T cells adhere strongly to APC if cognate peptide is present. By measuring cells which do not express the main adhesion contributor LFA-1, we could show that the peptide interaction is below 2 nN and can thus not be responsible for the high adhesion forces. Rather, cells actively react to the presence of peptide and activate their integrins by accumulation (*t-events*) and activation (*j-events*).

Accumulation time-scale observed for tethers corresponds remarkably well to other studies that see the pSMAC, where the adhesion molecules are located, forming fully after 10-15 min Fig. 9.16. The graph E in Fig. 9.16 resembles pretty remarkably what we have measured in t-events and, thus, corresponds to Fig. 9.11 (lower panel). The rising number of adhesion proteins in the contact interface correlates to the increase in rupture force in our t-events.

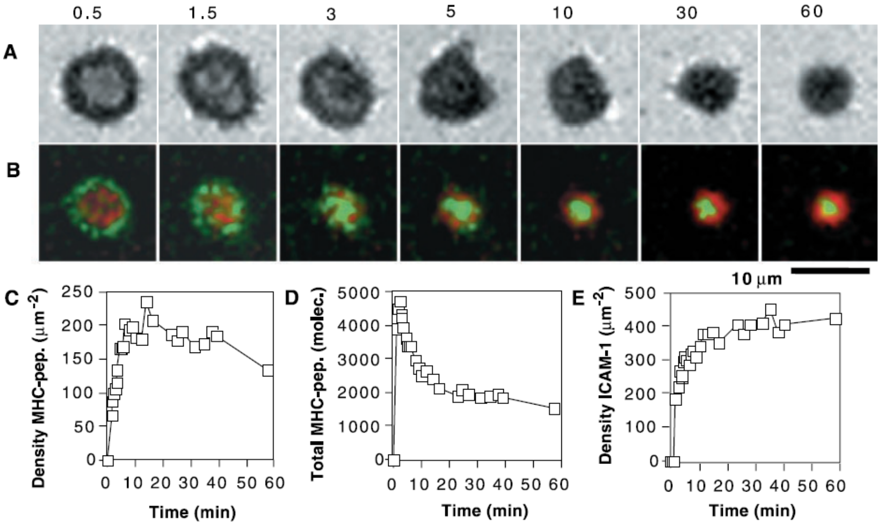

Figure 9.16: Immune synapse formation: (B) Images of MHC-peptide (green) and ICAM-1 (red) accumulation. (E) Density of accumulated ICAM-1. Adapted from [78].

The increase and subsequent decrease in tether rupture forces between 15 and 30 min in the unpulsed case indicates that T cells require this time span to realize the absence of peptide of the apposed cell surface. Since only a tiny fraction of MHC are loaded with foreign peptide, it might actually take this time to integrate all signals and to confirm that there is no peptide.

j-events helped us to identify to loading rate regimes for rupture forces which are perfectly fitted by the theoretical Bell model. In the case of present peptide j-events show that the cell can react on a faster time-scale. After two minutes a higher loading regimes is seen in rupture forces indicating that integrins either become activated (affinity regulation) or attached to the cytoskeleton (adhesion strengthening). Future experiments including new theoretical frameworks might be able to resolve which mechanism is responsible for the increase.

Part IV

Conclusion and Outlook

Chapter

10

Conclusion

Quantifying separation forces between cells has been investigated for over 70 years because it has been known for a long time that cell adhesion plays a major role in many cellular processes. In our immune system T cells must first engage and communicate with antigen-presenting cells (APCs) to identify intrusion of pathogens. The details of this adhesion process are intriguing and even though it has been studied extensively our understanding of this complex and fascinating recognition mechanisms developed by nature is still very rudimentary. Advances in biophysical techniques allow nowadays precise measurement of forces in cell conjugates and start revealing the underlying protein dynamics. In this study, for the first time, we successfully implemented a protocol to measure T cell/APC separation forces over a wide range of contact times using atomic force microscopy.

The main objective of this work was to investigate separation forces that occur at the cellular level. Therefore, we could not falsify any of the three hypotheses defined in the motivation for this study, cf. Chapter 7:

1. Total adhesion forces increase over time in T cell/APC pairs where the APC carries peptide and decrease at later timepoints.
2. If no peptide is present on the APC, total adhesion forces remain unchanged at around 2-4 nN which is probably the background separation force for these cell corresponding to receptor-ligand pairs, ICAM-1 and LFA-1, which are present on these cells, since a fraction of these molecules is always in an active state.

Adding to this, when we investigated cells that do not carry the ICAM ligand (L cells), the background dropped and we could measure the contribution of pMHC/TCR binding after 2 min.

Moreover, when evaluating force spectra we realized that we could confirm the proposed model depicted in Fig. 7.1 on multiple levels. Looking at the details of AFM force curves, tethers rupture and *j-events*, clearly shows that cell adhesion is also significantly different when MHC molecules are loaded with cognate peptide. Tether rupture forces grow over time to reach a maximum at $T_C = 30$ min for pulsed cell pairs, indicating clustering of adhesion molecules, which correlates very well to density measurements of adhesion molecules at the contact interface in other studies [78]. This shows, that we can successfully measure increasing integrin aggregation using AFM. In the unpulsed case, molecules cluster after 15min but drop again, which signifies the time required for a cell to recognize that no foreign peptide is present on the APC.

When peptide was present *j-events* show that the cells react within 2 minutes of contact and either change the affinity state of their surface integrins or bind cytoskeleton to the cytoplasmic domain of the adhesion proteins, which is consistent with current theories: it is known that within minutes of T cell recognition of an APC, signaling is triggered that leads to rapid cytoskeletal polarization, involving actin polymerization, and microtubule re-organization [83, 184]. Probably, both of these effects play a role in increasing single rupture forces.

Summarizing, this study revealed biophysical characteristics of T cell/APC adhesion on several levels which are consistent which current theories and paradigms. Thus, the experiments performed in this thesis mark an important contribution to a better understanding of details governing immune cell interactions, in particular the formation, strength and onset in T cell/APC adhesion.

Chapter

11

Outlook

We have shown for the first time that the AFM is capable to measure long-time cell-cell adhesion forces and elucidated the protein interactions that are involved. However, many questions remain unanswered and the number of possibilities for future research are thus numerous.

Inhibition of integrin activation

We attribute the strengthening of adhesion to LFA-1 activation, thus, this hypothesis can be tested by suppressing the activation of integrins. Experiments with an inhibitor which suppresses integrin activation are under way. We performed some preliminary experiments with our collaboration partners, where the integrin activation inhibitor BIRT377 [185] was added in conjugate assays and lowered the fraction of T cell/B cell pairs in a conjugate assay. These promising results form the basis of future inhibition measurements at the AFM. Using BIRT377, in AFM experiments we hope to suppress cell adhesion in 3B11/LK35.2 experiments even when cognate peptide is present on MHC and expect values to drop to the unpulsed case.

Primary cells

It will be interesting to see how forces differ in primary cell pairs. So far, we have tried to measure several primary cell couples at the AFM and the cell stretcher but we could not conclude these experiments, since the handling of primary cells is much more difficult than cell lines. For one reason, because of their small size, future experiments with primary cells should employ smaller cantilevers with lower force constants. Moreover, it seemed that PLL was not the right choice for attaching the primary cells to glass which means that we have to establish a new protocol for measurements.

Biophysical characterization of membrane tethers

Even though this study was intended to measure differences in total adhesion, we gained additionally a great deal of insight into single molecule rupture events in our AFM spectra. In future experiments, we want to characterize tether formation using the model of Schmitz et. al. [66]. Employing their fitting routine might allows to gain more information of the onset of actin binding to the membrane receptors after contact cell-cell contact. This will help to elucidate further the internal protein coupling and respective signaling pathways which are triggered when a T cell encounters a cognate peptide carrying APC.

List of Figures

1.1 Structural components of a cell 4
1.2 Transmembrane adhesion molecules 7
1.3 Schematic of an adherens junction 8
1.4 Constant force applied to a bond 11
1.5 Loading rate dependence of adhesion bonds 12
1.6 Separation of two surfaces connected by receptor/ligand pairs 13
1.7 Leukocyte arrest 14

2.1 T cell-APC contact 16
2.2 Immune response caused by APC-T cell encounters 17
2.3 Side view of a mature immune synapse 17
2.4 Immune synapse formation 18

3.1 First cell-cell separation force measurements from 1944 21
3.2 1954 Cell Elastimer 22
3.3 Micropipette Aspiration Suction 23
3.4 Overview of micropipette aspiration techniques 24
3.5 Micropipette step pressure technique 25
3.6 Illustration of optical tweezers 27
3.7 Magnetic Tweezers Setup 28
3.8 Optical stretcher 29
3.9 Momentum transfer in light transmission 29
3.10 Uniaxial substrate stretching device 31

4.1 Schematic view of the cell stretcher apparatus 36
4.2 Cell stretcher microplates 36
4.3 Cell placement between two microplates 37
4.4 Cell Stretcher: experimental chamber and glass fiber 39
4.5 LabVIEW control program, main window 40
4.6 Early adhesion contrast experiments 41
4.7 Cell Stretcher in adhesion contrast mode 42
4.8 Processed cell stretcher images in adhesion contrast experiments 43
4.9 Compartment displacement in adhesion contrast experiments 44

5.1 First AFM Setup by Binnig et. al. 46
5.2 Force measuring principle of an AFM cell-cell experiment 47
5.3 AFM force spectrum illustration 48
5.4 Single ruptures of tethers in AFM spectra (t-events) 49
5.5 SE micrograph of an AFM Cantilever 50
5.6 Sensitivity calibration of an AFM cantilever 51
5.7 Microscopy Images of a Cell on AFM Cantilever 51

6.1 Schematic of a FACS machine 53
6.2 FACS Data of 3B11 and LK35.2 Cells 55

7.1 Inside-out signaling in T cell/APC adhesion 60
7.2 Integrin activation, switchblade model 61

8.1 Collecting Cells on the Bottom with the Cell Stretcher 64
8.2 Cell Stretcher Used a Single Cell Spectroscope 64
8.3 Representative Force in Cell-Cell Separation Experiment 66
8.4 Cell Conjugate Separation with the Cell Stretcher 67
8.5 Dendritic Cell scans T cell 68
8.6 Series images showing tethers in cell separation 69

9.1 Survival of CD4+T cell hybridoma 72
9.2 IL2 assay and immune synapse formation in 3B11/LK35.2 pairs 73
9.3 FACS data for 3B11/LK35.2 conjugate formation 74
9.4 Modified Glass Cover Slip 75
9.5 Illustration of an AFM Cell Separation Experiment 77
9.6 3B11/LK35.2 Separation Force Dynamics 78
9.7 Scatter plots for 15, 30 and 60 min experiments 80
9.8 Histogram of Unpulsed Separation Experiments 81
9.9 Contact zone of 3B11/LK35.2 conjugates over time 82
9.10 Single rupture t-events for 2 and 30 minutes of adhesion 84
9.11 Rupture Forces of t-events in 3B11/LK35.2 AFM experiments 85
9.12 j-event rupture forces as function of r_f 86
9.13 j-events plotted over loading rate 87
9.14 ICAM expression in L cells measured with FACS 89
9.15 3B11/LK35.2 compared to 1934.4/L cell experiments for T_C = 2min 90
9.16 Immune synapse formation 91

Bibliography

[1] Bruce Alberts. *Molecular Biology of the Cell*. Garland, 2006. 3, 5

[2] Raja Paul, Patrick Heil, Joachim P Spatz, and Ulrich S Schwarz. Propagation of mechanical stress through the actin cytoskeleton toward focal adhesions: model and experiment. *Biophys J*, 94(4):1470–1482, Feb 2008. 3

[3] H. Herrmann and U. Aebi. Intermediate filaments and their associates: multi-talented structural elements specifying cytoarchitecture and cytodynamics. *Curr Opin Cell Biol*, 12(1):79–90, Feb 2000. 3

[4] R. D. Goldman, S. Khuon, Y. H. Chou, P. Opal, and P. M. Steinert. The function of intermediate filaments in cell shape and cytoskeletal integrity. *J Cell Biol*, 134(4):971–983, Aug 1996. 4

[5] Clifford P Brangwynne, Frederick C MacKintosh, Sanjay Kumar, Nicholas A Geisse, Jennifer Talbot, L. Mahadevan, Kevin K Parker, Donald E Ingber, and David A Weitz. Microtubules can bear enhanced compressive loads in living cells because of lateral reinforcement. *J Cell Biol*, 173(5):733–741, Jun 2006. 4

[6] G. Wiche. Role of plectin in cytoskeleton organization and dynamics. *J Cell Sci*, 111 (Pt 17):2477–2486, Sep 1998. 4

[7] J. C. Jones, J. Asmuth, S. E. Baker, M. Langhofer, S. I. Roth, and S. B. Hopkinson. Hemidesmosomes: extracellular matrix/intermediate filament connectors. *Exp Cell Res*, 213(1):1–11, Jul 1994. 4

[8] E. Zamir and B. Geiger. Molecular complexity and dynamics of cell-matrix adhesions. *J Cell Sci*, 114(Pt 20):3583–3590, Oct 2001. 4

[9] Harald Herrmann, Harald Bär, Laurent Kreplak, Sergei V Strelkov, and Ueli Aebi. Intermediate filaments: from cell architecture to nanomechanics. *Nat Rev Mol Cell Biol*, 8(7):562–573, Jul 2007. 4

[10] Thomas D. Pollard and William C. Earnshaw. *Cell Biology*. Elsevier, 2002. 4, 7

[11] Nicole King, Christopher T Hittinger, and Sean B Carroll. Evolution of key cell signaling and adhesion protein families predates animal origins. *Science*, 301(5631):361–363, Jul 2003. 5

[12] J. Maynard-Smith and E. Szathmary. *The Major Transitions in Evolution.* New York: Oxford University Press, 1997. 5

[13] Scott A Nichols, William Dirks, John S Pearse, and Nicole King. Early evolution of animal cell signaling and adhesion genes. *Proc Natl Acad Sci U S A*, 103(33):12451–12456, Aug 2006. 5

[14] Bernhard Wehrle-Haller and Beat A Imhof. Integrin-dependent pathologies. *J Pathol*, 200(4):481–487, Jul 2003. 5

[15] Yan-Yang Zhao, Motoko Takahashi, Jian-Guo Gu, Eiji Miyoshi, Akio Matsumoto, Shinobu Kitazume, and Naoyuki Taniguchi. Functional roles of N-glycans in cell signaling and cell adhesion in cancer. *Cancer Sci*, 99(7):1304–1310, Jul 2008. 5

[16] B. M. Gumbiner. Cell adhesion: the molecular basis of tissue architecture and morphogenesis. *Cell*, 84(3):345–357, Feb 1996. 5

[17] David A Calderwood. Integrin activation. *J Cell Sci*, 117(Pt 5):657–666, Feb 2004. 6

[18] Yun-Bi Lu, Kristian Franze, Gerald Seifert, Christian Steinhäuser, Frank Kirchhoff, Hartwig Wolburg, Jochen Guck, Paul Janmey, Er-Qing Wei, Josef Käs, and Andreas Reichenbach. Viscoelastic properties of individual glial cells and neurons in the cns. *Proc Natl Acad Sci U S A*, 103(47):17759–17764, Nov 2006. 6

[19] Christopher V Carman and Timothy A Springer. Integrin avidity regulation: are changes in affinity and conformation underemphasized? *Curr Opin Cell Biol*, 15(5):547–556, Oct 2003. 6, 59

[20] Patrick T Caswell and Jim C Norman. Integrin trafficking and the control of cell migration. *Traffic*, 7(1):14–21, Jan 2006. 6

[21] Teijo Pellinen and Johanna Ivaska. Integrin traffic. *J Cell Sci*, 119(Pt 18):3723–3731, Sep 2006. 6

[22] David Traynor and Robert R Kay. Possible roles of the endocytic cycle in cell motility. *J Cell Sci*, 120(Pt 14):2318–2327, Jul 2007.

[23] Mark S Bretscher. On the shape of migrating cells – a ‚front-to-back' model. *J Cell Sci*, 121(Pt 16):2625–2628, Aug 2008. 6

[24] M. J. Humphries. Integrin structure. *Biochem Soc Trans*, 28(4):311–339, 2000. 6, 9

[25] Eliane J Müller, Lina Williamson, Carine Kolly, and Maja M Suter. Outside-in signaling through integrins and cadherins: a central mechanism to control epidermal growth and differentiation? *J Invest Dermatol*, 128(3):501–516, Mar 2008. 6

[26] A. J. Valentijn, N. Zouq, and A. P. Gilmore. Anoikis. *Biochem Soc Trans*, 32(Pt3):421–425, Jun 2004. 6

[27] A. Paul Mould and Martin J Humphries. Regulation of integrin function through conformational complexity: not simply a knee-jerk reaction? *Curr Opin Cell Biol*, 16(5):544–551, Oct 2004. 7, 59, 61

[28] P. L. Ryan, A. F. Valentine, and C. A. Bagnell. Expression of epithelial cadherin in the developing and adult pig ovary. *Biol Reprod*, 55(5):1091–1097, Nov 1996. 8

[29] B. P. Wijnhoven, W. N. Dinjens, and M. Pignatelli. E-cadherin-catenin cell-cell adhesion complex and human cancer. *Br J Surg*, 87(8):992–1005, Aug 2000. 8

[30] Clara Martinez-Rico, Frederic Pincet, Eric Perez, Jean Paul Thiery, Kazuya Shimizu, Yoshimi Takai, and Sylvie Dufour. Separation force measurements reveal different types of modulation of e-cadherin-based adhesion by nectin-1 and -3. *J Biol Chem*, 280(6):4753–4760, Feb 2005. 8, 24, 66

[31] V. Vasioukhin, C. Bauer, M. Yin, and E. Fuchs. Directed actin polymerization is the driving force for epithelial cell-cell adhesion. *Cell*, 100(2):209–219, Jan 2000. 8

[32] G. K. Ragsdale, J. Phelps, and K. Luby-Phelps. Viscoelastic response of fibroblasts to tension transmitted through adherens junctions. *Biophys J*, 73(5):2798–2808, Nov 1997. 8

[33] Elaine Fuchs and Srikala Raghavan. Getting under the skin of epidermal morphogenesis. *Nat Rev Genet*, 3(3):199–209, Mar 2002. 8

[34] R. O. Hynes. Integrins: a family of cell surface receptors. *Cell*, 48(4):549–554, Feb 1987. 9

[35] Richard O Hynes. Integrins: bidirectional, allosteric signaling machines. *Cell*, 110(6):673–687, Sep 2002. 9

[36] Thomas Ludwig, Robert Kirmse, Kate Poole, and Ulrich S Schwarz. Probing cellular microenvironments and tissue remodeling by atomic force microscopy. *Pflugers Arch*, 456(1):29–49, Apr 2008. 9

[37] F. G. Giancotti and E. Ruoslahti. Integrin signaling. *Science*, 285(5430):1028–1032, Aug 1999. 9

[38] E. Ruoslahti and B. Obrink. Common principles in cell adhesion. *Exp Cell Res*, 227(1):1–11, Aug 1996.

[39] S. P. Holly, M. K. Larson, and L. V. Parise. Multiple roles of integrins in cell motility. *Exp Cell Res*, 261(1):69–74, Nov 2000. 9

[41] R. J. Pelham and Y. Wang. Cell locomotion and focal adhesions are regulated by substrate flexibility. *Proc Natl Acad Sci U S A*, 94(25):13661–13665, Dec 1997. 9

[40] B. Geiger, A. Bershadsky, R. Pankov, and K. M. Yamada. Transmembrane crosstalk between the extracellular matrix–cytoskeleton crosstalk. *Nat Rev Mol Cell Biol*, 2(11):793–805, Nov 2001. 9

[42] H. B. Wang, M. Dembo, S. K. Hanks, and Y. Wang. Focal adhesion kinase is involved in mechanosensing during fibroblast migration. *Proc Natl Acad Sci U S A*, 98(20):11295–11300, Sep 2001. 9

[43] D. Riveline, E. Zamir, N. Q. Balaban, U. S. Schwarz, T. Ishizaki, S. Narumiya, Z. Kam, B. Geiger, and A. D. Bershadsky. Focal contacts as mechanosensors: externally applied local mechanical force induces growth of focal contacts by an mdia1-dependent and rock-independent mechanism. *J Cell Biol*, 153(6):1175–1186, Jun 2001.

[44] N. Q. Balaban, U. S. Schwarz, D. Riveline, P. Goichberg, G. Tzur, I. Sabanay, D. Mahalu, S. Safran, A. Bershadsky, L. Addadi, and B. Geiger. Force and focal adhesion assembly: a close relationship studied using elastic micropatterned substrates. *Nat Cell Biol*, 3(5):466–472, May 2001.

[45] Benjamin Geiger and Alexander Bershadsky. Exploring the neighborhood: adhesion-coupled cell mechanosensors. *Cell*, 110(2):139–142, Jul 2002.

[46] Tom Shemesh, Benjamin Geiger, Alexander D Bershadsky, and Michael M Kozlov. Focal adhesions as mechanosensors: a physical mechanism. *Proc Natl Acad Sci U S A*, 102(35):12383–12388, Aug 2005.

[47] Alexander Bershadsky, Michael Kozlov, and Benjamin Geiger. Adhesion-mediated mechanosensitivity: a time to experiment, and a time to theorize. *Curr Opin Cell Biol*, 18(5):472–481, Oct 2006.

[48] Donald E Ingber. Cellular mechanotransduction: putting all the pieces together again. *FASEB J*, 20(7):811–827, May 2006. 9

[49] Adam J Engler, Shamik Sen, H. Lee Sweeney, and Dennis E Discher. Matrix elasticity directs stem cell lineage specification. *Cell*, 126(4):677–689, Aug 2006. 9

[50] Z. Huang, S. Li, and R. Korngold. Immunoglobulin superfamily proteins: structure, mechanisms, and drug discovery. *Biopolymers*, 43(5):367–382, 1997. 9

[51] A. Radu Aricescu and E. Yvonne Jones. Immunoglobulin superfamily cell adhesion molecules: zippers and signals. *Curr Opin Cell Biol*, 19(5):543–550, Oct 2007. 9

[52] G. I. Bell. Models for the specific adhesion of cells to cells. *Science*, 200(4342):618–627, May 1978. 10

[53] E. Evans and K. Ritchie. Dynamic strength of molecular adhesion bonds. *Biophys J*, 72(4):1541–1555, Apr 1997. 10, 84

[54] Yuriy V. Pereverzev and Oleg V. Prezhdo. Universal laws in the force-induced unraveling of biological bonds. *Physical Review E (Statistical, Nonlinear, and Soft Matter Physics)*, 75(1):011905, 2007.

[55] Felix Hanke and Hans Jurgen Kreuzer. Breaking bonds in the atomic force microscope: Theory and analysis. *Physical Review E (Statistical, Nonlinear, and Soft Matter Physics)*, 74(3):031909, 2006.

[56] Philippe Robert, Anne-Marie Benoliel, Anne Pierres, and Pierre Bongrand. What is the biological relevance of the specific bond properties revealed by single-molecule studies? *J Mol Recognit*, 20(6):432–447, 2007. 14

[57] Emily B Walton, Sunyoung Lee, and Krystyn J Van Vliet. Extending bell's model: how force transducer stiffness alters measured unbinding forces and kinetics of molecular complexes. *Biophys J*, 94(7):2621–2630, Apr 2008. 10

[58] Henry Eyring. The activated complex in chemical reactions. *The Journal of Chemical Physics*, 3(2):107–115, 1935. 10

[59] H. A. Kramers. Brownian motion in a field of force and the diffusion model of chemical reactions. *Physica*, 7(4):284–304, April 1940.

[60] Peter Hänggi, Peter Talkner, and Michal Borkovec. Reaction-rate theory: fifty years after Kramers. *Rev. Mod. Phys.*, 62(2):251–341, Apr 1990. 10

[61] R. Merkel, P. Nassoy, A. Leung, K. Ritchie, and E. Evans. Energy landscapes of receptor-ligand bonds explored with dynamic force spectroscopy. *Nature*, 397(6714):50–53, Jan 1999. 10, 12, 26

[62] Ewa P Wojcikiewicz, Midhat H Abdulreda, Xiaohui Zhang, and Vincent T Moy. Force spectroscopy of LFA-1 and its ligands, ICAM-1 and ICAM-2. *Biomacromolecules*, 7(11):3188–3195, Nov 2006. 12, 86

[63] Emilie Perret, Anne-Marie Benoliel, Pierre Nassoy, Anne Pierres, Véronique Delmas, Jean-Paul Thiery, Pierre Bongrand, and Hélène Feracci. Fast dissociation kinetics between individual e-cadherin fragments revealed by flow chamber analysis. *EMBO J*, 21(11):2537–2546, Jun 2002.

[64] Bryan T Marshall, Krishna K Sarangapani, Jizhong Lou, Rodger P McEver, and Cheng Zhu. Force history dependence of receptor-ligand dissociation. *Biophys J*, 88(2):1458–1466, Feb 2005. 10

[65] P. Hinterdorfer, W. Baumgartner, H. J. Gruber, K. Schilcher, and H. Schindler. Detection and localization of individual antibody-antigen recognition events by atomic force microscopy. *Proc Natl Acad Sci U S A*, 93(8):3477–3481, Apr 1996. 11

[66] Julia Schmitz, Martin Benoit, and Kay-Eberhard Gottschalk. The viscoelasticity of membrane tethers and its importance for cell adhesion. *Biophys J*, 95(3):1448–1459, Aug 2008. 11, 84, 97

[67] Manoj Gopalakrishnan, Kimberly Forsten-Williams, Matthew A Nugent, and Uwe C Täuber. Effects of receptor clustering on ligand dissociation kinetics: theory and simulations. *Biophys J*, 89(6):3686–3700, Dec 2005. 12

[68] G. I. Bell, M. Dembo, and P. Bongrand. Cell adhesion. competition between nonspecific repulsion and specific bonding. *Biophys J*, 45(6):1051–1064, Jun 1984. 12

[69] Udo Seifert. Rupture of multiple parallel molecular bonds under dynamic loading. *Phys. Rev. Lett.*, 84(12):2750–2753, Mar 2000.

[70] T. Erdmann and U. S. Schwarz. Stability of adhesion clusters under constant force. *Phys. Rev. Lett.*, 92(10):108102, Mar 2004.

[71] Thorsten Erdmann and Ulrich S Schwarz. Bistability of cell-matrix adhesions resulting from nonlinear receptor-ligand dynamics. *Biophys J*, 91(6):L60–L62, Sep 2006. 12

[72] Vishwanath Ramachandran, Marcie Williams, Tadayuki Yago, David W Schmidtke, and Rodger P McEver. Dynamic alterations of membrane tethers stabilize leukocyte rolling on P-selectin. *Proc Natl Acad Sci U S A*, 101(37):13519–13524, Sep 2004. 13

[73] R. Alon, D. A. Hammer, and T. A. Springer. Lifetime of the P-selectin-carbohydrate bond and its response to tensile force in hydrodynamic flow. *Nature*, 374(6522):539–542, Apr 1995. 13

[74] J. Fritz, A. G. Katopodis, F. Kolbinger, and D. Anselmetti. Force-mediated kinetics of single p-selectin/ligand complexes observed by atomic force microscopy. *Proc Natl Acad Sci U S A*, 95(21):12283–12288, Oct 1998. 13

[75] M. B. Lawrence and T. A. Springer. Leukocytes roll on a selectin at physiologic flow rates: distinction from and prerequisite for adhesion through integrins. *Cell*, 65(5):859–873, May 1991. 13

[76] Ronen Alon and Michael L Dustin. Force as a facilitator of integrin conformational changes during leukocyte arrest on blood vessels and antigen-presenting cells. *Immunity*, 26(1):17–27, Jan 2007. 14, 15, 16, 60

[77] C. R. Monks, B. A. Freiberg, H. Kupfer, N. Sciaky, and A. Kupfer. Three-dimensional segregation of supramolecular activation clusters in t cells. *Nature*, 395(6697):82–86, Sep 1998. 15, 16

[79] D. M. Davis, I. Chiu, M. Fassett, G. B. Cohen, O. Mandelboim, and J. L. Strominger. The human natural killer cell immune synapse. *Proc Natl Acad Sci U S A*, 96(26):15062–15067, Dec 1999.

[78] A. Grakoui, S. K. Bromley, C. Sumen, M. M. Davis, A. S. Shaw, P. M. Allen, and M. L. Dustin. The immunological synapse: a molecular machine controlling T cell activation. *Science*, 285(5425):221–227, Jul 1999. 16, 59, 82, 91, 95

[80] J. Delon. The immunological synapse. *Curr Biol*, 10(6):R214, Mar 2000. 15, 19

[81] Charles A. Janeway, Paul Travers, Mark Walport, and Mark J. Shlomchik. *Immunobiology: The Immune System in Health and Disease - Sixth Edition.* Garland Science, 2007. 15

[82] Eleonora Market and F. Nina Papavasiliou. V(D)J recombination and the evolution of the adaptive immune system. *PLoS Biol*, 1(1):E16, Oct 2003. 15

[83] Daniel D Billadeau, Jeffrey C Nolz, and Timothy S Gomez. Regulation of T-cell activation by the cytoskeleton. *Nat Rev Immunol*, 7(2):131–143, Feb 2007. 16, 19, 96

[84] J. Delon and R. N. Germain. Information transfer at the immunological synapse. *Curr Biol*, 10(24):R923–R933, 2000. 16, 18, 19

[85] Thomas R Weikl and Reinhard Lipowsky. Pattern formation during T-cell adhesion.ts. *Biophys J*, 87(6):3665–3678, Dec 2004. 16, 19, 66

[86] S. Demotz, H. M. Grey, and A. Sette. The minimal number of class II MHC-antigen complexes needed for T cell activation. *Science*, 249(4972):1028–1030, Aug 1990. 18

[87] P. A. van der Merwe. The tcr triggering puzzle. *Immunity*, 14(6):665–668, Jun 2001. 18

[88] Nigel John Burroughs and Christoph Wülfing. Differential segregation in a cell-cell contact interface: the dynamics of the immunological synapse. *Biophys J*, 83(4):1784–1796, Oct 2002. 19

[89] Daniel Coombs, Micah Dembo, Carla Wofsy, and Byron Goldstein. Equilibrium thermodynamics of cell-cell adhesion mediated by multiple ligand-receptor pairs. *Biophys J*, 86(3):1408–1423, Mar 2004.

[90] Philippos K Tsourkas, Nicole Baumgarth, Scott I Simon, and Subhadip Raychaudhuri. Mechanisms of B-cell synapse formation predicted by Monte Carlo simulation. *Biophys J*, 92(12):4196–4208, Jun 2007. 19

[91] A. I. Sperling, J. R. Sedy, N. Manjunath, A. Kupfer, B. Ardman, and J. K. Burkhardt. Tcr signaling induces selective exclusion of cd43 from the t cell-antigen-presenting cell contact site. *J Immunol*, 161(12):6459–6462, Dec 1998. 19

[92] Jérôme Delon, Sabine Stoll, and Ronald N Germain. Imaging of T-cell interactions with antigen presenting cells in culture and in intact lymphoid tissue. *Immunol Rev*, 189:51–63, Nov 2002. 19

[93] M. L. Dustin and J. A. Cooper. The immunological synapse and the actin cytoskeleton: molecular hardware for t cell signaling. *Nat Immunol*, 1(1):23–29, Jul 2000. 19

[94] J. Delon, K. Kaibuchi, and R. N. Germain. Exclusion of CD43 from the immunological synapse is mediated by phosphorylation-regulated relocation of the cytoskeletal adaptor moesin. *Immunity*, 15(5):691–701, Nov 2001. 19, 59

[95] Tal Ilani, Chand Khanna, Ming Zhou, Timothy D Veenstra, and Anthony Bretscher. Immune synapse formation requires zap-70 recruitment by ezrin and cd43 removal by moesin. *J Cell Biol*, 179(4):733–746, Nov 2007. 19, 59

[96] Alain Trautmann and Salvatore Valitutti. The diversity of immunological synapses. *Curr Opin Immunol*, 15(3):249–254, Jun 2003. 19

[97] Peter Friedl, Annemieke Th den Boer, and Matthias Gunzer. Tuning immune responses: diversity and adaptation of the immunological synapse. *Nat Rev Immunol*, 5(7):532–545, Jul 2005. 19, 68

[98] Dale Rex Coman. Decreased mutual adhesiveness, a property of cells from squamous cell carcinomas. *Cancer Res*, 4(10):625–629, October 1944. 21

[99] Martin A. Hubbe. Adhesion and detachment of biological cells in vitro. *Progress in Surface Science*, 11(2):65–137, 1981. 21

[100] J. M. Mitchison and M. M. Swann. The mechanical properties of the cell surface: I. the cell elastimeter. *J Exp Biol*, 31(3):443–460, September 1954. 22

[101] J. M. Mitchison and M. M. Swann. The mechanical properties of the cell surface: II. the unfertilized sea-urchin egg. *J Exp Biol*, 31(3):461–472, September 1954. 22

[102] M. A. Tsai, R. S. Frank, and R. E. Waugh. Passive mechanical behavior of human neutrophils: power-law fluid. *Biophys J*, 65(5):2078–2088, Nov 1993. 22

[103] A. Yeung and E. Evans. Cortical shell-liquid core model for passive flow of liquid-like spherical cells into micropipets. *Biophys J*, 56(1):139–149, Jul 1989. 22

[104] R. M. Hochmuth. Micropipette aspiration of living cells. *J Biomech*, 33(1):15–22, Jan 2000. 23

[105] E. Evans and A. Yeung. Apparent viscosity and cortical tension of blood granulocytes determined by micropipet aspiration. *Biophys J*, 56(1):151–160, Jul 1989. 23

[106] Jin-Yu Shao, Gang Xu, and Peng Guo. Quantifying cell-adhesion strength with micropipette manipulation: principle and application. *Front Biosci*, 9:2183–2191, Sep 2004. 23, 24

[107] KL Sung, LA Sung, M Crimmins, SJ Burakoff, and S Chien. Determination of junction avidity of cytolytic T cell and target cell. *Science*, 234(4782):1405–1408, December 1986. 24

[108] Yeh-Shiu Chu, William A Thomas, Olivier Eder, Frederic Pincet, Eric Perez, Jean Paul Thiery, and Sylvie Dufour. Force measurements in E-cadherin-mediated cell doublets reveal rapid adhesion strengthened by actin cytoskeleton remodeling through Rac and Cdc42. *J Cell Biol*, 167(6):1183–1194, Dec 2004. 24, 25, 81

[109] E. Evans, K. Ritchie, and R. Merkel. Sensitive force technique to probe molecular adhesion and structural linkages at biological interfaces. *Biophys J*, 68(6):2580–2587, Jun 1995. 25

[110] Gang Xu and Jin-Yu Shao. Double tether extraction from human neutrophils and its comparison with CD4+ T-lymphocytes. *Biophys J*, 88(1):661–669, Jan 2005. 26, 70

[111] Gaurav Girdhar, Yong Chen, and Jin-Yu Shao. Double-tether extraction from human umbilical vein and dermal microvascular endothelial cells. *Biophys J*, 92(3):1035–1045, Feb 2007.

[112] Gaurav Girdhar and Jin-Yu Shao. Simultaneous tether extraction from endothelial cells and leukocytes: observation, mechanics, and significance. *Biophys J*, 93(11):4041–4052, Dec 2007. 26, 70

[113] A. Ashkin. Acceleration and trapping of particles by radiation pressure. *Phys. Rev. Lett.*, 24(4):156–159, Jan 1970. 26

[114] Steven Chu. Nobel lecture: The manipulation of neutral particles. *Rev. Mod. Phys.*, 70(3):685–706, Jul 1998. 26

[115] Claude N. Cohen-Tannoudji. Nobel lecture: Manipulating atoms with photons. *Rev. Mod. Phys.*, 70(3):707–719, Jul 1998.

[116] William D. Phillips. Nobel lecture: Laser cooling and trapping of neutral atoms. *Rev. Mod. Phys.*, 70(3):721–741, Jul 1998. 26

[117] S. M. Block, L. S. Goldstein, and B. J. Schnapp. Bead movement by single kinesin molecules studied with optical tweezers. *Nature*, 348(6299):348–352, Nov 1990. 26, 28

[118] Jeffrey R Moffitt, Yann R Chemla, Steven B Smith, and Carlos Bustamante. Recent advances in optical tweezers. *Annu Rev Biochem*, 77:205–228, 2008. 26

[119] D. Choquet, D. P. Felsenfeld, and M. P. Sheetz. Extracellular matrix rigidity causes strengthening of integrin-cytoskeleton linkages. *Cell*, 88(1):39–48, Jan 1997. 26

[120] S. C. Kuo and M. P. Sheetz. Force of single kinesin molecules measured with optical tweezers. *Science*, 260(5105):232–234, Apr 1993. 28

[121] T. Nishizaka, H. Miyata, H. Yoshikawa, S. Ishiwata, and K. Kinosita. Unbinding force of a single motor molecule of muscle measured using optical tweezers. *Nature*, 377(6546):251–254, Sep 1995. 28

[122] A. Ashkin and J. M. Dziedzic. Optical trapping and manipulation of viruses and bacteria. *Science*, 235(4795):1517–1520, Mar 1987. 28

[123] S. Suresh, J. Spatz, J. P. Mills, A. Micoulet, M. Dao, C. T. Lim, M. Beil, and T. Seufferlein. Connections between single-cell biomechanics and human disease states: gastrointestinal cancer and malaria. *Acta Biomater*, 1(1):15–30, Jan 2005. 28, 35

[124] O. Thoumine, P. Kocian, A. Kottelat, and J. J. Meister. Short-term binding of fibroblasts to fibronectin: optical tweezers experiments and probabilistic analysis. *Eur Biophys J*, 29(6):398–408, 2000. 28

[125] A. R. Bausch, F. Ziemann, A. A. Boulbitch, K. Jacobson, and E. Sackmann. Local measurements of viscoelastic parameters of adherent cell surfaces by magnetic bead microrheometry. *Biophys J*, 75(4):2038–2049, Oct 1998. 28

[126] A. R. Bausch, W. Möller, and E. Sackmann. Measurement of local viscoelasticity and forces in living cells by magnetic tweezers. *Biophys J*, 76(1 Pt 1):573–579, Jan 1999. 28

[127] Linhong Deng, Nigel J Fairbank, Ben Fabry, Paul G Smith, and Geoffrey N Maksym. Localized mechanical stress induces time-dependent actin cytoskeletal remodeling and stiffening in cultured airway smooth muscle cells. *Am J Physiol Cell Physiol*, 287(2):C440–C448, Aug 2004. 28

[128] G. N. Maksym, B. Fabry, J. P. Butler, D. Navajas, D. J. Tschumperlin, J. D. Laporte, and J. J. Fredberg. Mechanical properties of cultured human airway smooth muscle cells from 0.05 to 0.4 hz. *J Appl Physiol*, 89(4):1619–1632, Oct 2000. 28

[129] Nadine Walter, Christine Selhuber, Horst Kessler, and Joachim P Spatz. Cellular unbinding forces of initial adhesion processes on nanopatterned surfaces probed with magnetic tweezers. *Nano Lett*, 6(3):398–402, Mar 2006. 29

[130] Anthony H B de Vries, Bea E Krenn, Roel van Driel, and Johannes S Kanger. Micro magnetic tweezers for nanomanipulation inside live cells. *Biophys J*, 88(3):2137–2144, Mar 2005. 29

[131] J. Guck, R. Ananthakrishnan, H. Mahmood, T. J. Moon, C. C. Cunningham, and J. Käs. The optical stretcher: a novel laser tool to micromanipulate cells. *Biophys J*, 81(2):767–784, Aug 2001. 29

[132] Ulf Leonhardt. Optics: Momentum in an uncertain light. *Nature*, 444(7121):823–824, December 2006. 30

[133] H. Minkowski. Die Grundgleichungen für die elektromagnetischen Vorgänge in bewegten Köpern. *Nachrichten von der Gesellschaft der Wissenschaften zu Göttingen*, 53:53–111, 1908. 30

[134] A. Ashkin and J. M. Dziedzic. Radiation pressure on a free liquid surface. *Phys. Rev. Lett.*, 30(4):139–142, January 1973. 30

[135] Jochen Guck, Stefan Schinkinger, Bryan Lincoln, Falk Wottawah, Susanne Ebert, Maren Romeyke, Dominik Lenz, Harold M Erickson, Revathi Ananthakrishnan, Daniel Mitchell, Josef Käs, Sydney Ulvick, and Curt Bilby. Optical deformability as an inherent cell marker for testing malignant transformation and metastatic competence. *Biophys J*, 88(5):3689–3698, May 2005. 30

[136] Simon Jungbauer, Huajian Gao, Joachim P Spatz, and Ralf Kemkemer. Two characteristic regimes in frequency dependent dynamic reorientation of fibroblasts on cyclically stretched substrates. *Biophys J*, May 2008. 31

[137] Hirotaka Ohishi, Ken-Ichi Furukawa, Koei Iwasaki, Kazumasa Ueyama, Akihiro Okada, Shigeru Motomura, Seiko Harata, and Satoshi Toh. Role of prostaglandin i2 in the gene expression induced by mechanical stress in spinal ligament cells derived from patients with ossification of the posterior longitudinal ligament. *J Pharmacol Exp Ther*, 305(3):818–824, Jun 2003. 31

[138] K. Iwasaki, K-I. Furukawa, M. Tanno, T. Kusumi, K. Ueyama, M. Tanaka, H. Kudo, S. Toh, S. Harata, and S. Motomura. Uni-axial cyclic stretch induces cbfa1 expression in spinal ligament cells derived from patients with ossification of the posterior longitudinal ligament. *Calcif Tissue Int*, 74(5):448–457, May 2004. 31

[139] C-Y. Charles Huang, Kristen L Hagar, Lauren E Frost, Yubo Sun, and Herman S Cheung. Effects of cyclic compressive loading on chondrogenesis of rabbit bone-marrow derived mesenchymal stem cells. *Stem Cells*, 22(3):313–323, 2004. 31

[140] O. Thoumine, A. Ott, O. Cardoso, and J. J. Meister. Microplates: a new tool for manipulation and mechanical perturbation of individual cells. *J Biochem Biophys Methods*, 39(1-2):47–62, Feb 1999. 35

[141] Michael Beil, Alexandre Micoulet, Götz von Wichert, Stephan Paschke, Paul Walther, M. Bishr Omary, Paul P Van Veldhoven, Ulrike Gern, Elke Wolff-Hieber, Juliane Eggermann, Johannes Waltenberger, Guido Adler, Joachim Spatz, and Thomas Seufferlein. Sphingosylphosphorylcholine regulates keratin network architecture and visco-elastic properties of human cancer cells. *Nat Cell Biol*, 5(9):803–811, Sep 2003. 35

[142] Pablo Fernández, Pramod A Pullarkat, and Albrecht Ott. A master relation defines the nonlinear viscoelasticity of single fibroblasts. *Biophys J*, 90(10):3796–3805, May 2006. 35

[143] Nicolas Desprat, Alain Richert, Jacqueline Simeon, and Atef Asnacios. Creep function of a single living cell. *Biophys J*, 88(3):2224–2233, Mar 2005.

[144] N. Desprat, A. Guiroy, and A. Asnacios. Microplates-based rheometer for a single living cell. *Review of Scientific Instruments*, 77(5):055111, 2006. 35, 65

[145] Alexandre Micoulet, Joachim P Spatz, and Albrecht Ott. Mechanical response analysis and power generation by single-cell stretching. *ChemPhysChem*, 6(4):663–670, Apr 2005. 35, 36, 38

[146] Alexandre Micoulet. *Uniaxial Mechanical Assays on Adherent Living Single Cells : Animal Embryonic Fibroblasts and Human Pancreas Cancer Cells*. PhD thesis, Universität Heidelberg, Fakultät für Physik und Astronomie, 2004. 37, 38

[147] E. Gladilin, A. Micoulet, B. Hosseini, K. Rohr, J. Spatz, and R. Eils. 3D finite element analysis of uniaxial cell stretching: from image to insight. *Phys Biol*, 4(2):104–113, Jun 2007. 41, 42, 43

[148] Vincent Dupres, Claire Verbelen, and Yves F Dufrêne. Probing molecular recognition sites on biosurfaces using afm. *Biomaterials*, 28(15):2393–2402, May 2007. 42

[149] N. Wang, K. Naruse, D. Stamenović, J. J. Fredberg, S. M. Mijailovich, I. M. Tolić-Norrelykke, T. Polte, R. Mannix, and D. E. Ingber. Mechanical behavior in living cells consistent with the tensegrity model. *Proc Natl Acad Sci U S A*, 98(14):7765–7770, Jul 2001. 42, 43

[150] G. Binnig, C. F. Quate, and Ch. Gerber. Atomic force microscope. *Phys. Rev. Lett.*, 56(9):930–933, March 1986. 45, 46

[151] Daniel J. Muller and Yves F. Dufrene. Atomic force microscopy as a multifunctional molecular toolbox in nanobiotechnology. *Nat Nano*, 3(5):261–269, May 2008. 45

[152] Michael D. Ward. Materials science: Snapshots of crystal growth. *Science*, 308(5728):1566–1567, 2005. 45

[153] Bhanu P. Jena and J.K. Heinrich Hörber, editors. *Atomic Force Microscopy in Cell Biology*. Academic Press, 2002. 45

[154] E. L. Florin, V. T. Moy, and H. E. Gaub. Adhesion forces between individual ligand-receptor pairs. *Science*, 264(5157):415–417, Apr 1994. 45

[155] Paul A Wiggins, Thijn van der Heijden, Fernando Moreno-Herrero, Andrew Spakowitz, Rob Phillips, Jonathan Widom, Cees Dekker, and Philip C Nelson. High flexibility of DNA on short length scales probed by atomic force microscopy. *Nat Nanotechnol*, 1(2):137–141, Nov 2006. 45

[156] Yann Gilbert, Marie Deghorain, Ling Wang, Bing Xu, Philipp D Pollheimer, Hermann J Gruber, Jeff Errington, Bernard Hallet, Xavier Haulot, Claire Verbelen, Pascal Hols, and Yves F Dufrêne. Single-molecule force spectroscopy and imaging of the vancomycin/d-ala-d-ala interaction. *Nano Lett*, 7(3):796–801, Mar 2007. 45

[157] M. Benoit, D. Gabriel, G. Gerisch, and H. E. Gaub. Discrete interactions in cell adhesion measured by single-molecule force spectroscopy. *Nat Cell Biol*, 2(6):313–317, Jun 2000. 45, 46, 78, 84, 88

[158] Jonne Helenius, Carl-Philipp Heisenberg, Hermann E Gaub, and Daniel J Muller. Single-cell force spectroscopy. *J Cell Sci*, 121(Pt 11):1785–1791, Jun 2008. 46

[159] Martin Benoit and Hermann E Gaub. Measuring cell adhesion forces with the atomic force microscope at the molecular level. *Cells Tissues Organs*, 172(3):174–189, 2002. 46, 78, 91

[160] A. Vinckier and G. Semenza. Measuring elasticity of biological materials by atomic force microscopy. *FEBS Lett*, 430(1-2):12–16, Jun 1998. 48

[161] M. Radmacher, R. W. Tillamnn, M. Fritz, and H. E. Gaub. From molecules to cells: imaging soft samples with the atomic force microscope. *Science*, 257(5078):1900–1905, Sep 1992.

[162] M. Radmacher, M. Fritz, C. M. Kacher, J. P. Cleveland, and P. K. Hansma. Measuring the viscoelastic properties of human platelets with the atomic force microscope. *Biophys J*, 70(1):556–567, Jan 1996.

[163] Jérme Solon, Ilya Levental, Kheya Sengupta, Penelope C Georges, and Paul A Janmey. Fibroblast adaptation and stiffness matching to soft elastic substrates. *Biophys J*, 93(12):4453–4461, Dec 2007.

[164] David C. Lin and Ferenc Horkay. Nanomechanics of polymer gels and biological tissues: A critical review of analytical approaches in the hertzian regime and beyond. *Soft Matter*, 4(4):669–682, 2008. 48

[165] J. P. Cleveland, S. Manne, D. Bocek, and P. K. Hansma. A nondestructive method for determining the spring constant of cantilevers for scanning force microscopy. *Review of Scientific Instruments*, 64(2):403–405, 1993. 49, 76

[166] Christine Selhuber. *Biological Adhesion on Nanopatterned Substrates Studied with Force Spectroscopy and Microinterferometry*. PhD thesis, Universität Heidelberg, Fakultät für Physik und Astronomie, 2006. 50

[167] Peter Friedl and Julian Storim. Diversity in immune-cell interactions: states and functions of the immunological synapse. *Trends Cell Biol*, 14(10):557–567, Oct 2004. 59, 68

[168] Timothy A Springer. Predicted and experimental structures of integrins and beta-propellers. *Curr Opin Struct Biol*, 12(6):802–813, Dec 2002. 59, 61

[169] Jonathan T Pribila, Angie C Quale, Kristen L Mueller, and Yoji Shimizu. Integrins and t cell-mediated immunity. *Annu Rev Immunol*, 22:157–180, 2004.

[170] Bing-Hao Luo and Timothy A Springer. Integrin structures and conformational signaling. *Curr Opin Cell Biol*, 18(5):579–586, Oct 2006. 59

[171] J. Kappler, J. White, D. Wegmann, E. Mustain, and P. Marrack. Antigen presentation by Ia+ B cell hybridomas to H-2-restricted T cell hybridomas. *Proc Natl Acad Sci U S A*, 79(11):3604–3607, Jun 1982. 65, 68, 71

[172] Kyeong-Hee Lee, Amy D Holdorf, Michael L Dustin, Andrew C Chan, Paul M Allen, and Andrey S Shaw. T cell receptor signaling precedes immunological synapse formation. *Science*, 295(5559):1539–1542, Feb 2002. 66

[173] L. C. Bonifaz, S. Arzate, and J. Moreno. Endogenous and exogenous forms of the same antigen are processed from different pools to bind MHC class II molecules in endocytic compartments. *Eur J Immunol*, 29(1):119–131, Jan 1999. 68

[174] Mingzhai Sun, John S Graham, Balazs Hegedüs, Françoise Marga, Ying Zhang, Gabor Forgacs, and Michel Grandbois. Multiple membrane tethers probed by atomic force microscopy. *Biophys J*, 89(6):4320–4329, Dec 2005. 70, 82, 84

[175] F. Momburg, S. Fuchs, J. Drexler, R. Busch, M. Post, G. J. Hmmerling, and L. Adorini. Epitope-specific enhancement of antigen presentation by invariant chain. *J Exp Med*, 178(4):1453–1458, Oct 1993. 71

[176] M. Thie, R. Rspel, W. Dettmann, M. Benoit, M. Ludwig, H. E. Gaub, and H. W. Denker. Interactions between trophoblast and uterine epithelium: monitoring of adhesive forces. *Hum Reprod*, 13(11):3211–3219, Nov 1998. 78, 81

[177] Anna Taubenberger, David A Cisneros, Jens Friedrichs, Pierre-Henri Puech, Daniel J Muller, and Clemens M Franz. Revealing early steps of alpha2beta1 integrin-mediated adhesion to collagen type I by using single-cell force spectroscopy. *Mol Biol Cell*, 18(5):1634–1644, May 2007. 81

[178] Jens Friedrichs, Juha M Torkko, Jonne Helenius, Terhi P Tervinen, Joachim Fllekrug, Daniel J Muller, Kai Simons, and Aki Manninen. Contributions of galectin-3 and -9 to epithelial cell adhesion analyzed by single cell force spectroscopy. *J Biol Chem*, 282(40):29375–29383, Oct 2007. 78

[179] Guido H Wabnitz, Thomas Kcher, Philipp Lohneis, Christoph Stober, Mathias H Konstandin, Beate Funk, Urban Sester, Matthias Wilm, Martin Klemke, and Yvonne Samstag. Costimulation induced phosphorylation of L-plastin facilitates surface transport of the T cell activation molecules CD69 and CD25. *Eur J Immunol*, 37(3):649–662, Mar 2007. 79, 118

[180] S. Vedula, T. Lim, P. Kausalya, E. Lane, G. Rajagopal, W. Hunziker, and C. Lim. Quantifying Forces Mediated by Integral Tight Junction Proteins in Cell-Cell Adhesion. *Experimental Mechanics*, pages –, 2007. 81

[181] Xiaohui Zhang, Ewa Wojcikiewicz, and Vincent T Moy. Force spectroscopy of the leukocyte function-associated antigen-1/intercellular adhesion molecule-1 interaction. *Biophys J*, 83(4):2270–2279, Oct 2002. 86

[182] Xiaohui Zhang, Susan E Craig, Hishani Kirby, Martin J Humphries, and Vincent T Moy. Molecular basis for the dynamic strength of the integrin alpha4beta1/VCAM-1 interaction. *Biophys J*, 87(5):3470–3478, Nov 2004. 86

[183] D. C. Wraith, D. E. Smilek, D. J. Mitchell, L. Steinman, and H. O. McDevitt. Antigen recognition in autoimmune encephalomyelitis and the potential for peptide-mediated immunotherapy. *Cell*, 59(2):247–255, Oct 1989. 89

[184] Janis K Burkhardt, Esteban Carrizosa, and Meredith H Shaffer. The actin cytoskeleton in T cell activation. *Annu Rev Immunol*, 26:233–259, 2008. 96

[185] Jiang-Ping Wu, Jonathan Emeigh, Donghong A Gao, Daniel R Goldberg, Daniel Kuzmich, Clara Miao, Ian Potocki, Kevin C Qian, Ronald J Sorcek, Deborah D Jeanfavre, Kei Kishimoto, Elizabeth A Mainolfi, Gerald Nabozny, Charline Peng, Patricia Reilly, Robert Rothlein, Rosemarie H Sellati, Joseph R Woska, Shirlynn Chen, Jocelyn A Gunn, Drane O'Brien, Stephen H Norris, and Terence A Kelly. Second-generation lymphocyte function-associated antigen-1 inhibitors: 1H-imidazo[1,2-alpha]imidazol-2-one derivatives. *J Med Chem*, 47(22):5356–5366, Oct 2004. 97

[186] C. Reis e Sousa and R. N. Germain. Major histocompatibility complex class I presentation of peptides derived from soluble exogenous antigen by a subset of cells engaged in phagocytosis. *J Exp Med*, 182(3):841–851, Sep 1995. 118

Acknowledgments

First and foremost, I would like to express my gratitude to Prof. Dr. Joachim P. Spatz, who supported me in the best possible way. Thank you for taking me on as PhD student in your lab and for giving me the chance to pursuit science with no boundaries. Also, I want to thank Prof. Heinz Horner who readily agreed to be the second referee for this thesis. Vielen Dank auch Prof. Harald Herrmann und Prof. Markus Oberthaler, die spontan zusagten an der Disputation teilzunehmen.

The author acknowledges the support of many other people who helped to make this thesis possible. I want to thank Dominik Djandji (DKFZ) who helped with many of the AFM experiments. I enjoyed our nightly visits to Mandy's when we had our burger cravings ;-) Also, I wish to thank Prof. Günter Hämmerling (DKFZ) who made great efforts to ensure that our AFM experiments were successful and who taught a good deal of immunology. Thanks to Vamsi Kodali, who introduced me to Kishore Kunapuli who came up with the idea to do T cell/APC experiments in the first place.

I am indebted to my fellow lab colleagues who helped to make this thesis possible. Alexandre Micoulet, the cell „stretcher daddy”, trained me to use the machine I spent so many hours with. I have to thank Ilia Louban, who introduced me to the AFM technique. I enjoyed our daily coffee breaks which included many hours of physics talk ;-) Ich möchte mich bei Jacques Blümmel, bedanken, mit dem ich in der Anfangsphase ein Büro teilte und mir das eine oder andere Mal zur Seite stand, so dass ich mir als Physiker im Chemielabor nicht ganz so verloren vorkam... Thanks to Daniel Aydin, who helped us resolving many issues related to surface functionalisation. Kai Uhrig, Daniel Aydin and Theobald Lohmüller were a vital and refreshing source in many helpful discussions, not only in the field of science ;-) Vielen anderen aktiven und ehemaligen Mitgliedern der Gruppe sei an dieser Stelle für die unzähligen fachlichen Diskussionen gedankt.

Vor allem in der Anfangsphase bildete die 8-Uhr-Frühstücks-Gruppe mit Christian Schmitz, Kai Uhrig und Heike Böhm die Grundlage für einen überaus interssanten und motivierenden Start in den Tag. Ich werde die Zeit in sehr guter Erinnerung behalten und hoffe, dass wir bald das Sparschwein schlachten können... Simon Schulz danke ich für die lustigen Kurzpausen, die Fahrt nach Aarhus und all den anderen Kram, den wir zusammen erlebt haben.

Ein großer Dank geht an unseren HiWi Thomas Kriesche, der mit seinem unermüdlichem Einsatz geholfen hat einige Experimente auszuwerten und dessen exzellentes AFM Filmchen immer großen Eindruck in Voträgen gemacht hat. Einen besonderen Gruß sende ich nach Schweden/Dänemark an Christine Selhuber, die Vorreiterin im AK Spatz in Sachen AFM war und die Grundlagen für den erfolgreichen Betrieb der Maschine in HD geschaffen hat. Kai Uhrig, Daniel Aydin, Ilia Louban und Ada Cavalcanti danke ich herzlich für die gründliche Durchsicht und das Korrekturlesen der Arbeit. Technisch sehr unterstüzt haben mich Richard Morlang, Sigrid Riese und nicht zuletzt Nadja Bulbuc vom DKFZ, die unermüdlich Zellen für unsere Experimente preparierte. Vielen Dank!

Ich bedanke mich ganz herzlich bei unseren Sekräterinnen, Frau Bozcek und Frau Pfeilmeier. Besonders für die Doktoranden in Heidelberg war Frau Boczek, die gute Seele des AK Spatz, ein stets hilfsbereiter Ansprechpartner. Ihrem Organisationtalent und ihrer Zuverlässigkeit verdanken wir den reibungslosen Ablauf im AK. Ohne ihre grünen Äpfel hätte ich den ein oder anderen Abend im Labor nicht überstanden...

Das Beste am AK Spatz sind seine Mitglieder! Die Zusammenarbeit mit euch hat mir viel Spaß gemacht. Besonders hervorzuheben sind die halbjährlichen gemeinsamen Ausflüge nach Ringberg, Weingarten und Antholz, die sehr lehr- und zugleich erlebnisreich waren. Vor allem die “Crew” bestehend aus Ferdi, Marco, Ilia, Janosch, Huber Kai, Voggelfisch Theo, Fischvoggel Daniel und Bulz Simon war Garant für viele spannende Momente ;-) Misch!

Außerhalb der Uni möchte ich allen meinen Freunden danken, die mich stets unterstüzt haben. Im besonderen danke ich Navid, Thomas, Babak, Janosch, Sebastian und Henryk die immer für mich da waren, auch in den schwierigeren Zeiten.

Meiner Familie habe ich das Meiste zu verdanken. Ohne die Gelassenheit meiner Eltern und meiner Schwester Narges wäre ich heute sicher nicht so weit. Für ihre Rücksicht und ihre Unterstützung bin ich ihnen zu großem Dank verpflichtet. Ich widme diese Arbeit daher meinen Eltern.

Evelyne musste am meisten unter meinem Dissertation-Stress leiden. Für ihre fortwährende Geduld, ihr Vertrauen und ihre stete Unterstützung bin ich sehr dankbar. Thanks for loving me back. ♡

Appendix

A

Appendix

A.1 Abbreviations

APC Antigen Presenting Cell

AFM Atomic Force Microscope

BFP Bio-membrane Force Probe

CAM Cell Adhesion Molecule

ConA Concanavalin A

CD Cluster of Differentiation

DC Dendritic Cell

DNA Deoxyribonucleic Acid

ECM Extracellular Matrix

FACS Fluorescent-Activated Cell Sorting

FC Flow Cytometry

HEL$_{34-45}$ Hen Egg Lysozome (peptide 34-45)

ICAM-1 Intercellular Adhesion Molecule-1

Ig-CAM Immunoglobulin Cell Adhesion Molecule

IgSF Immunoglobulin Superfamily

IL-2 Interleukin-2

IS Immune Synapse

LFA-1 Lymphocyte Function-associated Antigen-1

MIFC Multispectral Imaging Flow Cytometry

MHC Major Histocompatibility Complex

pMHC peptide loaded Major Histocompatibility Complex

PI Propidium Iodide

PLL Poly-L-Lysine

OT Optical Tweezers

TCR T Cell Receptor

SD Standard Deviation

SMAC Supramolecular Activation Cluster

SCFS Single-Cell Force Spectroscopy

A.2 IL2 Sandwich ELISA

The IL-2 level in culture supernatants was measured by sandwich ELISA performed as previously described [186]. Briefly, a monoclonal antibody specific for IL-2 is coated on a 96-well plate (rat IgG2a capture antibody, clone JES6-1A12, BD Pharmingen, 554424). Standards and samples are added to the wells, and any IL-2 present binds to the immobilized antibody. The wells are washed and streptavidin-horseradish peroxidase (SA-HRP) conjugate mixed with biotinylated anti-murine IL-2 antibody (biotinylated rat IgG2b detection antibody, clone JES6-5H4, BD Pharmingen, 554426) is added, producing an antibody-antigen-antibody "sandwich". The substrate for HRP is O-phenylenediamine (OPD, 1mg/ml) with an absorbance maximum at 492 nm. OPD yields a water soluble yellow-orange product when reacted with peroxidase. Hydrogen peroxide (H_2O_2) was added at the concentration of 1µl/ml of substrate buffer and 100µl of substrate solution per well was added, waited until the color changed from color less solution to olive green. This usually takes around 3-10min depending on the amount of antibody in the test sample. Color development may start in 2-5 min. Under these conditions, the assay is linear to an OD of ≈ 2.5 at 490nm. Absolute levels of IL-2 produced in the various experiments were generally between 0 and 5×10^5 IL-2 units/ml.

A.3 Analysis of the Immune Synapse Using ImageStream

Conjugate formation analysis between 3B11 T cells and HEL_{34-45} pulsed or unpulsed LK35.2 B cells was performed according to standard experimental procedure described in [179]. Briefly, LK35.2 B cells were adjusted to a density of 4×10^6 cells per ml. For the peptide loading HEL_{34-45} was added (100µmol/ml) and the cells were incubated at 37°C for 2h. Thereafter, unbound peptide was removed by two sequential washing steps with phosphate buffered saline. The LK35.2 pellet was re-suspended in 250µl culture medium containing the 3B11 T cells (4×10^6 per ml). The cells were pelleted to allow conjugate formation and immediately re-suspended in 50µl culture medium. After the incubation at 37°C for the indicated time points, cells were stained with fluorescently labeled antibodies against specific cell surface antigens as indicated (anti-CD3-Biotin, Streptavidin-PE-TexasRed and anti-CD18-FITC; purchased from BD-Biocience, Heidelberg, Germany) and Hoechst nuclear dye (Hoechst33342, Invitrogen). Data acquisition was performed with an ImageStream system (Amnis, Seattle, USA) and data were analyzed with IDEAS 3.0 software (Amnis, Seattle, USA). To find the contact zone between 3B11 and LK35.2 cells, total events were gated on true T cell/B cell pairs and a Hoechst dependent valley mask was defined between these cell couples. To specify the mask to the T cells the valley mask was combined with a T cell mask, which is dependent on the CD3 surface staining. This results in the Immune-Synapse-mask (IS-mask). Thereafter, protein accumulation was calculated as ratio between the mean pixel intensity (MPI) of the respective protein, i.e. CD3 or CD18, in the IS-mask and the MPI of the same protein in the T cells mask.